Performance and Receiver Structures for OFDM on Rayleigh Fading Channels

by

William S. Burchill

B. Eng. (Electrical) Carleton University, 1981

M. Eng. (Systems and Computer) Carleton University, 1985

A THESIS SUBMITTED IN PARTIAL FULFILLMENT OF

THE REQUIREMENTS FOR THE DEGREE OF

DOCTOR OF PHILOSOPHY

in

THE FACULTY OF GRADUATE STUDIES

ELECTRICAL ENGINEERING

We accept this thesis as conforming

to the required standard

THE UNIVERSITY OF BRITISH COLUMBIA

March 1997

In presenting this thesis in partial fulfilment of the requirements for an advanced degree at the University of British Columbia, I agree that the Library shall make it freely available for reference and study. I further agree that permission for extensive copying of this thesis for scholarly purposes may be granted by the head of my department or by his or her representatives. It is understood that copying or publication of this thesis for financial gain shall not be allowed without my written permission.

Department of Electrical Engineering

The University of British Columbia
Vancouver, Canada

Date May 5/1997

DE-6 (2/88)

Abstract

This thesis is a study of performance and receiver structures for Orthogonal Frequency Division Multiplexing (OFDM) on land mobile radio channels characterized by flat or frequency-selective Rayleigh fading.

The type of OFDM considered is a parallel modulation scheme in which N data symbols are assembled and used to simultaneously modulate N frequency-orthogonal tones, forming the OFDM symbol or block. Relative to a conventional serial modulation scheme of comparable bandwidth, OFDM has an extended signaling interval which allows for channel averaging in fading conditions. However, the channel variation over the duration of an OFDM block impairs the orthogonality of the modulated tones, causing intersymbol interference.

A new matched filter bound is derived which does not require that the channel remain constant over the signaling interval, and has Doppler frequency as a parameter. Pulse shape, diversity order, and interray correlation may also be varied. The matched filter bound is used to establish analytic performance limits on the probability of bit error for any receiver of uncoded OFDM on flat or frequency-selective Rayleigh fading channels. In contrast to the AWGN channel, the optimal pulse shape used in the receive correlator is time-varying and the transmitter pulse shape affects the probability of error.

Using the Maximum Likelihood Sequence Estimation (MLSE) criterion, an optimal receiver for OFDM on flat fading channels is derived. This turns out to require a constraint length $L = N - 1$, which is generally infeasible due to complexity constraints. However for BPSK OFDM a suboptimal truncated version of the MLSE receiver is able to approach the MFB to within 1 dB for a wide range of Doppler rates. For QPSK OFDM simple truncated MLSE is found to be impractical due to the required constraint length, which is greater than for BPSK OFDM.

The Minimum Mean Square Error (MMSE) criterion is used to derive optimal linear and nonlinear decision feedback equalizing receivers for OFDM on flat fading channels. A continuous-time analysis is used to show that the optimal linear MMSE receiver requires a sampling rate in excess of N samples per OFDM block, and that the optimal weighting function applied to the received signal to mitigate channel fading is tone-dependent. Approximations are considered to remove the tone-dependency, yielding a result consistent with previous work.

An MMSE-based criterion is proposed and used to derive a method for modifying the channel impulse response to an optimal desired impulse response having a specified constraint length. This limits error propagation with decision feedback and reduces the complexity of sequence estimation, making the latter feasible for QPSK OFDM as well as BPSK OFDM. The resulting nonlinear receiver structures have probability of error performances which improve on previously published results for the same modulation and channel.

Finally optimal and suboptimal receivers for OFDM on frequency-selective Rayleigh fading channels based on MLSE and MMSE criteria are derived. The additional complexities of receiver design arising from the presence of delay spread are studied analytically and evaluated by simulation. It is shown that for the MLSE receiver, long blocklength OFDM is relatively insensitive to the distribution of signal strengths between the rays of the two-ray frequency-selective Rayleigh fading channel model.

Table of Contents

Glossary

Acronyms

AWGN	Additive White Gaussian Noise
BOFDM	BPSK OFDM
BPSK	Binary Phase Shift Keying
DIR	Desired Impulse Response
DFE	Decision Feedback Equalization
DFFT	Discrete Frequency Fourier Transform
DFT	Discrete Fourier Transform
FEC	Forward Error Correction
FFT	Fast Fourier Transform
GSM	Groupe Spécial Mobile
iDFFT	inverse DFFT
ISI	Inter-Symbol Interference
MFB	Matched Filter Bound
MLSE	Maximum Likelihood Sequence Estimation
MMSE	Minimum Mean Square Error
MSE	Mean Square Error
kbaud	kilosymbols/sec
OFDM	Orthogonal Frequency Division Multiplexing
PAM	Pulse Amplitude Modulation
PCS	Personal Communications Systems
QOFDM	QPSK OFDM
QPSK	Quadrature Phase Shift Keying
SNR	Signal to Noise Ratio
ZF	Zero-Forcing

Symbols

a_k	data symbol
E_a	energy of a data symbol
E_b	energy of a data bit
f_c	carrier frequency
f_D	maximum Doppler frequency / spread
f_N	normalized maximum Doppler frequency
f_s	sampling frequency
$J_0(\cdot)$	zeroth order Bessel function of the first kind
L	sequence estimator constraint length
N	number of data symbols in an OFDM block
N_0	power spectral density of AWGN
P_b	probability of a bit error
P_e	probability of a bit or symbol error
P_s	probability of a symbol error
$p(t)$	transmitted pulse shape
$q(t)$	received pulse shape
$r(t)$	received signal
$s(t)$	transmitted OFDM block / signal
Δt	sampling interval
T_0	nominal OFDM block period
U_n	matched filter output
V_n	tone correlation
$w(t)$	output of a noiseless channel
$z(t)$	complex Gaussian random process
$z(\sigma, t)$	impulse response of a linear channel

Greek Symbols

α	rolloff factor of a raised cosine pulse
α_i	amplitude scaling factor of fading waveform
$\delta(t)$	delta function
δ_n	unit sample function
η^2	noise to signal ratio N_0/E_a
ρ	correlation coefficient
σ^2	variance
τ	delay
τ_{max}	maximum delay spread
λ	Viterbi metric / eigenvalue

List of Figures

Acknowledgment

This thesis is dedicated to my parents, William Joseph and Joyce Eleanor (Meikle) Burchill for getting things started. Many friends and colleagues in Ottawa and Vancouver who encouraged my graduate studies were influential. In particular I would like to thank my thesis advisor Dr. Cyril Leung for his constant patience and critical thinking. Thanks also go to the members of my thesis examination committee, and to the external examiner for their time and effort.

This work was supported in part by a B.C. Science Council Great Award, and NSERC grant #OGP0001731.

Chapter 1

Introduction

We are at the dawn of the era of universal wireless personal communications systems (PCS). The goal of PCS is to provide access to a global communications network without regard to location or mobility. These systems represent the third generation of public wireless services and will be completely digital [1].

It is unlikely that any single technology can be applied to all areas of PCS because of the fundamentally different economic and technical issues of *low-tier* and *high-tier* PCS situations. Low-tier applications are characterized by low power and low complexity, for example a hand held cordless telephone for pedestrian use. High-tier applications are characterized by large macrocells and high-speed mobility, the most important example being communication with a vehicle over land mobile radio channels. Communications devices may be optimized for a particular tier [2] but intercommunicate when appropriate, such as having a pedestrian phone relay its information through a high-tier device when used inside a vehicle.

From the perspective of modulation and detection, it is the high-tier situation, and in particular the vehicular digital mobile radio, which presents the most interesting and challenging technical problems. This is due to the severe and random nature of the channel distortion encountered.

Land mobile radio channels suffer from random signal fading which corrupts both the amplitude and phase of the received signal, causing dropouts whose frequency varies with the vehicle's speed, and there can be significant delay spread introducing random frequency selectivity. Assuming that the transmitter cannot anticipate the random channel[1] some form of diversity is required to obtain error rates comparable to those attainable on an additive white Gaussian noise (AWGN) channel.

[1] In certain situations, e.g. if the channel varies slowly relative to the rate at which its state can be assessed and communicated from the receiver back to the transmitter, some anticipation is possible.

Some early forms of diversity [3] took the form of multiple transmissions or receptions in the time, frequency, or less often, polarization planes[2]. These methods effectively halve the transmission rate. Another approach is to combine forward error correction (FEC) with any non-diversity modulation method. Although not generally viewed as a diversity technique, FEC provides an effective diversity by delocalizing the information content of a specific data symbol. Its bandwidth cost is $1 - R_c$, where R_c is the code rate. More recently some researchers have been advocating spread-spectrum modulation which has inherent frequency diversity in combination with FEC [4]. Its bandwidth cost or gain remains a subject of debate [2].

A novel method for dealing with the impairments of the land mobile radio channel was proposed in [5]. The idea was to use a version of orthogonal frequency division multiplexing (OFDM) with signaling elements chosen long enough to enable channel averaging, a type of inherent time diversity essentially without bandwidth cost, except for a small portion reserved for channel measurement. Simulation results presented in [5] showed substantial gains for channel-averaging OFDM over conventional modulation techniques without FEC in fast fading conditions.

Motivated by the results of [5] and the importance of the land-mobile radio channel, this thesis is concerned with the further development of OFDM theory. In particular we seek to establish the best performance achievable with this technique. We begin by deriving a new matched filter bound (MFB) for fast Rayleigh fading channels. This bound is unique in that it does not assume the fading channel remains constant over the duration of a signaling element, and establishes analytic limits on the probability of bit error (P_b) performance of any uncoded OFDM receiver with the maximum fading rate as a parameter. In subsequent chapters, several new receiver structures are derived via maximum-likelihood sequence estimation (MLSE) and minimum mean-square error

---

[2] Space diversity is does not halve the transmission rate.

(MMSE) optimality criteria. Their P_b or probability of symbol error (P_s) performances are evaluated by simulation for mutual comparison and for comparison to the bounds based on the MFB work. This is done for both flat (i.e. non-frequency-selective) and frequency-selective Rayleigh fading channels. The P_s performances of the receiver structures derived in this thesis meet, or in most cases substantially exceed previously published results on channel-averaging OFDM.

The rest of this introduction is organized as follows. OFDM is introduced in Section 1.1 and the effects of fading on it are outlined. The research contributions of this thesis are summarized in Section 1.3. Section 1.4 presents the organization of the rest of this thesis.

1.1 OFDM Modulation

OFDM can be described as a parallel modulation in which N data symbols are assembled and simultaneously modulated onto N orthogonal carriers. The modulator outputs are summed and the resulting waveform is further shaped by the unit energy pulse $p(t)$ to form $s(t)$, the transmitted waveform of a single OFDM block. This is

$$s(t) = p(t) \sum_{k=0}^{N-1} a_k e^{j\frac{2\pi}{T_0}kt} \tag{1.1.1}$$

where a_k is a data symbol, generally complex, and $p(t)$ is a pulse shaping function. The nominal duration of the block is $T_0 = NT_s$, where T_s is the data symbol interval in a comparable serial scheme having the same signaling rate. The frequency interval between adjacent complex tones is $1/T_0$. This is shown in Figure 1.1.

The bank of modulators need not appear explicitly in a digital implementation. An efficient method for generating an OFDM signal takes advantage of the inverse Fourier transform relationship between a_k and $s(t)$ seen in (1.1.1). If we sample the time-domain waveforms at intervals Δt, letting $x_m = x(m\Delta t)$, then a discrete version of (1.1.1) is

$$s_m = p_m \sum_{k=0}^{N-1} a_k e^{j\frac{2\pi}{T_0}km\Delta t}. \tag{1.1.2}$$

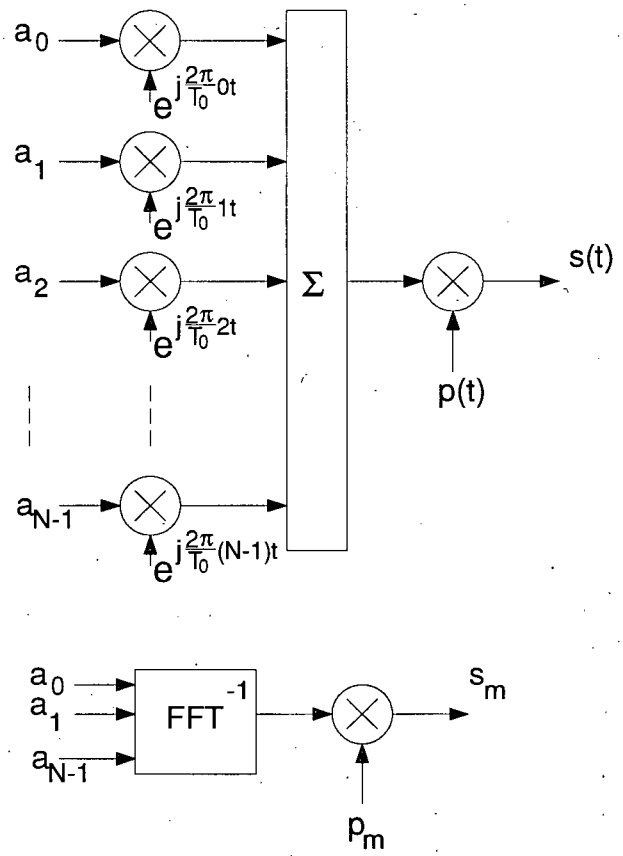

Figure 1.1 Parallel QAM and FFT based OFDM transmitters

Choose $N'\Delta t = T_0$, $N' \geq N$, and define $a_k = 0,\ k \geq N$. Then s_m can be written as

$$s_m = p_m \sum_{k=0}^{N'-1} a_k e^{j\frac{2\pi}{N'}km} \tag{1.1.3}$$

which is clearly an inverse discrete Fourier transform (DFT) [6] of the data post-multiplied by a shaping function. Since N' can be chosen for convenience, such as a power of 2, the fast Fourier transform (FFT) [6] algorithm can be used to evaluate (1.1.3) very efficiently. The choice of Δt affects the accuracy of the signal representation and is considered in Chapter 4. Previous work on land mobile radio channels [5], [7] has used $\Delta t = T_0/N$ with rectangular pulse shaping.

We will also need to consider the more general time-domain root raised cosine pulse shape $p(t)$ given by

$$p(t) = \sqrt{p_{sq}(t)},$$
$$p_{sq}(t) = \begin{cases} \frac{1}{2T_0}\left(1+\cos\left(\frac{\pi(t-\alpha T_0)}{\alpha T_0}\right)\right), & 0 \le t < \alpha T_0 \\ 1/T_0, & \alpha T_0 \le t \le T_0 \\ \frac{1}{2T_0}\left(1+\cos\left(\frac{\pi(t-T_0)}{\alpha T_0}\right)\right), & T_0 < t \le T_0(1+\alpha) \\ 0, & \text{otherwise} \end{cases} \tag{1.1.4}$$

where $0 \le \alpha \le 1$ is a rolloff factor describing the percentage of the pulse duration beyond T_0. The total time interval for which the pulse is nonzero is $T_0(1+\alpha)$, where T_0 is the time interval between the inflection-points of its leading and trailing edges as shown in Figure 1.2. As subsequent blocks of N data symbols are formed into OFDM blocks, they are transmitted serially over the channel at intervals of T, yielding

$$\begin{aligned} s_s(t) &= \sum_n s(t-nT) \\ &= \sum_n p(t-nT) \sum_{k=0}^{N-1} a_{n_k} e^{j\frac{2\pi}{T_0}k(t-nT)}, \end{aligned} \tag{1.1.5}$$

where a_{n_k} is the k^{th} data symbol of the n^{th} block. This is also shown in Figure 1.2. We will assume throughout that $T \ge T_0(1+\alpha)$ so that interblock interference (IBI) is not an issue. Additionally, on delay spread channels we will assume that

$$T \ge T_0(1+\alpha) + \tau_{max} \tag{1.1.6}$$

where τ_{max} is the maximum value of delay spread for the same reason. Typically $\tau_{max} \le 0.01\ T_0$ so that (1.1.6) is a mild requirement for OFDM. With IBI precluded we can henceforth confine our attention to the transmission and reception of a single OFDM block.

To a close approximation[3] the bandwidth of OFDM is the same as that of a conventional serial modulation transmitting data symbols at the same rate. This follows

[3] At this point we are not considering overhead for channel measurement, or effects of α and τ_{max}.

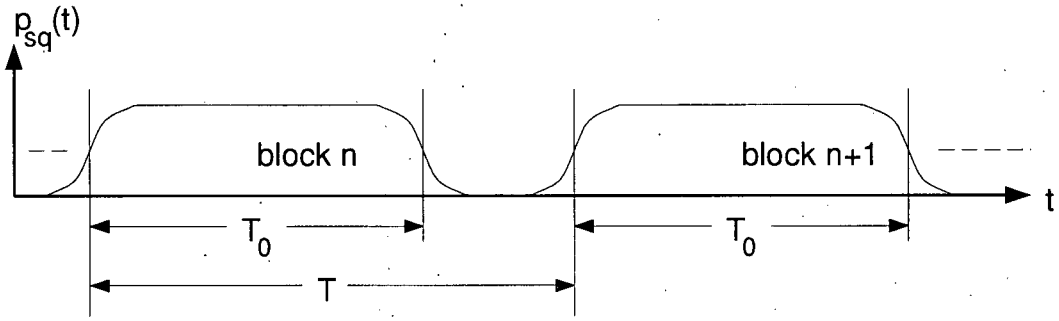

Figure 1.2 Definitions of T_0 and T

from noting that the bandwidth expansion due to transmitting N data symbols on frequency orthogonal carriers is compensated for by the bandwidth reduction due to each data symbol being transmitted N times more slowly. This extension in time of the data symbols is the key to the channel averaging ability of OFDM.

We note that the preceding description of OFDM as a parallel modulation scheme is convenient but not required. OFDM could equally well be viewed as a serial modulation with a nominal OFDM symbol duration of T_0 and possibly a very large alphabet of M^N OFDM symbols, where M is the size of the data symbol alphabet.

1.1.1 Modulation Constellation

In principle the individual tones comprising the OFDM signal could be modulated with points from any quadrature amplitude modulation (QAM) constellation. However the E_b/N_0 required to obtain a specified P_b, where E_b is the energy per bit and N_0 is the noise power spectral density, increases with constellation size [8]. Since we are primarily interested in low E_b/N_0 environments, we will confine our attention to BOFDM and QOFDM. BOFDM denotes OFDM with binary phase shift keying (BPSK) modulation of the OFDM tones and QOFDM denotes OFDM with quadrature phase shift keying (QPSK) modulation of the tones.

1.1.2 Bandwidth of OFDM

The bandwidth of OFDM is readily derived from first principles [9]. The general approach is to first determine the autocorrelation function of the modulated waveform, which turns out to be a cyclostationary process, and then remove the time dependency by averaging over one period of the process. The data symbols are assumed to be mutually independent and of equal energy. A Fourier transform of the time-averaged autocorrelation function gives the desired power spectral density as

$$\frac{E_a}{T_0}\sum_{k=0}^{N-1}\left|P\left(f-\frac{k}{T_0}\right)\right|^2 \tag{1.1.7}$$

where $E_a = \mathrm{E}\left[|a_k|^2\right]$ is the energy of a data symbol and $P(f) = \int p(t)e^{-j\frac{2\pi}{T_0}kt}dt$ is the Fourier transform of the shaping pulse. Note that T does not appear in (1.1.7); this is a consequence of the independent data assumption.

An interesting consequence of (1.1.7) is that the bandwidth of OFDM is only mildly influenced by $p(t)$ when N is large. To illustrate, if we consider two serial modulations, one with $p_1(t) = \mathrm{sinc}(t/T_s)$ and the other with $p_2(t) = \mathrm{rect}(t/T_s)$ pulse shaping, and measure bandwidth as the distance between the mainlobe's first nulls, then the bandwidth in the first case is $1/T_s$ which is only half that in the second. Similarly, we compare two OFDM modulations, one with $p_1(t) = \mathrm{sinc}(t/T_0)$ and the other with $p_2(t) = \mathrm{rect}(t/T_0)$ pulse shaping. The bandwidths for these two cases are N/T_0 and $(N+1)/T_0$ respectively, a factor of $(N+1)/N$ change. Since $(N+1)/N \approx 1$ for N large, the bandwidth for OFDM is approximately $1/T_s$ in both cases, showing low sensitivity to the pulse shape.

1.1.3 Channel Measurement

The type of OFDM system we have been describing is a type of coherent amplitude and phase modulation applied to a channel with randomly time-varying amplitude and

phase characteristics. Therefore optimal detection of the data requires knowledge of the channel parameters at the receiver. We assume this knowledge is obtained by allocating a small portion of the available bandwidth to channel estimation. The idea is to insert known pilot tones or pilot symbols into the transmitted signal. At the receiver these can be used to estimate the channel's impulse response.

The amount of bandwidth which must be allocated for channel measurement purposes follows from Nyquist's criterion, which states that the channel must be sampled at a rate higher than $2f_D$. This represents only about 2% of the data bandwidth since typically $f_D \leq 0.01/T_s$, e.g. $f_D = 100$ Hz and $f_s = 1/T_s = 10$ kbaud. This could be considered a lower limit since it makes no provision for guard intervals to protect pilots from Doppler spread data nor does it provide for mutual pilot signal orthogonality in an interference environment. These issues have been addressed in the literature. Comparative studies of pilot symbol and pilot tone techniques appear in [10] and [11] in the context of serial modulation and flat fading channels. The Groupe Spécial Mobile (GSM) standards [12] specify a 26 symbol pilot sequence for estimating frequency-selective channels in an interference environment. The original OFDM for land mobile radio study [5] presents pilot tone based techniques for estimating flat and frequency-selective fading channels.

In this thesis we do not develop the channel estimation problem further. The channel is assumed known to the receiver, and the focus is then on optimal detection. An exception occurs in Chapter 4 where an analysis is performed to estimate the deterioration in P_b due to using a noisy versus perfect channel estimate, and the result is verified by simulation.

1.1.4 Effect of Fading on OFDM

The extended symbol interval of OFDM that was introduced to provide channel averaging also causes it to suffer a serious impairment on fading channels. Fading impairs the orthogonality of the tones comprising the OFDM signal. The result is a type

of convolution of the data symbols within an OFDM block with a channel-dependent waveform [5], [7]. The convolution introduces intersymbol interference (ISI) amongst the data symbols. It is shown in subsequent chapters that the exact type of convolution depends on the signal representation. Similarly, there is also intrasymbol interference[4] when the data symbols are complex. This is generally not a problem for serial modulation schemes because the channel is approximately constant over a symbol's duration.

On frequency-selective fading channels the problem is compounded by additional ISI arising from multiple arrivals of the same block, each of which suffers from its own pattern of ISI.

1.2 Previous Work

Historically, many names have been used for OFDM, e.g. multichannel modulation, multicarrier modulation, or multitone modulation, depending upon the author. The basic idea is to subdivide a channel into a set of frequency-orthogonal subchannels. The complex exponential tones of the preceding OFDM description are the subchannel carrier frequencies of a multichannel description.

An early work on OFDM considered data communication on telephone channels [13]. Use of an FFT to construct the OFDM block was introduced in [14]. Application of OFDM to fading channels was proposed in [15] and [16]. The former considered HF band communications which are slowly fading such that Doppler spread induced ISI was of little importance. The latter considered digital audio broadcasting on land mobile radio channels, but used OFDM blocklengths much shorter than the channel's coherence time. Thus in these previous works the channel is essentially constant during the OFDM block and the motivation for OFDM is not channel averaging but simplified equalization. The simplified equalization follows from observing that individual OFDM subchannels are much narrower in bandwidth than the entire signal, therefore there is relatively less

[4] Interference of the in-phase and quadrature components.

change in the channel over the bandwidth of a subchannel as compared to the entire channel bandwidth.

In this work the OFDM blocks exceed the coherence time of the channel and OFDM is considered for its channel averaging ability. Only a few publications have been found to date (1997) which explore this approach. The first is [5] which makes the original proposal for OFDM on land mobile radio channels. This work related time-domain fading to frequency-domain ISI[5] and proposed simplified equalization structures for flat-fading and frequency-selective fading channels. A channel-averaging variation of OFDM in combination with FM transmission on flat-fading channels was considered in [17]. This work also presented a type of parallel decision feedback called decision feedback correction (DFC). Conventional decision feedback equalization (DFE) for OFDM of the type proposed in [5] was studied in [7].

In this thesis OFDM refers exclusively to coherent OFDM of the channel-averaging type. We study OFDM without FEC so that the effects of fading channels on OFDM can be observed without the artifacts of a particular code choice.

1.3 Thesis Contribution

The main contributions of this thesis are listed below:

1. A new matched filter bound for fast flat and frequency-selective Rayleigh fading channels is derived. This bound does not assume that the fading channel remains constant for the duration of a signaling element. It establishes analytic limits for the P_b performance of any receiver for uncoded OFDM, with maximum Doppler rate as a parameter. Arbitrary power levels and correlations between multiple rays due either to delay spread or diversity can be accommodated. Previous results for slow[6] fading Rayleigh channels are special cases of this result.

[5] What we call ISI was also called ICI in [5].

[6] The term *slow* is used to refer to a channel whose characteristics remain approximately constant over an entire symbol interval.

2. An optimal receiver for OFDM on flat Rayleigh fading channels is derived using the principles of maximum likelihood sequence estimation (MLSE). A suboptimal version of the MLSE receiver is introduced to reduce complexity and its performance evaluated by simulation. An approximate analysis of the effects on P_b of a noisy channel estimate is presented and verified by simulation.
3. The theory of equalization as modified for OFDM in flat Rayleigh fading is developed, resulting in the derivation of a new decision feedback equalization (DFE) structure having substantial complexity and performance benefits over the current state of the art. A method is devised for modifying the channel impulse response to a desired impulse response (DIR) which could also be applied to conventional serial modulation schemes.
4. Optimal and suboptimal receivers for OFDM on frequency-selective Rayleigh fading channels based on MLSE and MMSE criteria are derived. The additional complexities of receiver design arising from the presence of delay spread are studied analytically and evaluated by simulation.

1.4 Thesis Organization

In Chapter 2 background material on the land mobile fading channel is presented, and the modeling of flat and frequency-selective Rayleigh fading channels with one and two-ray models is described.

In Chapter 3, matched filter bounds for fast Rayleigh fading channels are presented. The MFB system model for time-varying channels with AWGN is presented in Section 3.2. An analysis to determine P_b is presented in Section 3.3. Section 3.4 extends the results to accommodate K–channel diversity. Examples of the MFB evaluated for flat and frequency-selective Rayleigh fading channels are given in Section 3.5.

In Chapter 4, the MLSE receiver for OFDM in flat Rayleigh fading is derived and evaluated. Section 4.1 describes the transmitter and channel model. Section 4.2 presents

the theoretical derivation of an optimal maximum likelihood receiver, in the sense of sequence estimation. Evaluation of two key parameters, matched filter outputs and tone correlations, by FFTs in a digital implemention and determination of the required sampling rate is examined in Section 4.3. Section 4.4 describes the truncation of the constraint length used by the sequence estimator to make it less complex and Section 4.5 presents a criterion for choosing a non-rectangular pulse shape. Section 4.6 presents simulation results for P_b as a function of E_b/N_0, of BOFDM for a variety of parameters and compares them to the MFBs of Chapter 3. Section 4.7 develops an approximate analysis to predict the effect of using an imperfect channel estimate. Section 4.8 shows a limitation of the truncated MLSE receiver when applied to QOFDM.

In Chapter 5, linear and decision feedback receivers for OFDM in flat Rayleigh fading are derived and evaluated. Section 5.1 derives the optimal linear MMSE equalizer for OFDM in flat Rayleigh fading. Section 5.2 derives a discrete symbol-spaced equalizer, also by the MMSE criterion. Section 5.3 reviews classical DFE as developed for serial modulation and Section 5.4 describes the application of this approach to OFDM in previous work. The idea of reshaping the overall impulse response of the transmitter, channel, and front-end filter[7] to some desired impulse response (DIR) is reviewed in Section 5.5. Section 5.6 derives a DIR DFE based on the zero-forcing criterion (ZFDIRDFE) and in Section 5.7, an improved DIR DFE based on the MMSE criterion (MSEDIRDFE) is derived. The combination of a Viterbi-type sequence estimator in combination with MSEDIR shaping is considered in Section 5.8. A theoretical comparison in terms of MSE performance surfaces for a simplified fading channel model appears in Section 5.9, and simulation results for the receivers are presented in Sections 5.10 and 5.11.

In Chapter 6 some of our previous work for flat fading channels is extended to frequency-selective channels. Receivers for OFDM on frequency-selective Rayleigh

[7] The term *front-end filter* is defined in Section 5.3.

fading channels are derived and evaluated, based on the optimization of MLSE and MMSE performance criteria. Section 6.1 describes the channel modeling. Derivation of optimal and truncated MLSE receivers is presented in Section 6.2. Methods for evaluating matched filter outputs and tone correlations are given in Section 6.2.1, and the effect of pulse shaping on the tone correlations is considered in Section 6.2.2. Performance results obtained by simulation of the MLSE receivers are presented in Section 6.2.3. In Section 6.3 optimal linear MMSE receivers are derived. Direct and alternate implementations are described in Sections 6.3.1 and 6.3.2. Methods for evaluating matched filter outputs and tone correlations are given in Section 6.3.3. The relationship between the integral equation and matrix formulations of the estimation problem is examined in Section 6.3.4, and an efficient matrix formulation for rate N/T_0 sampling is outlined in Section 6.3.5. The performance results obtained by simulation of the MMSE receivers are presented in Section 6.3.6.

In Chapter 7 the conclusions of this thesis are summarized, and some suggestions for future work are presented.

Chapter 2

The Land Mobile Fading Channel

In this chapter background material on the land mobile fading channel is presented, and the modeling of flat and frequency-selective Rayleigh fading channels with one and two-ray models is described.

In the case of the land mobile radio channel there is generally no line of sight path, and the transmitted signal propagates to the vicinity of the receiver over multiple paths via reflection and diffraction. Each of the paths has a potentially different attenuation and delay. Time variations of the multipath channel arise from motion of the receiver which alters the significance of different paths. *Fading* occurs when the receiver moves through an area of destructive interference. The fading is commonly described as either *flat*, meaning that all frequencies in the signaling bandwidth are similarly affected, or *frequency-selective*, meaning that different frequencies may undergo different fading.

Useful characterizations are the coherence time Δt_c, a measure of how long the channel stays approximately constant, and the coherence bandwidth Δf_c, a measure of the bandwidth over which signals spaced in frequency will be similarly affected. Alternatively the Doppler spread and delay spread may be used. The Doppler spread f_D is a measure of the width of the received spectrum when a single sine wave is transmitted through the channel, and the delay spread τ is a measure of the width of the received signal in the time-domain when a single impulse excites the channel. It can be shown [9] that $\Delta t_c \approx 1/f_D$ and $\Delta f_c \approx 1/\tau$.

A rule-of-thumb for categorizing a channel as flat or frequency-selective for a digital signal relates the symbol interval to the rms delay spread [18]. Channels with rms delay spread less than about 10% of the symbol interval are considered flat and conversely those with a greater rms delay spread are considered frequency-selective. This is based

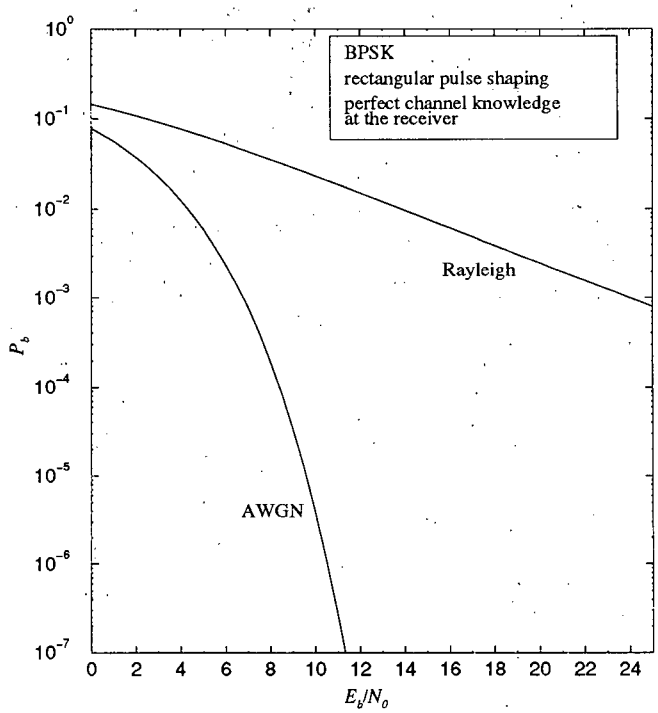

Figure 2.1 BPSK on AWGN and Rayleigh channels

on work which shows $P_b \leq 10^{-3}$ can be obtained without equalization for the channels categorized as flat fading.

Fading can be quite detrimental to the average P_b performance of a standard modulation format as compared to P_b on an AWGN channel. For example, Figure 2.1 compares the P_b of BPSK on an AWGN channel to its P_b on a Rayleigh flat fading channel. At $P_b = 10^{-3}$, a difference of over 17 dB difference is seen.

We will focus on the land mobile radio application with AWGN as the dominant impairment. Although this is somewhat unrealistic in the context of cellular systems which tend to be interference limited, it does provide insight and has the important advantages of being mathematically tractable and broadly understood.

The output of a linear channel with AWGN may be written in terms of its input and impulse response as

$$w(t) = \int z(\sigma, t)s(t - \sigma)d\sigma + n(t) \tag{2.1}$$

where $s(t)$ is the channel input, $n(t)$ is AWGN, and $w(t)$ is the channel output. Equation (2.1) is in terms of the complex lowpass equivalents of bandpass waveforms [9], which are used throughout this thesis. The channel impulse response $z(\sigma, t)$ is defined as the response of the channel at time t to an impulse applied at time $t - \sigma$. In this section, expressions for $z(\sigma, t)$ are sought which model both flat and frequency-selective Rayleigh fading channels. The approach follows that of [9].

The mobile receiver typically receives the transmitted signal as the sum of several attenuated and delayed versions resulting from paths with reflectors and diffractors [3]. The effect of delay on a bandpass signal appears as a delay and phase rotation of its lowpass equivalent [9]. Neglecting noise for the moment, the received signal from a multipath channel is

$$w(t) = \sum_n \alpha_n(t) s(t - \tau_n(t)) e^{-j2\pi f_c \tau_n(t)} \tag{2.2}$$

where f_c is the carrier frequency of the bandpass signal, and $\alpha_n(t)$ and $\tau_n(t)$ are the attenuation and delay of the n^{th} path at time t respectively. Comparing (2.1) and (2.2) it is apparent that

$$z(\sigma, t) = \sum_n \alpha_n(t) e^{-j2\pi f_c \tau_n(t)} \delta(\sigma - \tau_n(t)). \tag{2.3}$$

Equation (2.3) could be written as a general integral expression to accommodate a continuous distribution of paths, but for simplicity we consider mainly one and two-ray models.

Suppose that several of the path delays are closely distributed about a mean delay $\overline{\tau}_1$ and that the remainder of the path delays are closely distributed about $\overline{\tau}_2$. By closely distributed it is meant that the differences in path delays are small relative to a symbol interval.

Writing

$$\begin{aligned} \tau_{n_1}(t) &= \overline{\tau}_1 + \Delta\tau_{n_1}(t) \\ \tau_{n_2}(t) &= \overline{\tau}_2 + \Delta\tau_{n_2}(t) \end{aligned} \tag{2.4}$$

and indexing the paths grouped about $\overline{\tau}_1$ with n_1 and those about $\overline{\tau}_2$ with n_2 we have

$$\begin{aligned} z(\sigma,\tau) = e^{-j2\pi f_c\overline{\tau}_1} \sum_{n_1} \alpha_{n_1}(t) e^{-j2\pi f_c \Delta\tau_{n_1}(t)} \delta(\sigma - \overline{\tau}_1 - \Delta\tau_{n_1}(t)) \\ + e^{-j2\pi f_c\overline{\tau}_2} \sum_{n_2} \alpha_{n_2}(t) e^{-j2\pi f_c \Delta\tau_{n_2}(t)} \delta(\sigma - \overline{\tau}_2 - \Delta\tau_{n_2}(t)) \end{aligned} \tag{2.5}$$

where $\overline{\tau}_1$ is the mean of $\tau_{n_1}(t)$ over n_1 and $\overline{\tau}_2$ is the mean of $\tau_{n_2}(t)$ over n_2 at some arbitrary time within the duration of an OFDM block.

In order to simplify our model, it would be convenient to drop the $\Delta\tau_{n_i}(t)$ terms in (2.5). To ensure this is reasonable, we upper bound the magnitude of $\Delta\tau_{n_i}(t)$.

The geometry which causes the greatest change in delay spread during the reception of an OFDM block is the same as that which causes the maximum Doppler spread: motion of the vehicle directly in line with the direction of arrival of the signal. In this situation the path length will change by vT_0 over the duration of an OFDM block, where T_0 is the duration of an OFDM block. This establishes an upper bound on $|\Delta\tau_{n_i}(t)|$ of $\Delta\tau_{max} = \frac{v}{c}T_0$, where c is the speed of light. Since $\Delta\tau_{max}$ is several orders of magnitude smaller than T_0, $\Delta\tau_{n_i}(t)$ can be dropped from the delta functions in (2.5). However because of the large factor f_c in the complex exponentials, those terms remain. It is assumed that the phase distribution over the paths is uniform and that there are several terms in each of the summations. Setting $\overline{\tau}_1 = 0$ and $\tau = \overline{\tau}_2$, and applying the Central Limit Theorem [19], (2.5) approaches

$$z(\sigma,t) = z_1(t)\delta(\sigma) + e^{-j2\pi f_c\tau} z_2(t)\delta(\sigma - \tau) \tag{2.6}$$

where $z_1(t)$ and $z_2(t)$ are independent complex Gaussian random processes. The exponential rotation factor in (2.6) is a constant; it can be included in the definition of $z_2(t)$ without altering its statistics. Additionally, it is convenient to normalize

$\mathrm{E}\left[|z_1(t)|^2\right] = \mathrm{E}\left[|z_2(t)|^2\right] = 1.0$ and use the explicit factors α_1 and α_2 to indicate the relative strengths of the rays, yielding for our two-ray model

$$z(\sigma, t) = \alpha_1 z_1(t)\delta(\sigma) + \alpha_2 z_2(t)\delta(\sigma - \tau). \tag{2.7}$$

The channel described in (2.7) is in general both time varying and frequency-selective; specialized to a Rayleigh flat fading model it requires only one term

$$z(\sigma, t) = z_1(t)\delta(\sigma). \tag{2.8}$$

Equations (2.7) and (2.8) are widely used for modeling channels with serial modulations. The purpose of outlining their derivations is to ensure that the assumptions leading to their final forms are not invalidated by the extended duration of the OFDM block.

Additional characterizations of Rayleigh fading are derived in [3]. We will find use for both the power density spectrum $\Phi_{z_i}(f)$ and autocorrelation function $\phi_{z_i}(\tau)$ of the process $z_i(t)$. They are

$$\Phi_{z_i}(f) = \frac{1}{2\pi f_D}\left(1 - \left(\frac{f - f_c}{f_D}\right)^2\right)^{-1/2} \tag{2.9}$$

and

$$\phi_{z_i}(\tau) = J_0(2\pi f_D \tau) \tag{2.10}$$

where $J_0(\cdot)$ is the zeroth-order Bessel function of the first kind.

Chapter 3

Matched Filter Bounds for Fast Fading Rayleigh Channels

3.1 Introduction

Many analyses of digital signaling on a Rayleigh fading channel assume that the Doppler rate is small compared to the symbol rate, allowing the channel to be treated as constant for the duration of a single symbol. This chapter presents a matched filter bound (MFB) analysis of BPSK on a Rayleigh fading channel in which the normalized Doppler rate is unrestricted, including the slowly fading model as a special case. It is shown that the optimal matched filter receiver is time varying, and in contrast to matched filter reception on the AWGN or slowly fading channels, it is found that the probability of error depends on the transmitted pulse shape.

Compared to a single carrier modulation of similar bandwidth and bit rate, the duration of an OFDM block period is increased in proportion to the number of carriers used. Previous studies [5], [17] have used simulation to show gains of several dB due to the channel averaging of OFDM on Rayleigh fading channels, where the savings increase with the Doppler rate.

The maximum Doppler rate f_D encountered in land mobile radio systems operating near 900 MHZ is typically about 100 Hz. For a transmission rate $1/T$ of about $10,000$ symbols/sec, the normalized Doppler rate $f_N = f_D T$[8] is on the order of 1%. At such a low rate the channel characteristics may often be treated as constant over a single symbol period. We will refer to channels for which $f_D T \leq 0.01$ as slow fading channels. Conversely, a fast fading channel will be defined as one which changes significantly during a symbol period, i.e. $f_D T > 0.01$. Since OFDM systems may use hundreds of

[8] We are using T as opposed to T_0, because at this point we are not necessarily considering just an OFDM block, but rather any symbol of duration T.

tones, an analysis applicable to fast fading is required. For OFDM systems having up to 512 tones we are interested in a normalized Doppler rate in the range $0 < f_N < 5.12$. As a first step, this work considers the transmission of a single pulse over fast fading Rayleigh channels of *arbitrary* normalized Doppler rate, where it is assumed that the receiver is a matched filter with perfect channel state information. The resulting error rate gives the Matched Filter Bound [20].

Although developed in terms of a matched filter bound, the results presented for cases of zero delay spread are equivalent to a probability of bit error (P_b) analysis for continuous BPSK signaling with perfect channel state information available at the receiver.

The analysis also allows for delay spreads due to multiple rays and K channel diversity, where the correlations between rays and between channels are arbitrary and each channel may have a different impulse response.

While previous works [20], [21] with the slow fading Rayleigh channel have considered delay spread and channel diversity, the extension to arbitrary Doppler rates as well as the examination of correlations and differing impulse responses, are believed to be new contributions.

3.2 System Model

Figure 3.1 shows the system model in terms of the complex baseband equivalents of passband signals. Although we consider BPSK modulation for simplicity, our method is valid for any pulse amplitude modulated (PAM) scheme with minor modifications. The modulator sends a single pulse $+Ap(t)$ over a Rayleigh fading channel whose complex impulse response is given by $z(\sigma, t)$, which denotes the response of the channel at time t to an impulse applied at time $t - \sigma$ [9]. The pulse $p(t)$ has duration T_0 and unit energy, therefore the energy per bit E_b is A^2. The real and imaginary components of $z(\sigma, t)$ are independent zero-mean Gaussian processes of identical variances, and the maximum

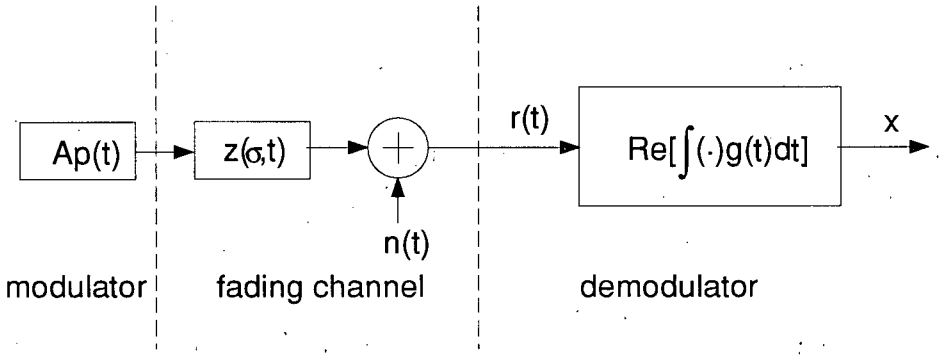

Figure 3.1 System Model

delay spread is τ_{max}. We assume that $z(\sigma, t)$ is wide-sense stationary so that we may use its autocorrelation function defined as

$$\phi_z(\sigma_a, \sigma_b; t_a - t_b) = E[z(\sigma_a, t_a)z^*(\sigma_b, t_b)]. \tag{3.2.1}$$

The received signal is given by

$$r(t) = A \int_0^{\tau_{max}} z(\sigma, t)p(t - \sigma)d\sigma + n(t) \tag{3.2.2}$$

where $n(t)$ is zero-mean complex AWGN of variance $\sigma_n^2 = N_o$. The receiver uses $r(t)$ to form the decision variable

$$x = \mathrm{Re}\left[\int r(t)g(t)dt\right] \tag{3.2.3}$$

where $g(t)$ is the pulse shape used in the receiver's correlator, and the integration is performed over the interval for which $g(t)$ is nonzero.

3.3 Analysis

Denoting the signal component of x by

$$y = \mathrm{Re}\left[\int \int_0^{\tau_{max}} z(\sigma, t)p(t - \sigma)d\sigma\ g(t)dt\right] \tag{3.3.1}$$

and the noise component by

$$n_1 = \mathrm{Re}\left[\int n(t)g(t)dt\right] \tag{3.3.2}$$

we have

$$x = Ay + n_1. \tag{3.3.3}$$

Given $g(t)$, n_1 is a zero-mean Gaussian random variable with variance

$$\sigma_{n_1}^2 = \frac{N_o}{2}\int |g(t)|^2 dt. \tag{3.3.4}$$

The probability density function (*pdf*) of x conditioned on y is Gaussian with mean Ay,

$$p_x(x \mid y) = \frac{1}{\sqrt{2\pi}\sigma_{n_1}} e^{\frac{-(x-Ay)^2}{2\sigma_{n_1}^2}}. \tag{3.3.5}$$

The probability P_c of a correct decision is the probability that x is greater than zero

$$P_c = \int_0^\infty \int_{-\infty}^\infty \frac{1}{\sqrt{2\pi}\sigma_{n_1}} e^{\frac{-(x-Ay)^2}{2\sigma_{n_1}^2}} p_y(y)dy\, dx. \tag{3.3.6}$$

Changing the order of integration and recognizing the error function

$$\mathrm{erf}(x) = \frac{2}{\sqrt{\pi}}\int_0^x e^{-t^2} dt \tag{3.3.7}$$

we have for the probability of bit error

$$P_b = \frac{1}{2} - \frac{1}{2}\int_{-\infty}^\infty \mathrm{erf}\left(\sqrt{\frac{A^2y^2}{2\sigma_{n_1}^2}}\right) p_y(y)dy. \tag{3.3.8}$$

To proceed further we must specify the pulse shape $g(t)$ used in the demodulator correlator. It is well known [9] that the optimal demodulator for a pulse transmitted on a nonfading AWGN channel is a matched filter demodulator, where the demodulator filter is matched to the transmitted pulse shape. From the receiver's viewpoint, we observe

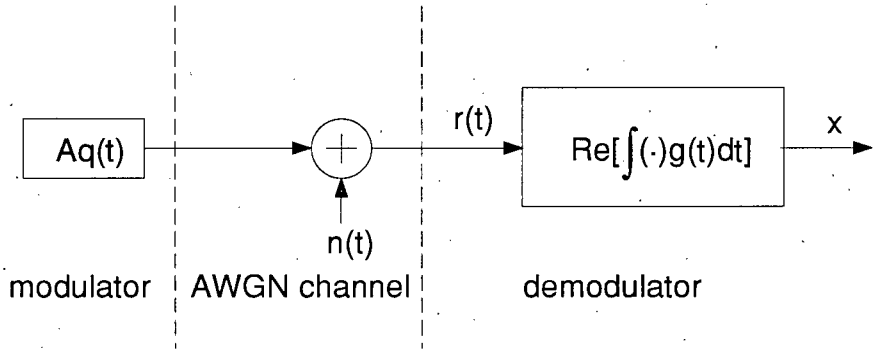

Figure 3.2 Equivalent system in terms of an AWGN channel

that the fixed-shape pulse $Ap(t)$ entering the fading channel of Figure 3.1 is equivalent to a time varying transmit pulse, $Aq(t) = A\int_0^{\tau_{max}} z(\sigma,t)p(t-\sigma)d\sigma$, entering a nonfading AWGN channel as shown in Figure 3.2. Then it is clear that the optimal receive correlator pulse *shape* is also time varying, $g(t) = \int_0^{\tau_{max}} z^*(\sigma,t)p^*(t-\sigma)d\sigma$.

For the matched filter case (3.3.1) and (3.3.2) become

$$\begin{aligned} y &= \int \left| \int_0^{\tau_{max}} z(\sigma,t)p(t-\sigma)d\sigma \right|^2 dt \\ &= \int |q(t)|^2 dt \end{aligned} \tag{3.3.9}$$

and

$$n_1 = \mathrm{Re}\left[\int n(t) \int_0^{\tau_{max}} z^*(\sigma,t)p^*(t-\sigma)d\sigma \, dt \right], \tag{3.3.10}$$

where the noise variance is

$$\sigma_{n_1}^2 = \frac{N_o}{2} y. \tag{3.3.11}$$

Note that the variance $\sigma_{n_1}^2$ is itself a random variable. The expression for P_b in (3.3.8) can be written as

$$P_b = \frac{1}{2} - \frac{1}{2}\int_0^{\infty} \mathrm{erf}\left(\sqrt{\frac{E_b y}{N_o}}\right) p_y(y)dy. \tag{3.3.12}$$

Since y is nonnegative from (3.3.9), the lower limit in the integral has been replaced by 0.

We will refer to E_b/N_o as the transmitted signal to noise ratio (SNR). The quantity $E_b y/N_o$ is the received SNR at the output of the matched filter, shown with its equivalent implementation as a matched correlator in Figure 3.2. Equation (3.3.12) states that the P_b for our analysis is given by the average over all received SNRs of the P_b for a static AWGN channel. This expression has the same general form as that which results from a slow fading analysis [9], except that the *pdf* of y is harder to obtain. The effects of fast fading, correlations, and diversity are reflected solely in how they affect the *pdf* of y.

The average received SNR is given by $\gamma_{br} = E[y]E_b/N_o$. Taking the expectation of (3.3.9) yields

$$\mathrm{E}[y] = \int_0^{\tau_{max}} \int_0^{\tau_{max}} \phi_z(\sigma_a, \sigma_b; 0) p(t-\sigma_a) p^*(t-\sigma_b) d\sigma_a d\sigma_b dt. \tag{3.3.13}$$

Using the autocorrelation function of the pulse $p(t)$

$$f(\sigma_b - \sigma_a) = \int p(t-\sigma_a) p^*(t-\sigma_b) dt \tag{3.3.14}$$

we have

$$\mathrm{E}[y] = \int_0^{\tau_{max}} \int_0^{\tau_{max}} \phi_z(\sigma_a, \sigma_b; 0) f(\sigma_b - \sigma_a) d\sigma_a d\sigma_b. \tag{3.3.15}$$

Equation (3.3.15) will be used to obtain more specific results in Section 3.5.

To derive the *pdf* of y, we approximate (3.3.9) arbitrarily closely using a finite summation

$$y = \Delta t \sum_{i=1}^{M} |q_i|^2 \tag{3.3.16}$$

where $q_i = q\big((i-\frac{1}{2})\Delta t\big)$ and $M = \left\lfloor \frac{T_0(1+\alpha)+\tau_{max}}{\Delta t} \right\rfloor$[9]. The $|q_i|^2$ are correlated random variables with a chi-squared degree 2 *pdf*. Defining the vector $\mathbf{q}^{\mathrm{H}} = \sqrt{\Delta t}[q_1^*, q_2^*, \ldots, q_M^*]$ (3.3.16) can be written as

$$y = \mathbf{q}^{\mathrm{H}}\mathbf{q}. \tag{3.3.17}$$

[9] $\lfloor \cdot \rfloor$ means the integer part of.

To obtain an expression for y as a sum of uncorrelated random variables, we apply a discrete version of the Karhunen-Loeve [22] expansion to $\mathbf{q}$ as

$$\mathbf{q}^{\mathrm{H}} = \mathbf{u}^{\mathrm{H}}\sqrt{\mathbf{\Lambda}}\mathbf{P}^{\mathrm{H}} \tag{3.3.18}$$

where

$$\mathbf{u}^{\mathrm{H}} = [u_1^*, u_2^*, \ldots, u_M^*], \quad \mathrm{E}\left[\mathbf{u}\mathbf{u}^{\mathrm{H}}\right] = \mathbf{I} \tag{3.3.19}$$

$$\mathbf{\Lambda} = \mathrm{diag}(\lambda_1, \lambda_2, \ldots, \lambda_M) \tag{3.3.20}$$

and

$$\mathbf{P} = [\mathbf{p_1}, \mathbf{p_2}, \ldots, \mathbf{p_M}], \quad \mathbf{P}^{\mathrm{H}}\mathbf{P} = \mathrm{I}. \tag{3.3.21}$$

Defining the Hermitian matrix

$$\mathbf{Q} = \mathrm{E}\left[\mathbf{q}\mathbf{q}^{\mathrm{H}}\right] = \mathbf{P}\mathbf{\Lambda}\mathbf{P}^{\mathrm{H}} \tag{3.3.22}$$

the $\lambda_i's$ are recognized as the eigenvalues of $\mathbf{Q}$ and are also real and nonnegative [23]. We have for the $(n,m)^{th}$ element of $\mathbf{Q}$

$$\mathbf{Q}_{\mathrm{n,m}} = \Delta t \int_0^{\tau_{max}} \int_0^{\tau_{max}} \phi_z(\sigma_a, \sigma_b; (n-m)\Delta t) p(n'\Delta t - \sigma_a) p^*(m'\Delta t - \sigma_b) d\sigma_a d\sigma_b \tag{3.3.23}$$

where $n' = n - 1/2$, $m' = m - 1/2$ and $1 \leq n, m \leq M$.

Using (3.3.18) in (3.3.17) we can write y as a weighted sum of independent chi-squared random variables of degree 2

$$y = \sum_{i=1}^{R} \lambda_i |u(i)|^2 \tag{3.3.24}$$

where R is the number of nonzero eigenvalues of $\mathbf{Q}$, which is equal to its rank.

Equation (3.3.24) indicates that the characteristic function of y , $\Phi_y(v)$, expressed in terms of the characteristic function of $|u_i|^2$, $\Phi_{|u_i|^2}(v)$, is

$$\Phi_y(v) = \prod_{i=1}^{R} \Phi_{|u_i|^2}(\lambda_i v). \tag{3.3.25}$$

The characteristic function for degree 2 chi-squared random variables is given in [9] as

$$\Phi_{|u_i|^2}(v) = \frac{1}{(1 - j2v\sigma_r^2)} \tag{3.3.26}$$

where we set $\sigma_r^2 = 1/2$ in order to normalize $\mathrm{E}\left[|u_i|^2\right] = 1$.

The simple form of $\Phi_{|u_i|^2}(v)$ allows the *pdf* of y to be found analytically. Combining (3.3.25) and (3.3.26)

$$\Phi_y(v) = \prod_{i=1}^{R} \frac{1}{1 - j\lambda_i v}. \tag{3.3.27}$$

Equation (3.3.27) may be rewritten using a partial fraction expansion [24] as

$$\Phi_y(v) = \sum_{i=1}^{D} \sum_{k=1}^{n_i} \frac{A_{ik}}{(1 - j\lambda_i v)^k} \tag{3.3.28}$$

where the constants A_{ik} are given by

$$A_{ik} = \frac{1}{(n_i - k)!(-j\lambda_i)^{n_i - k}} \left[\frac{d^{n_i - k}}{dv^{n_i - k}} (1 - j\lambda_i v)^{n_i} \Phi_y(jv) \right]_{v = \frac{1}{j\lambda_i}}. \tag{3.3.29}$$

D is the number of distinct $\lambda_i's$, n_i is the order of λ_i. Equation (3.3.28) is easily inverted by recognizing the inverses of its individual terms as

$$\text{Inverse}\left\{ \frac{A_{ik}}{(1 - j\lambda_i v)^k} \right\} = \begin{cases} \frac{A_{ik}}{(k-1)!\lambda_i^k} y^{k-1} e^{-y/\lambda_i}, & y \geq 0 \\ 0, & \text{otherwise.} \end{cases} \tag{3.3.30}$$

The *pdf* of y is then

$$p_y(y) = \begin{cases} \sum_{i=1}^{D} \sum_{k=1}^{n_i} \frac{A_{ik}}{(k-1)!\lambda_i^k} y^{k-1} e^{-y/\lambda_i}, & y \geq 0 \\ 0, & \text{otherwise} \end{cases} \tag{3.3.31}$$

and combining with (3.3.12) for P_b yields

$$P_b = \frac{1}{2} - \frac{1}{2} \sum_{i=1}^{R} \sum_{k=1}^{n_i} \frac{A_{ik}}{(k-1)!\lambda_i^k} \int_0^\infty \mathrm{erf}\left(\sqrt{\frac{E_b y}{N_0}} \right) y^{k-1} e^{-y/\lambda_i} dy. \tag{3.3.32}$$

The integral in (3.3.32) is evaluated in Appendix A.1. The resulting expression for P_b is

$$P_b = \frac{1}{2} - \frac{1}{2}\sum_{i=1}^{R}\sum_{k=1}^{n_i} A_{ik} \sum_{l=0}^{k-1} \frac{(2l-1)!!}{(2l)!!}\sqrt{\frac{\lambda_i E_b/N_o}{(\lambda_i E_b/N_o + 1)^{2l+1}}} \quad . \tag{3.3.33}$$

An expression having the same form as (3.3.33) was given in [21] for diversity reception on slowly fading channels. However, the formulation in [21] does not allow the fast fading channel case to be studied. In contrast, our model includes an arbitrary Doppler frequency as a parameter.

3.4 Extension to K-Channel Diversity

We can extend our technique for deriving the λ_i's to include K-channel space, frequency or time diversity reception by considering the channel impulse response $z(\sigma, t)$ in (3.3.9) to be the concatenation in σ of the K diversity channel impulse responses, which may in general be correlated. The vector $\mathbf{q}$ becomes the concatenation of vectors $\mathbf{q_i}$

$$\mathbf{q}^{\mathrm{H}} = \left[\mathbf{q}_1^{\mathrm{H}}, \mathbf{q}_2^{\mathrm{H}}, \ldots, \mathbf{q}_{\mathrm{K}}^{\mathrm{H}}\right], \tag{3.4.1}$$

where $\mathbf{q_i}$ is due to the i^{th} channel impulse response and where the k^{th} element of $\mathbf{q}_i^{\mathrm{H}}$ is

$$\mathbf{q}_{\mathrm{i_k}}^{*} = \int_0^{\tau_{max_i}} z_i^*\left(\sigma, \left(k - \frac{1}{2}\right)\Delta t\right) p^*\left(\left(k - \frac{1}{2}\right)\Delta t - \sigma\right) d\sigma. \tag{3.4.2}$$

Defining the matrices

$$\mathbf{Q_{ik}} = \mathrm{E}\left[\mathbf{q_i}\mathbf{q}_{\mathrm{k}}^{\mathrm{H}}\right] \tag{3.4.3}$$

we have

$$\mathbf{Q} = \begin{bmatrix} \mathbf{Q_{11}} & \mathbf{Q_{12}} & \cdots & \mathbf{Q_{1K}} \\ \mathbf{Q_{21}} & \mathbf{Q_{22}} & \cdots & \mathbf{Q_{2K}} \\ \vdots & \vdots & \cdots & \vdots \\ \mathbf{Q_{K1}} & \mathbf{Q_{K2}} & \cdots & \mathbf{Q_{KK}} \end{bmatrix}. \tag{3.4.4}$$

When the impulse responses of the different channels are uncorrelated, $\mathbf{Q}$ simplifies to a block diagonal matrix

$$\mathbf{Q}' = \begin{bmatrix} \mathbf{Q_{11}} & \mathbf{0} & .. & \mathbf{0} \\ \mathbf{0} & \mathbf{Q_{22}} & .. & \mathbf{0} \\ : & : & .. & : \\ \mathbf{0} & \mathbf{0} & .. & \mathbf{Q_{KK}} \end{bmatrix}. \tag{3.4.5}$$

It is easily shown that the matrix of eigenvalues of $\mathbf{Q}'$ is

$$\mathbf{\Lambda}' = \begin{bmatrix} \mathbf{\Lambda_{11}} & \mathbf{0} & .. & \mathbf{0} \\ \mathbf{0} & \mathbf{\Lambda_{22}} & .. & \mathbf{0} \\ : & : & .. & : \\ \mathbf{0} & \mathbf{0} & .. & \mathbf{\Lambda_{KK}} \end{bmatrix} \tag{3.4.6}$$

where $\mathbf{\Lambda_{ii}}$ is the diagonal matrix having as its elements the eigenvalues of $\mathbf{Q_{ii}}$. Thus the eigenvalues of $\mathbf{Q}'$ can be found by finding the eigenvalues of the smaller matrices $\mathbf{Q_{ii}}$, $1 \leq i \leq K$ independently. If we further assume that all diversity channels have the same autocorrelation function, then we need only find the eigenvalues of $\mathbf{Q_{11}}$, since the eigenvalues of $\mathbf{Q}'$ will be those of $\mathbf{Q_{11}}$, but with their orders increased by a factor of K.

3.5 Some MFB Results

3.5.1 Flat Rayleigh Fading

In flat Rayleigh fading there may be a fixed distortion of the power spectral density of the received signal, but during fades all frequency components are attenuated and phase shifted equally. This implies that the channel's impulse response is separable in the delay and time variables. In the simplest case, there is no fixed distortion and the channel's impulse response and autocorrelation function may be written as

$$\begin{aligned} z(\sigma, t) &= \delta(\sigma) z_1(t) \\ \phi_z(\sigma_a, \sigma_b; t_a - t_b) &= \delta(\sigma_a)\delta(\sigma_b)\phi_{z_1}(t_a - t_b). \end{aligned} \tag{3.5.1}$$

We will use the channel model of (3.5.1) to see how P_b is affected by the normalized Doppler rate f_N, transmitted SNR, and pulse shape in flat Rayleigh fading. We begin by considering the limiting cases of very slow ($f_N \to 0^+$) and very fast ($f_N \to \infty$) fading.

It has been shown [3] that the channel autocorrelation function for a mobile whip antenna moving through a field with isotropic scattering is given by

$$\phi_z((n-m)\Delta t) = J_0(\omega_D(n-m)\Delta t) \tag{3.5.2}$$

where $J_0(x)$ is a zeroth order Bessel function and $w_D = 2\pi f_D$ is the maximum Doppler frequency in radians. For this case the elements of the matrix $\mathbf{Q}$ as given by (3.3.23) simplify to

$$\mathbf{Q}_{\mathrm{n,m}} = \Delta t J_0(\omega_D(n-m)\Delta t)p(n'\Delta t)p^*(m'\Delta t). \tag{3.5.3}$$

For very slow fading, $J_0(w_D(n-m)\Delta t)$ in (3.5.3) is essentially constant, and so $\mathbf{Q}$ has only a single eigenvalue, which is $\lambda_0 = 1.0$. This follows from using (3.3.15) with (3.5.1) to show that $E[y] = f(0)\phi_{z_1}(0) = 1.0$. The pulse shape has no effect on the P_b since it does not influence λ_0. The P_b is given by the $R = 1$, $n_1 = 1$ case of (3.3.33), i.e.

$$P_b = \frac{1}{2} - \frac{1}{2}\sqrt{\frac{E_b/N_o}{E_b/N_o + 1}} \tag{3.5.4}$$

as is well known [9].

At the opposite extreme as $f_N \to \infty$ it can be shown (Appendix A.2) that the variance σ_y^2 approaches 0 for any unit energy pulse. Ultimately as $\sigma_y^2 \to 0$, the *pdf* of y becomes a delta function at $E[y] = 1.0$, i.e.

$$\lim_{f_N \to \infty} p(y) = \delta(y - 1.0). \tag{3.5.5}$$

Using this in (3.3.12) we find

$$\lim_{f_N \to \infty} P_b = \frac{1}{2} - \frac{1}{2}\,\mathrm{erf}\left(\sqrt{E_b/N_o}\right). \tag{3.5.6}$$

The P_b expression given by (3.5.6) is identical to that for BPSK signaling on a nonfading AWGN channel, as might be expected. Thus the use of an extremely long (relative to the

coherence time of the channel) signaling pulse of arbitrary shape has essentially made the fading channel look like a nonfading channel.

Between these extremes we might suspect that the pulse shape would be significant since the effective channel averaging or variance of y depends on the pulse shape. The matrix $\mathbf{Q}$ given by (3.5.3) was calculated for different pulse shapes, and for a range of normalized Doppler rates f_N and E_b/N_o values. The pulse shapes chosen were a rect pulse defined as

$$p_r(t) = \begin{cases} \frac{1}{\sqrt{T_0}}, & 0 \le t \le T_0 \\ 0, & \text{otherwise} \end{cases}, \tag{3.5.7}$$

a half sin pulse defined as

$$p_s(t) = \begin{cases} \sqrt{2/T}\ \sin(\pi t/T_0), & 0 \le t \le T_0 \\ 0, & \text{otherwise} \end{cases} \tag{3.5.8}$$

and the root raised cosine pulse given previously in (1.1.4) as

$$\begin{aligned} p(t) &= \sqrt{p_{sq}(t)}, \\ p_{sq}(t) &= \begin{cases} \frac{1}{2T_0}\left(1+\cos\left(\frac{\pi(t-\alpha T_0)}{\alpha T_0}\right)\right), & 0 \le t < \alpha T_0 \\ 1/T_0, & \alpha T_0 \le t \le T_0 \\ \frac{1}{2T_0}\left(1+\cos\left(\frac{\pi(t-T_0)}{\alpha T_0}\right)\right), & T_0 < t \le T_0(1+\alpha) \\ 0, & \text{otherwise.} \end{cases} \end{aligned} \tag{3.5.9}$$

A computer package [25] was used to find the eigenvalues resulting from each combination of pulse shape and normalized Doppler rate. In every case all R eigenvalues were found to be distinct, so that (3.3.29) and (3.3.33) simplify to

$$P_b = \begin{cases} \frac{1}{2} - \frac{1}{2}\sqrt{\frac{E_b/N_o}{E_b/N_o+1}}, & R = 1 \\ \frac{1}{2} - \frac{1}{2}\sum_{i=1}^{R}\prod_{\substack{l=1 \\ l\neq i}}^{R}\frac{\lambda_i}{\lambda_i-\lambda_l}\sqrt{\frac{\lambda_i E_b/N_o}{\lambda_i E_b/N_o+1}}, & R \ge 2. \end{cases} \tag{3.5.10}$$

Figure 3.3 shows the P_b curves for the rect pulse shape in solid lines for a range of normalized Doppler rates up to 5.12. A couple of curves for the half sin pulse shape are shown in dashed lines for comparison. The curve for the limiting case of very fast

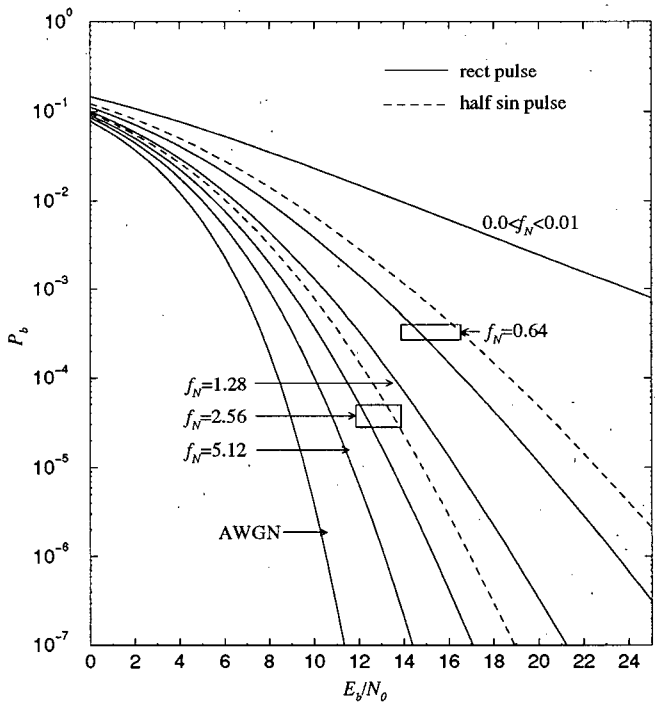

Figure 3.3 Effect of normalized Doppler rate and pulse shape for fast flat Rayleigh fading

fading ($f_N \to \infty$) is also shown. As noted previously, this curve is identical to the P_b curve for BPSK optimally received on a nonfading AWGN channel. For $P_b < 0.1$, substantial improvements over the slowly fading case of several dB are seen for all the curves presented. Below $P_b = 10^{-2}$, at least half of the achievable gain is obtained by increasing the pulse duration such that the normalized Doppler rate is 0.64 for the rect pulse or 1.28 for the sin pulse. Above these rates diminishing returns are clearly shown. Each succeeding curve corresponds to a doubling of the normalized Doppler rate, but the incremental improvement decreases with each curve. At $P_b = 10^{-2}$, both pulse shapes are within approximately 1 dB of nonfading AWGN channel performance, for $f_N \geq 5.12$. For finite positive values of f_N, the P_b for the half sin pulse is worse than that for the rect pulse, due to its inferior channel averaging.

Figure 3.4 shows the effect of varying the rolloff parameter α for the root raised cosine pulse defined by (3.5.9) at $f_N = 0.32$ and $f_N = 1.28$. There is very little change

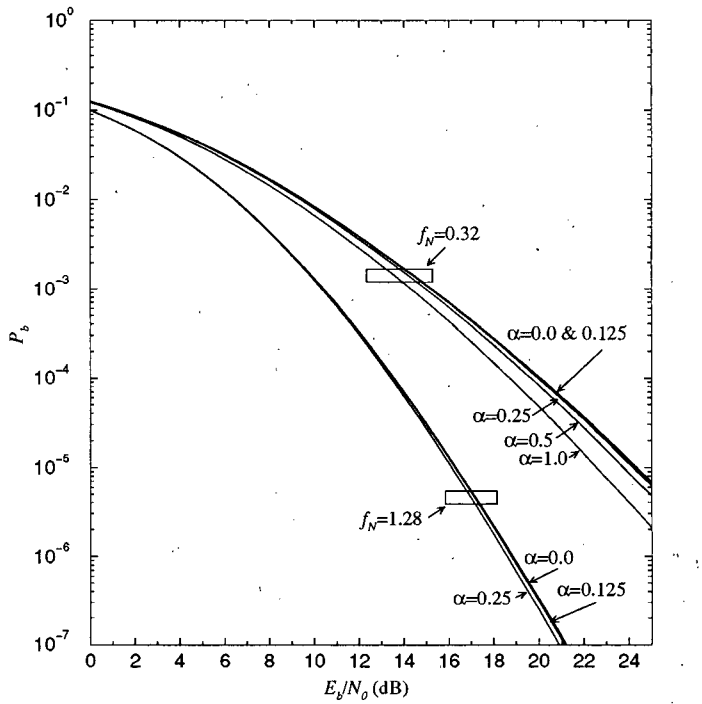

Figure 3.4 Effect of rolloff on P_b

in the curves for $\alpha \leq 0.25$, curves for $\alpha \leq 0.125$ are practically coincident over much of the graph's range. For $\alpha \geq 0.5$ loss in channel averaging ability is more significant. These curves indicate the tradeoff between pulse smoothing and channel averaging which is an important consideration in Chapter 6.

3.5.2 Frequency-Selective Rayleigh Fading

In frequency-selective Rayleigh fading the fading at different frequencies of the power density spectrum is not completely correlated. This implies a significant delay spread compared to the pulse duration. A common example [20] is when the transmitted pulse and a delayed version arrive at the receiver after having travelled over different fading paths. We model this channel impulse response with

$$z(\sigma, t) = \alpha_1 \delta(\sigma) z_1(t) + \alpha_2 \delta(\sigma - \tau) z_2(t) \tag{3.5.11}$$

where $\tau_1 = 0$ and $\tau = \tau_2 - \tau_1$. Its autocorrelation function is

$$\begin{aligned}\phi_z(\sigma_a, \sigma_b; t_a - t_b) = {} & \alpha_1^2 \delta(\sigma_a)\delta(\sigma_b)\phi_{z_1}(t_a - t_b) \\ & + \alpha_1\alpha_2\delta(\sigma_a)\delta(\sigma_b - \tau)\phi_{z_1 z_2}(t_a - t_b) \\ & + \alpha_1\alpha_2\delta(\sigma_a - \tau)\delta(\sigma_b)\phi_{z_2 z_1}(t_a - t_b) \\ & + \alpha_2^2\delta(\sigma_a - \tau)\delta(\sigma_b - \tau)\phi_{z_2}(t_a - t_b).\end{aligned} \tag{3.5.12}$$

We would like to consider the general case where the processes $z_1(t)$ and $z_2(t)$ may be correlated. To facilitate comparison with the flat Rayleigh fading case, we assume that they each have the same, to within a constant, autocorrelation function as used in the one-ray case

$$\phi_{z_1}((n-m)\Delta t) = \phi_{z_2}((n-m)\Delta t) = J_0(\omega_D(n-m)\Delta t) \tag{3.5.13}$$

and

$$\phi_{z_1 z_2}((n-m)\Delta t) = \rho J_0(\omega_D(n-m)\Delta t) \tag{3.5.14}$$

where ρ is a normalized cross-correlation coefficient having $|\rho| \leq 1$. The elements of $\mathbf{Q}$ for this case are

$$\begin{aligned}\mathbf{Q}_{\mathrm{n,m}} = {} & \Delta t J_0(\omega_D(n-m)\Delta t)\big[p(n'\Delta t)p^*(m'\Delta t) \\ & + \alpha\rho p(n'\Delta t)p^*(m'\Delta t - \tau) \\ & + \alpha\rho^* p(n'\Delta t - \tau)p^*(m'\Delta t) \\ & + \big[\alpha^2 p(n'\Delta t - \tau)p^*(m'\Delta t - \tau)\big].\end{aligned} \tag{3.5.15}$$

Normalization

Evaluating (3.3.15) for our two-ray model we obtain

$$\begin{aligned} \mathrm{E}[y] &= \phi_{z_1}(0)\big((\alpha_1^2+\alpha_2^2)f(0) + 2\alpha_1\alpha_2\mathrm{Re}[\rho f(\tau)]\big) \\ &= 1 + 2\alpha_1\alpha_2\mathrm{Re}[\rho f(\tau)] \end{aligned} \tag{3.5.16}$$

assuming $\alpha_1^2 + \alpha_2^2 = 1.0$.

Assuming for the moment that both rays have equal power we see that the average received SNR γ_{br} depends on the correlation between the rays and the amount of pulse overlap, and different combinations can yield the same γ_{br}. Thus there are several plausible ways for comparing P_e plots. If diversity occurs because extra antennas are being added at the receiver then it might be appropriate to have γ_{br} increase with each additional ray received. On the other hand, if we have a fixed amount of total power to radiate and want to compare the merits of sending it with or without diversity then it would likely be more insightful to assume the power per ray is reduced as the number of diversity channels is increased. A third option is to compare on the basis of a constant γ_{br}.

The choice made in producing Figures 3.5 and 3.6 is to assume that each of the two rays has a variance of $\alpha_1^2 = \alpha_2^2 = 1/2$ and this remains fixed independently of how the correlation and pulse overlap are varied. This makes two independently faded pulses with 100% overlap equivalent to the transmission of a single pulse. To limit the number of curves presented, the relative attenuation factor, α_2/α_1, between the two rays was not varied.

Two-ray slow Rayleigh fading

Figure 3.5 shows some P_b curves for two-ray slow Rayleigh fading for several combinations of the normalized delay spread τ and normalized correlation ρ between rays. The results for independent rays are the same as those in [20], while the results for nonzero ρ are new. A rect pulse shape was used in the calculation of **Q** by (3.5.15). The two

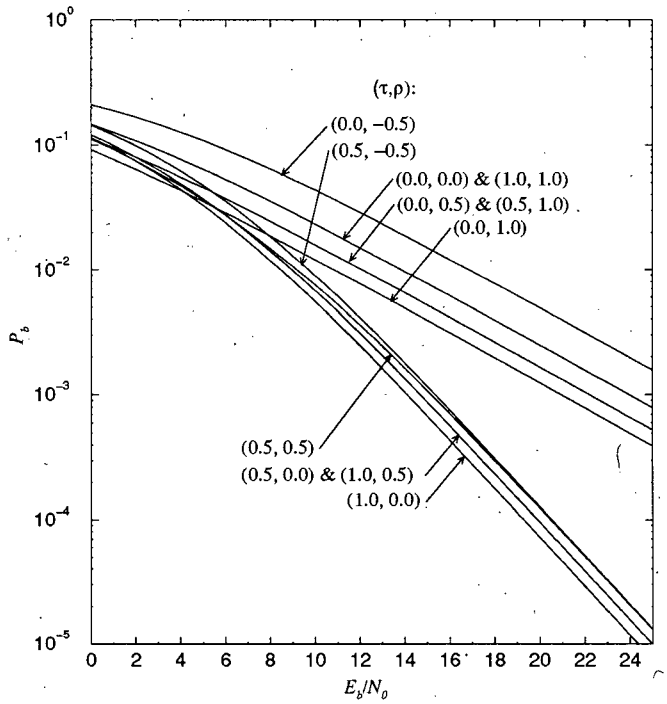

Figure 3.5 Effect of delay spread and correlation between rays, for two-ray very slow Rayleigh fading.

coincident curves with $(\tau, \rho) = (0.0, 0.0)$ & $(1.0, 1.0)$ are equivalent to the transmission of a single pulse on a single ray with the same E_b/N_o and have the poorest performance for $\rho \geq 0.0$. Several connections between τ and ρ are apparent. For the cases where $\rho = 1$, the greater the overlap of the received pulses the better the performance, but the maximum difference is only 3 dB. For the $\rho = 0$ cases, the better performance occurs with smaller overlap and the dB advantage can be significantly greater depending on the point of comparison, for example > 9.5 dB at $P_b = 10^{-3}$. The reasons for the gain occurring in each case are also different. In the former, the gain occurs because the noise added to each pulse is independent and so combines noncoherently, but the pulse components are able to combine coherently. In the latter case, the gain occurs because of the more important effect of diversity, where it is unlikely that both pulses fade simultaneously.

For intermediate values of ray correlation there ought to be some point where the gains and losses due to overlap oppose each other and the trend is not so clear, but as the curves show, most of the gain obtainable is achieved even for values of (τ, ρ) as high as $(0.5, 0.5)$. Additionally, each (τ, ρ) pair is seen to have a dual in the sense that there is more than one (τ, ρ) combination that produces the same curve. The **Q** matrices produced by the duals are generally different but their eigenvalues are of course identical. For $\rho \geq 0$ the dual to (τ, ρ) is given by $(1-\rho, 1-\tau)$. The combinations $(0.0, 1.0)$, $(1.0, 0.0)$ and $(0.5, 0.5)$ are their own duals.

The P_b curves were calculated by (3.5.10) except when $(\tau, \rho) = (1.0, 0.0)$. This is equivalent to diversity with two independent channels as described in Section 3.4. Therefore there are $R/2$ distinct eigenvalues of order 2. In this case (3.3.33) simplifies to

$$P_b = \frac{1}{2} - \frac{1}{2}\sum_{i=1}^{\frac{R}{2}} \left[(A_{i1} + A_{i2}) \sqrt{\frac{\lambda_i E_b/N_0}{\lambda_i E_b/N_0 + 1}} + \frac{1}{2} A_{i2} \sqrt{\frac{\lambda_i E_b/N_0}{(\lambda_i E_b/N_0 + 1)^3}} \right] \tag{3.5.17}$$

where

$$\begin{aligned} A_{i1} &= -\frac{1}{\lambda_i} \sum_{\substack{n=1 \\ n \neq i}}^{\frac{R}{2}} \frac{2\lambda_n}{(1 - \lambda_n/\lambda_i)^3} \prod_{\substack{l=0 \\ l \neq i,n}}^{\frac{R}{2}-1} \frac{1}{(1 - \lambda_l/\lambda_i)^2} \\ A_{i2} &= \prod_{\substack{l=0 \\ l \neq i}}^{\frac{R}{2}-1} \frac{1}{(1 - \lambda_i/\lambda_l)^2}. \end{aligned} \tag{3.5.18}$$

Two-ray fast Rayleigh fading

Figure 3.6 shows several P_b curves at a normalized Doppler rate of $f_N = 0.64$ for two-ray fast Rayleigh fading for several combinations of the normalized delay spread τ and normalized correlation ρ between rays. The variations of P_b with (τ, ρ) are similar to the slow fading case except the correlation between rays seems less important. Comparing the cases for $\tau = 1.0$ in Figure 3.6 with those of Figure 3.5 for slow fading, the dB spread is seen to be much reduced. This is because in slow fading the only source of diversity

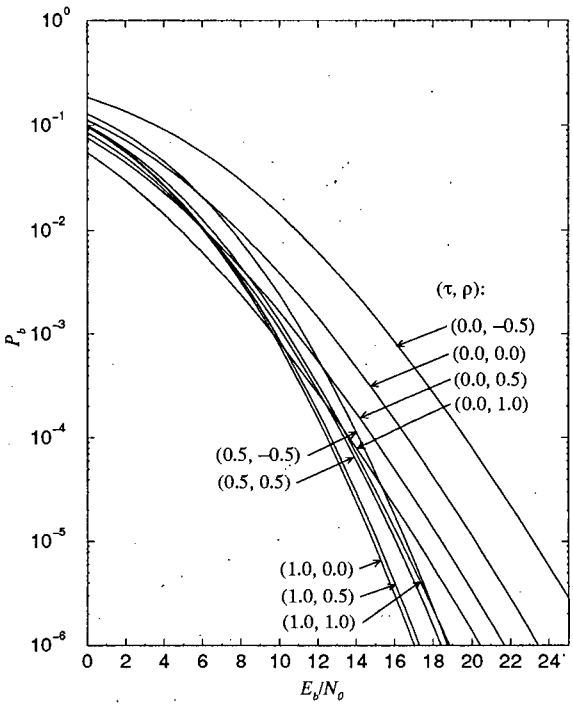

Figure 3.6 Effect of delay spread and correlation between rays, for two-ray fast Rayleigh fading. Normalized Doppler rate = 0.64.

is the extent of the two rays' independence, while in fast fading there is diversity within a single pulse.

3.6 Conclusion

A matched filter bound analysis was presented for BPSK signaling on fast Rayleigh fading channels. The effects of delay spread and correlation between the fading processes for multipath reception were included in the analysis, and several examples given.

The bit error rate performance was shown to improve with increasing f_N[10], eventually approaching the performance of BPSK on the nonfading AWGN channel. This result does not depend on the specific pulse shape. For $P_b = 10^{-2}$ and $f_N = 5.12$, the E_b/N_o

[10] This is consistent with previous work.

required is within 1 dB of that required on a nonfading channel for both the rect and half sin pulse shapes.

In contrast to the limiting case, for any finite normalized Doppler rate high enough that the channel gain cannot be assumed constant over the pulse duration, the pulse shape affects the P_b. This applies even in the case of a channel tracking receiver which ideally matches the impulse response of its correlator to the received pulse shape.

Delay spread was found to result in a lower P_b for both the slow and fast fading cases, when $\rho < 0.5$. The reduction was smaller in the latter case due to the inherent diversity present within a single pulse.

Chapter 4

A Maximum Likelihood Sequence Estimation Receiver for OFDM on Flat Rayleigh Fading Channels

The MFB analysis presented in Chapter 3 obtained performance bounds on the achievable P_b for OFDM in part by neglecting the ISI introduced by the channel fading. Since this ISI may be substantial, it remains an open question as to how closely these bounds may be approached by a receiver when ISI is not neglected.

In this chapter we derive an optimal receiver for OFDM based on the principles of maximum likelihood sequence estimation. A multiplicative fading channel model with AWGN is assumed in the derivation. The receiver's performance in flat Rayleigh fading is evaluated by simulation and compared to the MFB results derived in Chapter 3.

This chapter is organized as follows. Section 4.1 describes the transmitter and channel model for which the receiver is being derived. Section 4.2 presents the theoretical derivation of an optimal maximum likelihood receiver, in the sense of sequence estimation, for OFDM in flat Rayleigh fading. Evaluation of two key parameters, matched filter outputs and tone correlations, by FFTs in a digital implemention and the required sampling rate is examined in Section 4.3. Section 4.4 describes truncating the constraint length used by the sequence estimator to make it less complex and Section 4.5 presents a criterion for choosing a non-rectangular pulse shape. Section 4.6 presents simulation results for P_b as a function of E_b/N_0, assuming perfect channel knowledge, of BOFDM for a variety of parameters and compares them to the MFBs of Chapter 3. Section 4.7 develops an approximate analysis to predict the effect of using an imperfect channel estimate, and compares this result to a simulation with a noisy channel reference. Section 4.8 shows a limitation of the truncated MLSE receiver when applied to QOFDM and Section 4.9 summarizes the conclusions of this chapter.

4.1 The Transmitter and Channel Model

Figure 4.1 shows the transmitter and channel model in terms of the complex lowpass equivalents for bandpass signals. N data symbols are assembled and simultaneously modulated onto N frequency-orthogonal carriers. The modulator outputs are summed and the resulting waveform is further shaped by the unit energy pulse $p(t)$ to form $s(t)$, the transmitted waveform of a single OFDM block. The energy of an OFDM block is $E_0 = NE_a$, where E_a is the energy of a data symbol. Both the OFDM block and the data symbols comprising it have duration $(1+\alpha)T_0$.

The channel introduces multiplicative fading $z(t)$ and AWGN $n(t)$ of spectral density N_0. The channel fading is modeled as a complex Gaussian random process with a power spectrum

$$\Phi_{z_1}(f) = \frac{\sigma_z^2}{2\pi f_D}\left(1-\left(\frac{f-f_c}{f_D}\right)^2\right)^{-1/2} \tag{4.1.1}$$

and autocorrelation function

$$\phi_{z_1}(\tau) = J_0(2\pi f_D \tau) \tag{4.1.2}$$

appropriate for land mobile radio [3]. The AWGN is statistically independent of both the data and the fading.

4.2 Derivation of a Maximum Likelihood Receiver for OFDM

In order to determine the best possible performance attainable with an OFDM signal in Rayleigh fading, we derive an optimal receiver structure which assumes knowledge of the fading waveform $z(t)$ is available as side information at the receiver. In practice $z(t)$ might be estimated by reserving some of the OFDM tones for a pilot signal. Since the fading assumed is flat, the phase and amplitude changes impressed upon the pilot will be identical to those impressed upon the data tones, neglecting the effects of AWGN. We will not develop the estimate of $z(t)$ here, but merely assume that a perfect estimate

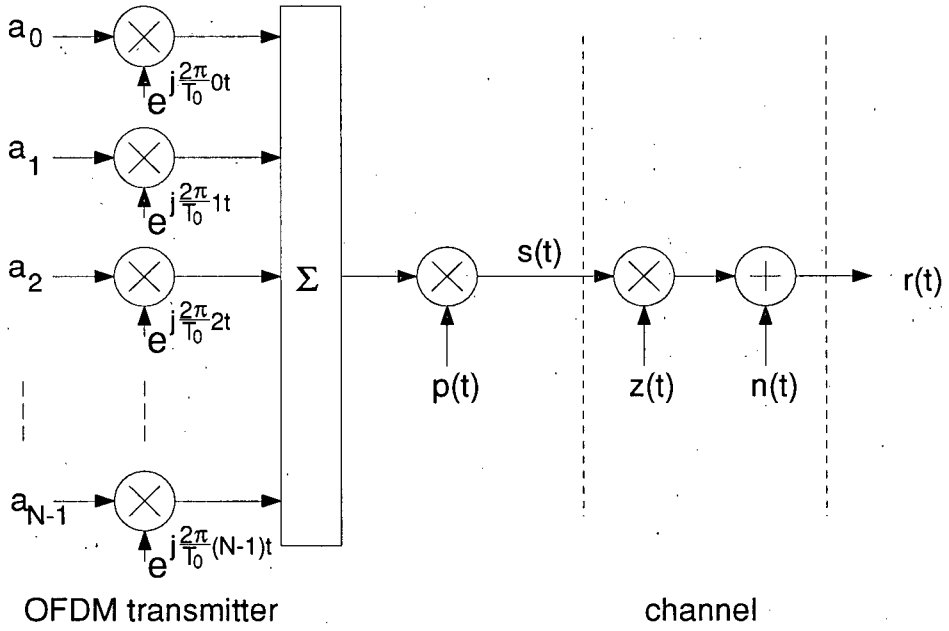

Figure 4.1 OFDM transmitter and channel model

is available. Later in Section 4.7 we will consider the effect of noise on the channel estimate, to verify that this assumption is not too brittle.

As previously noted, an OFDM block consists of N data symbols, and we are interested in the optimal detection of a single OFDM block. There are different possible interpretations of what is optimal. We could for example seek the minimum probability of a data symbol error or we could seek to minimize the probability of an OFDM block error. These criteria are not quite identical. In the latter case the problem is to find the optimal data symbol *sequence* composing an OFDM block. Experience with serial modulation [26] on ISI channels has shown that optimization by the sequence estimation criterion tends to perform well by the symbol optimization criterion as well. Related work in [27] shows that the symbol optimization criterion generally leads to a more computationally complicated receiver. With these points in mind, we choose to derive an optimal receiver in the sense of sequence estimation.

Consider a signal $w(t, \mathbf{a})$, dependent on a vector of data symbols $\mathbf{a}$, transmitted on an AWGN channel, where the noise is statistically independent of $w(t, \mathbf{a})$. The received signal is

$$r(t) = w(t, \mathbf{a}) + n(t). \tag{4.2.1}$$

It is well known from the principles of maximum likelihood sequence estimation [28] that the log-likelihood function for $\mathbf{a}$ is

$$\int |r(t) - w(t, \mathbf{a})|^2 dt \tag{4.2.2}$$

assuming the integral is finite. Equation (4.2.2) must be minimized over all possible choices for $\mathbf{a}$. Expanding (4.2.2) and retaining only the terms dependent on $\mathbf{a}$ we can show that minimizing (4.2.2) is equivalent to maximizing the metric

$$\lambda = \int \mathrm{Re}[r(t)w^*(t, \mathbf{a})] - \frac{1}{2}|w(t, \mathbf{a})|^2 dt \tag{4.2.3}$$

which is the form we shall work with here.

For the flat fading model, the received signal is given by

$$\begin{aligned} r(t) &= z(t)s(t) + n(t), \quad 0 \le t \le T_0(1+\alpha) \\ &= z(t)p(t) \sum_{n=0}^{N-1} a_n e^{j\frac{2\pi}{T_0}nt} + n(t) \end{aligned} \tag{4.2.4}$$

where

$$\begin{aligned} s(t) = p(t) \sum_{n=0}^{N-1} a_n e^{j\frac{2\pi}{T_0}nt}, \\ 0 \le t \le T_0(1+\alpha). \end{aligned} \tag{4.2.5}$$

Comparing with (4.2.1), it is apparent that

$$w(t, \mathbf{a}) = z(t)p(t) \sum_{n=0}^{N-1} a_n e^{j\frac{2\pi}{T_0}nt}. \tag{4.2.6}$$

Substituting (4.2.6) into (4.2.3) we have

$$\begin{aligned}\lambda = &\int \mathrm{Re}\left[r(t)z^*(t)p^*(t)\sum_{n=0}^{N-1} a_n^* e^{-j\frac{2\pi}{T_0}nt}\right]dt \\ &-\frac{1}{2}\int |z(t)|^2|p(t)|^2 \sum_{n=0}^{N-1}\sum_{m=0}^{N-1} a_n^* a_m e^{-j\frac{2\pi}{T_0}(n-m)t}dt\end{aligned} \tag{4.2.7}$$

where the interval of integration is the interval over which $p(t)$ is nonzero, i.e. $0 \le t \le T_0(1+\alpha)$. Interchanging the orders of the integrations and summations

$$\begin{aligned}\lambda = &\mathrm{Re}\left[\sum_{n=0}^{N-1} a_n^* \int r(t)z^*(t)p^*(t)e^{-j\frac{2\pi}{T_0}nt}dt\right] \\ &-\frac{1}{2}\sum_{n=0}^{N-1}\sum_{m=0}^{N-1} a_n^* a_m \int |z(t)|^2|p(t)|^2 e^{-j\frac{2\pi}{T_0}(n-m)t}dt\end{aligned} \tag{4.2.8}$$

and defining

$$U_n = \int r(t)z^*(t)p^*(t)e^{-j\frac{2\pi}{T_0}nt}dt \tag{4.2.9}$$

and

$$V_n = \int |z(t)|^2|p(t)|^2 e^{-j\frac{2\pi}{T_0}nt}dt \tag{4.2.10}$$

we can write for the metric

$$\lambda = \mathrm{Re}\left[\sum_{n=0}^{N-1} a_n^* U_n\right] - \frac{1}{2}\sum_{n=0}^{N-1}\sum_{m=0}^{N-1} a_n^* a_m V_{n-m}. \tag{4.2.11}$$

Some insight into the meaning of U_n and V_n can be obtained with a little manipulation of (4.2.9) and (4.2.10). Let the equivalent pulse shape after transmission over the channel be $q(t) = p(t)z(t)$, and let $P(f) = \int p(t)e^{-j2\pi ft}dt$. Using this and applying Parseval's relation[11] to (4.2.9) yields

$$\begin{aligned}U_n &= \int_{-\infty}^{\infty} R(f)Q^*\left(f - \frac{n}{T_0}\right)df \\ &= \{R(f) \circledast Q^*(-f)\}|_{f=\frac{n}{T_0}},\end{aligned} \tag{4.2.12}$$

[11] $\int_{-\infty}^{+\infty} a(t)b^*(t)dt = \int_{-\infty}^{\infty} A(f)B^*(f)df.$

where $\circledast$ is a convolution operator. U_n can be interpreted as the output $U(f)$ of a filter matched to $Q(f)$ operating in the frequency-domain, evaluated at $f = n/T_0$. We will refer to U_n as the matched filter outputs. Using $q(t)$ in (4.2.10) we have

$$V_n = \int |q(t)|^2 e^{-j\frac{2\pi}{T_0}nt} dt. \tag{4.2.13}$$

V_n is the correlation between two complex tones spaced n/T_0 apart in frequency after shaping by the equivalent pulse. We will refer to V_n as the tone correlations.

Once we have obtained U_n and V_n, (4.2.11) gives λ in a form maximizable by the Viterbi algorithm. Specifically, it may be shown (Appendix C) that λ may be found recursively by defining

$$\lambda_n = \mathrm{Re}[a_n^* U_n] - \mathrm{Re}\left[a_n^* \sum_{k=n-L}^{n-1} a_k V_{n-k}\right] - \frac{1}{2}|a_n|^2 V_0 \tag{4.2.14}$$

and maximizing

$$\lambda = \sum_{n=0}^{N-1} \lambda_n. \tag{4.2.15}$$

Equation (4.2.14) results in an optimal sequence selection only for the selection of $L = n$, or equivalently if $V_n = 0$ for $n > L$.

The Viterbi algorithm is a search for an optimal path through a trellis with M^L states, where M is the number of symbols in the alphabet of a_n. Although much more efficient than an exhaustive search when $L < N$, it is still exponentially complex in L, and thus L must be fairly small in actual use or approximations become necessary.

4.3 FFT Evaluation of U_n and V_n

Both the matched filter outputs U_n and the tone correlations V_n, which are defined by continous-time integrals, must be evaluated from discrete samples of $r(t)$ and $z(t)$ in a digital implementation. While numerical integration techniques could be used, it is much

more efficient to take advantage of certain relations between continous-time and discrete-time Fourier transforms. If we define $U(f)$ as the Fourier transform of $r(t)z^*(t)p^*(t)$ and $V(f)$ as the Fourier transform of $|z(t)|^2|p(t)|^2$, then U_n and V_n are seen to be these transforms evaluated at $f = n/T_0$. This leads to a criterion for determining the sampling rate which will allow all N values of U_n and V_n to be evaluated accurately and simultaneously using FFTs.

If we have a discrete signal s_m related to a continuous signal $s(t)$ by sampling as $s_m = s(t)\sum_m \delta(t - m\Delta t)$, the relation between $\tilde{S}(f) = \sum_m s_m e^{-j2\pi f m\Delta t}$ and $S(f) = \int s(t)e^{-j2\pi ft}dt$ is [6]

$$\tilde{S}(f) = \frac{1}{\Delta t}\sum_n S\Big(f - \frac{n}{\Delta t}\Big), \tag{4.3.1}$$

which states that the spectrum of the discrete signal is a periodic version of that of the continuous signal. When (4.2.9) and (4.2.10) are converted to DFTs by sampling as in

$$\tilde{U}_n = \sum_m r_m z_m^* p_m^* e^{-j\frac{2\pi}{T_0}nm\Delta t} \tag{4.3.2}$$

$$\tilde{V}_n = \sum_m |z_m|^2|p_m|^2 e^{-j\frac{2\pi}{T_0}nm\Delta t} \tag{4.3.3}$$

we are actually calculating periodic approximations to U_n and V_n. Equation (4.3.1) indicates one period of $\Delta t\tilde{U}_n = U_n$ and one period of $\Delta t\tilde{V}_n = V_n$ if U_n and V_n are bandlimited and Δt is small enough to avoid aliasing. The bandwidth of $s(t)$ depends on how many sidelobes are considered significant components of $P(f)$. For rectangular pulse shaping, even considering only the first sidelobe on either side and choosing Δt to avoid these aliasing requires $\Delta t \leq T_0/(N+3)$. The bandwidth of the received signal is greater because of the multiplicative fading, and the bandwidth of the argument of (4.2.9), $r(t)z^*(t)p^*(t)$, exceeds that of $s(t)$ by twice the Doppler frequency. Since the Doppler frequency is assumed to be on the order of 1 % of the signal bandwidth only a slight decrease in Δt is required. The implication is that despite the invertibility of the

DFT, an N–point transform (corresponding to $\Delta t = T_0/N$) is inadequate to represent an N tone OFDM signal on a fading channel[12].

To allow an adequate guard interval, and because it is convenient to work with factors of 2 when using FFTs we use $\Delta t = \frac{T_0}{2N}$, and our DFT equation for U_n is

$$U_n = \frac{T_0}{2N} \sum_{m=0}^{N'-1} r_m z_m^* p_m^* e^{-j\frac{2\pi}{2N}nm}. \tag{4.3.4}$$

The upper limit N' must be large enough to cover the time interval $0 \leq t \leq T_0(1+\alpha)$, requiring N' greater than $2N$ for $\alpha > 0$. Again choosing a factor of 2 for convenience

$$U_n = \sum_{m=0}^{4N-1} r_m z_m^* p_m^* e^{-j\frac{2\pi}{2N}nm}, \tag{4.3.5}$$

where we have rescaled U_n to remove the leading factor of $\frac{T_0}{2N}$. This rescaling is also applied to V_n below and does not affect the optimal path selection as can be seen from (4.2.11).

Equation (4.3.5) can be calculated from two $2N$–point FFTs by using the periodicity of discrete complex exponentials. It is easily shown

$$U_n = \sum_{n=0}^{2N-1} \left(r_m z_m^* p_m^* + r_{m+2N} z_{m+2N}^* p_{m+2N}^*\right) e^{-j\frac{2\pi}{2N}nm}, \qquad 0 \leq n \leq N-1. \tag{4.3.6}$$

In (4.2.10) for V_n, $|z(t)|^2|p(t)|^2$ has a much narrower bandwidth than that of $r(t)z^*(t)p^*(t)$, permitting a much larger Δt than that required to evaluate U_n. However, if a shorter FFT is used an interpolator is required because the frequency samples V_n are spaced too far apart. Since an FFT is an efficient interpolator, we use the following expression for V_n

$$V_n = \sum_{n=0}^{2N-1} \left(|z_m|^2|p_m|^2 + |z_{m+2N}|^2|p_{m+2N}|^2\right) e^{-j\frac{2\pi}{2N}nm}, \qquad 0 \leq n \leq L. \tag{4.3.7}$$

[12] N-points are adequate for AWGN channels, because the Nyquist criterion need not be satisfied.

4.4 Truncated MLSE

We have noted in Section 4.2 that the complexity of the Viterbi algorithm used to evaluate the metric of (4.2.14) and (4.2.15) varies as M^L. From (4.2.14) L is potentially as large as $N-1$, or 1 less than the number of tones used. Even for $M = 2$, a binary signaling alphabet, the complexity of the optimal receiver rapidly becomes unsupportable for more than perhaps 10 tones. Optimal receivers for $L = 64$ or 128 are clearly impractical, yet we are interested in large numbers of tones for the channel averaging they provide. Thus the maximum value of L must be reduced, and the simplest means is to set a limit for it. Specifically, in the calculation of λ_n by (4.2.14), we allow $L = n$ to increase with n for $n = 0, 1, ..., L_{max}$, and then hold it fixed at L_{max} for $n = L_{max} + 1, L_{max} + 2, ..., N - 1$. By so limiting L the MLSE receiver is made suboptimal.

The indication that L may be limited while losing only a small portion of the attainable performance follows from the interpretation of V_n as the correlation between two tones. As the sidelobes of $Q(f)$ decrease with increasing distance from the mainlobe, it is apparent that inter-tone correlations will decrease as the frequency spacing between the tones increases. How rapidly this decorrelation occurs depends on the type of pulse shaping used and on the fading waveform during the signaling interval. The selection of the pulse shape is affected in part by a tradeoff between channel averaging and rapid sidelobe reduction. A raised cosine pulse, for example, has more rapidly decreasing sidelobes than a rectangular pulse, but is less effective at channel averaging. In the following sections the required L_{max} for BOFDM is found by simulations of the suboptimal receiver for both rectangular and raised cosine pulse shapes.

4.5 Pulse Shaping

Without foreknowledge of the fading waveform the most effective channel averaging in the interval T_0 is obtained with a rectangular pulse shape.

However in practice a pulse without discontinuities is desirable because of bandwidth limitations, and additionally it seems possible that a pulse with more rapidly decaying sidelobes might cause less ISI and therefore require a smaller L. A criterion for choosing $p(t)$ is to require that the basis functions of $s(t)$ remain orthonormal after shaping and matched filtering in the absence of fading:

$$\delta_{n-m} = \int |p(t)|^2 e^{-j\frac{2\pi}{T_0}(n-m)t} dt. \tag{4.5.1}$$

Let $p_{sq}(t) = |p(t)|^2$ and $P_{sq}(f) = \int p_{sq}(t)e^{-j2\pi ft}dt$, then

$$\begin{aligned} \delta_n &= P_{sq}(f)|_{f=n/T_0} \\ &= P_{sq_n}. \end{aligned} \tag{4.5.2}$$

Transforming both sides with an inverse discrete frequency Fourier transform (Appendix B) and scaling by $1/T_0$ yields

$$\sum_n p_{sq}(t - nT_0) = \frac{1}{T_0} \tag{4.5.3}$$

which is merely Nyquist's criterion for zero-ISI pulse shaping with the traditional roles of time-domain and frequency-domain expressions reversed.

An important consequence of (4.5.3) is that there is no pulse shape of duration less than or equal to T_0 (other than the rectangular) which satisfies the orthonormality criterion. Thus alternative pulses must have their duration extended relative to the rectangular pulse.

We consider the raised cosine family for $p_{sq}(t)$ since it is known to satisfy (4.5.3) and its spectral sidelobes decay approximately as $1/f^3$. The raised cosine pulse is given by

$$p_{sq}(t) = \begin{cases} \frac{1}{2T_0}\left(1 + \cos\left(\frac{\pi(t-\alpha T_0)}{\alpha T_0}\right)\right), & 0 \le t < \alpha T_0 \\ 1/T_0, & \alpha T_0 \le t \le T_0 \\ \frac{1}{2T_0}\left(1 + \cos\left(\frac{\pi(t-T_0)}{\alpha T_0}\right)\right), & T_0 < t \le T_0(1+\alpha) \\ 0, & \text{otherwise} \end{cases} \tag{4.5.4}$$

where $0 \le \alpha \le 1$ is a rolloff factor describing the percentage of the pulse duration beyond T_0. The pulse $p(t)$ satisfying (4.5.1) is $p(t) = \sqrt{p_{sq}(t)}$.

The need to project $p(t)$ onto complex exponentials $e^{j\frac{2\pi}{T_0}nt}$ of duration greater than T_0 leads to an interesting observation. Redefining the exponentials to include a linear phase shift, the shaped basis functions are

$$p(t)e^{j\frac{2\pi}{T_0}n(t-\sigma)}, \quad 0 \leq t \leq (1+\alpha)T_0. \tag{4.5.5}$$

The P_b, in contrast to the AWGN channel, is affected by the choice of σ. Figure 4.2 shows the sensitivity of P_b to the choice of σ for BPSK modulation of $N = 32$ tones and $\alpha = 0.125$. These errors are due entirely to ISI caused by flat Rayleigh fading as there is no AWGN. Matched filter detection is employed without MLSE. The optimal σ occurs at $\sigma = \alpha T_0/2$.

The effect occurs because $p(t)$ has been defined to start at $t = 0$. This causes pulse shapes with nonzero α to have a delay of $\tau_d = \alpha T_0/2$ relative to the rect pulse. Consider a single modulated tone from an OFDM block as in (4.5.6)

$$a_n p(t)e^{j\frac{2\pi}{T_0}nt}. \tag{4.5.6}$$

Time delay of the pulse, as shown in (4.5.7)

$$\begin{aligned} a_n p(t-\tau_d)e^{j\frac{2\pi}{T_0}nt} &= a_n p(t')e^{j\frac{2\pi}{T_0}n(t'+\tau_d)} \\ &= \left(a_n e^{j\frac{2\pi}{T_0}n\tau_d}\right)p(t')e^{j\frac{2\pi}{T_0}nt'} \\ &= a'_n p(t')e^{j\frac{2\pi}{T_0}nt'} \end{aligned} \tag{4.5.7}$$

where $t' = t - \tau_d$ and $a'_n = a_n e^{j\frac{2\pi}{T_0}n\tau_d}$, effectively alters the transmitted constellation by introducing a tone dependent rotation of the data symbol.

There is no effect from rotation on P_b for an AWGN channel because the received tones remain orthogonal. But P_b is increased when orthogonality is lost as on a fading channel, because the a'_n can be closer in signal space than the a_n.

The variation in P_b with σ is greater than $2:1$ without compensation, but can be entirely removed by prerotating the a_n by $e^{-j\pi n\alpha}$ when $\alpha \neq 0$. This is equivalent to

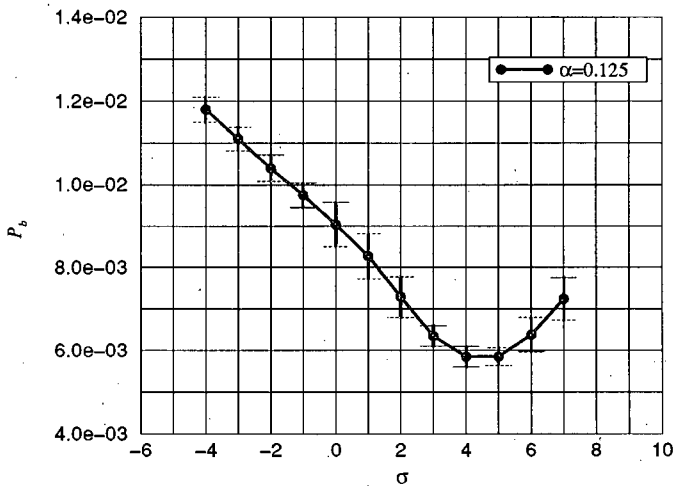

Figure 4.2 Variation of P_b with σ for $N = 32$ tones and various rolloff factors. Matched filter reception, no MLSE applied.

setting $\sigma = \alpha T_0/2$ in (4.5.5), and was done in producing the simulation results which follow.

4.6 Perfect Channel Knowledge

4.6.1 Simulation Framework

The probability of a bit error, P_b, was evaluated by simulation for several important cases. The OFDM blocks were generated as specified by (4.2.5) with $a_n = \pm\sqrt{E_a}$. This is independent BPSK modulation of each of the N tones comprising the OFDM block. Thus we have $E_a = E_b$, and the probability of a symbol error $P_s = P_b$. The simulation implements the transmitter and channel model shown in Figure 4.1, and the truncated MLSE receiver with suboptimal constraint length L derived in this chapter. The simulations were made long enough to obtain 95% confidence intervals of approximately $\pm 10\%$ of P_b.

The transmitted signal $s(t)$ is subjected to flat Rayleigh fading and AWGN as specified by (4.2.1) and (4.2.6). The received signal $r(t)$ is processed to produce the matched filter

outputs and tone correlations given by (4.3.6) and (4.3.7) respectively. These are then passed to a Viterbi algorithm which maximizes the metric λ given by (4.2.15).

The figures presented are annotated with f_N since it is this parameter upon which the P_b of the MFB of Chapter 3 depends. A maximum Doppler rate of $f_D = 0.01$ times the data symbol rate is assumed and the sampling rate and number of samples per block is such that $f_N = f_D T_0 = f_D N$. Therefore we always have $N = 100 f_N$ data symbols per OFDM block.

4.6.2 Rectangular Pulse Shape

We begin by considering a rectangular pulse shape $p(t) = \frac{1}{\sqrt{NT_0}} \operatorname{rect}(t/T_0)$ which has a $\sqrt{\frac{T_0}{N}} \operatorname{sinc}(T_0 f)$ amplitude spectrum. The sidelobes fall off only inversely with f and the first sidelobe is only 6.6 db down from the main lobe. It therefore seems possible that after channel fading has altered the special structure required to obtain orthogonality that L might be quite large, but our simulation results in comparison to the MFB indicate this is not always the case.

Figure 4.3 shows some simulation results for the MLSE receiver with various values of L. The OFDM signal uses BPSK modulation of 32 tones with rectangular pulse shaping on a flat Rayleigh fading channel. The normalized Doppler rate is $f_N = 0.32$, and the MFB for $f_N = 0.32$ is also shown for comparison. We observe that the truncated MLSE receiver is able to approach the MFB to within approximately 1 dB over a P_b range exceeding 10^{-2} to 10^{-4}, and that the discrepancy between the MFB and MLSE receiver increases only slightly with E_b/N_0. This is for a modest value of $L = 3$. If L is restricted to only 1 there is less than a 1 dB loss at 10^{-3}; increasing L to 5 results in negligible improvement over $L = 3$.

The $L = 0$ curve is simply matched filtering without sequence estimation. It exhibits an error floor slightly below 10^{-2}. This is due to the large amount of uncompensated ISI. The effect becomes more visible with increasing E_b/N_0 because the proportion of

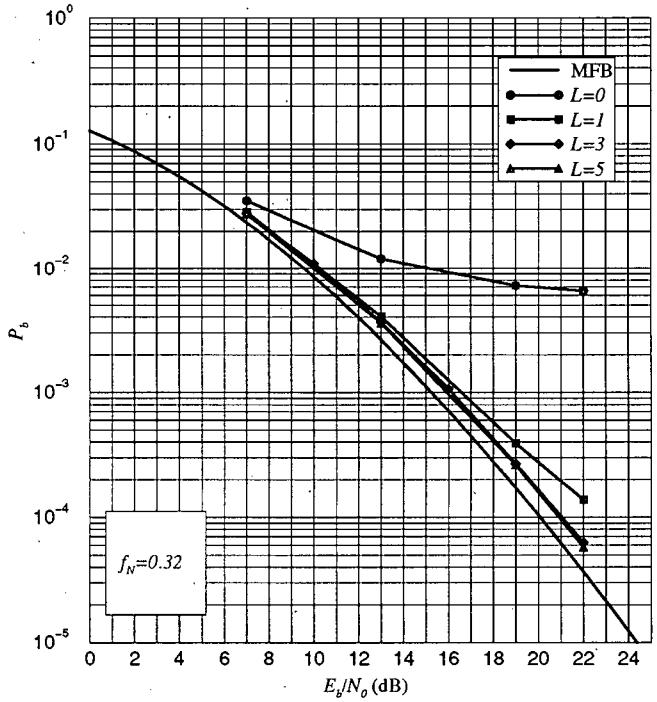

Figure 4.3 P_b of MLSE vs. L compared to the MFB for $f_N = 0.32$

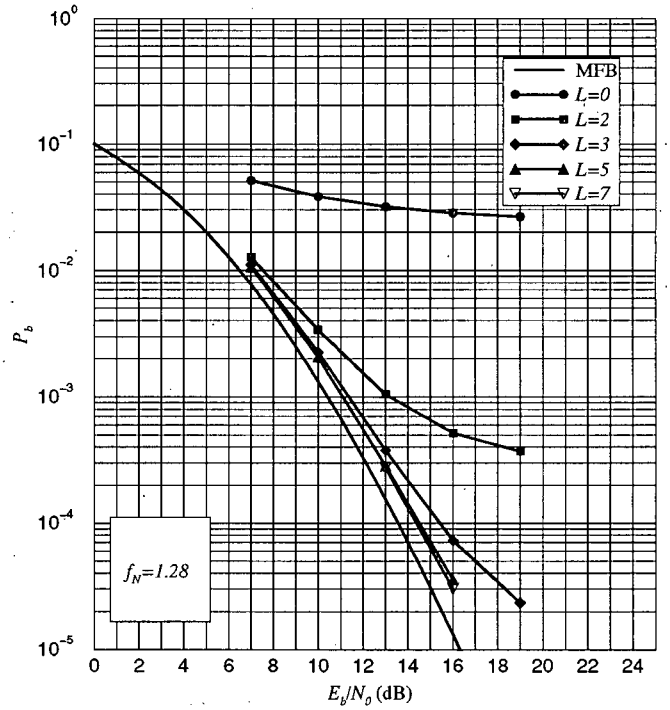

Figure 4.4 P_b of MLSE vs. L compared to the MFB for $f_N = 1.28$

error due to ISI relative to AWGN increases as well. Presumably error floors also exist for $L = 1$, 3, and 5, but at levels too low to measure by simulation.

Figure 4.4 shows results for the same parameters as Figure 4.3 except there are now 128 tones and $f_N = 1.28$. Again values of $L = 3$ or 5 are within 1 dB of the MFB at 10^{-3}, although the discrepancy between these curves becomes significant at lower error rates. Additional points show the inadequacy of $L = 2$ and a negligible improvement for $L = 7$ over $L = 5$.

4.6.3 Raised Cosine Pulse Shape

Here we compare the required L for raised cosine pulses of various α to the required L for a rectangular pulse. The pulse $p(t)$ is specified by (4.5.4) and (4.5.1). In comparing pulses of different α there is an unavoidable discrepancy in the overall signaling rate. This is because the orthonormality constraint of (4.5.1) requires a pulse of length $T_{p(t)} = T_0(1 + \alpha)$, and longer pulses imply fewer OFDM blocks can be transmitted in a given time.

Figure 4.5 shows P_b results for $f_N = 0.32$ with $L = 3$ for $\alpha = 0.0$ and $\alpha = 0.125$. It was shown previously that there is negligible improvement beyond $L = 3$ for this f_N. Not too surprisingly, the change in α has a negligible effect.

Figure 4.6 compares the P_b for various α at $f_N = 1.28$ and $L = 3$. Since $L = 3$ is noticeably worse than $L \geq 5$ at this f_N, it was thought that the reduced spectral sidelobe levels of the pulse shapes for $\alpha > 0.0$ might result in a lowered P_b relative to the $\alpha = 0.0$ case. However in the simulation results there is very little dependence on α from which we conclude that it is the ISI from nearby mainlobes which causes most errors over the simulated P_b range, and that the effect of ISI from sidelobes is relatively unimportant.

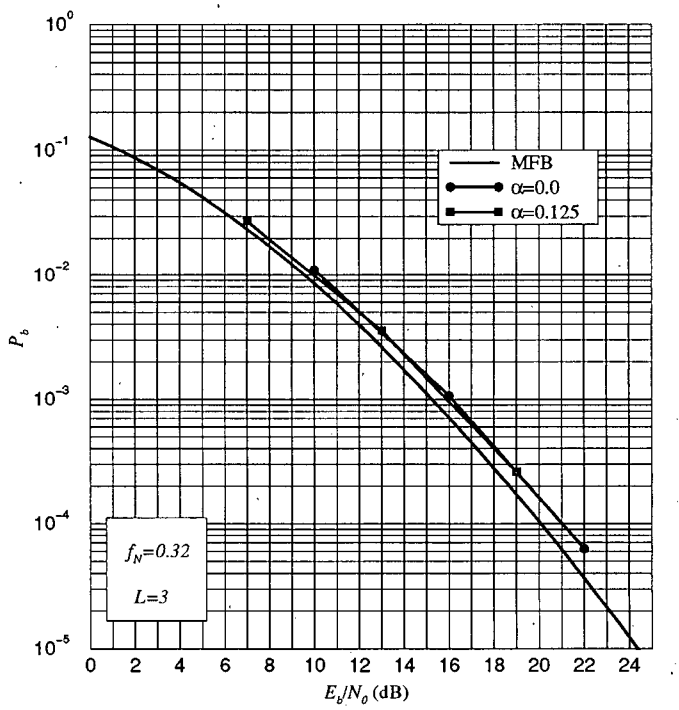

Figure 4.5 Effect of pulse shaping on the P_b of an MLSE for $f_N = 0.32$ and $L = 3$

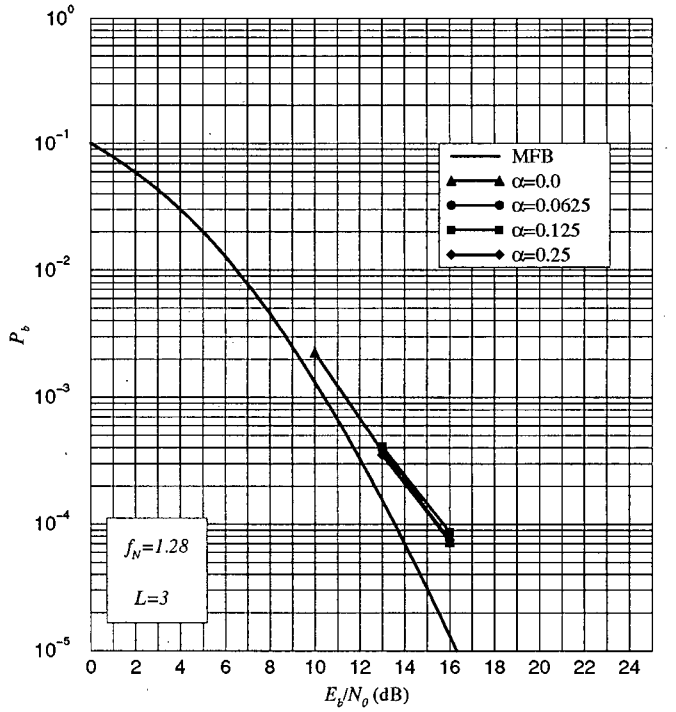

Figure 4.6 Effect of pulse shaping on the P_b of an MLSE for $f_N = 1.28$ and $L = 3$

4.7 Effect of an Imperfect Channel Estimate

In deriving and simulating the MLSE receiver we have so far assumed the availability of a perfect channel estimate $z(t)$ at the receiver. The problem of channel estimation by means of pilot signals for Rayleigh fading has been previously studied [5], [10], [11]. In this section we provide an approximate analysis of the effect of using a noisy estimate on the receiver's P_b performance and verify our result by simulation.

An imperfect channel estimate affects the MLSE receiver by introducing errors into the computation of the metric parameters U_n and V_n. We will focus on the matched filter outputs U_n since the results of Section 4.6 show the MLSE receiver to be tolerant of small errors in V_n.

We model the channel estimate $\hat{z}_m$ with

$$\hat{z}_m = z_m + n_{\hat{z}_m} \tag{4.7.1}$$

where $n_{\hat{z}_m}$ is AWGN with variance $\sigma_{\hat{z}}^2$, and is statistically independent of z_m.

Consider the term $r_m z_m^*$ from the argument of the summation in (4.3.5) used to calculate U_n. Substituting for r_m we have

$$\begin{aligned} r_m z_m^* &= [s_m z_m + n_m] z_m^* \\ &= w_m z_m^* + n_m' \end{aligned} \tag{4.7.2}$$

where $w_m z_m^*$ is a signal component and $n_m' = n_m z_m^*$ is an AWGN component of variance N_0. With the noisy estimate we have instead

$$\begin{aligned} r_m \hat{z}_m^* &= w_m \hat{z}_m^* + n_m \hat{z}_m^* \\ &= w_m \left[z_m^* + n_{\hat{z}_m}^* \right] + n_m \left[z_m^* + n_{\hat{z}_m}^* \right] \\ &\approx w_m z_m^* + n_m' + n_m'' \end{aligned} \tag{4.7.3}$$

where $n_m'' = w_m n_{\hat{z}_m}^*$ is an additional Gaussian noise term and the second order noise term $n_m n_{\hat{z}_m}^*$ has been dropped. Equation (4.7.3) is approximately equal to (4.7.2) with

the addition of an extra noise term n''_m. Its variance is

$$\mathrm{E}\left[\left|w_m n^*_{\hat{z}_m}\right|^2\right] = E_a \sigma^2_{n_{\hat{z}}} \tag{4.7.4}$$

which at first appears proportional to the energy per data symbol E_a.

We note n'_m and n''_m are independent, since they are assumed jointly Gaussian and their cross-correlation is

$$\begin{aligned} \mathrm{E}\left[n'_m n^{*\prime\prime}_m\right] &= \mathrm{E}[n_m z^*_m w^*_m n_{\hat{z}_m}] \\ &= w^*_m \mathrm{E}[n_m]\mathrm{E}[z^*_m]\mathrm{E}[n_{\hat{z}_m}] \\ &= 0. \end{aligned} \tag{4.7.5}$$

Therefore the noise powers add, and the ratio of signal energy to noise power in (4.7.3) is given by

$$\begin{aligned} \mathrm{SNR}' &= \frac{E_a}{\sigma^2_{n'} + \sigma^2_{n''}} \\ &= \frac{E_a/N_0}{1 + \frac{E_a}{N_0}\sigma^2_{n_{\hat{z}}}} \end{aligned} \tag{4.7.6}$$

where we have used $\mathrm{E}[z_m z^*_m] = 1$.

The variance $\sigma^2_{n_{\hat{z}}}$ depends on the type of estimator used to form $\hat{z}_m$. Suppose the channel is estimated by transmitting a pilot tone of energy E_l per data symbol interval. The received pilot is

$$l_{p_m} = \sqrt{\frac{E_l}{T_s}}\, z_m + n_{p_m} \tag{4.7.7}$$

where n_{p_m} is independent AWGN of spectral density N_0. l_{p_m} is bandpass filtered by an ideal rectangular filter of unity gain and bandwidth B_p. B_p is chosen wide enough to pass l_{p_m} undistorted except for band limiting the noise spectrum; i.e. $B_p \geq 2f_D$ with equality in the absence of frequency offsets. Adequate guard intervals (in frequency) are assumed to protect the pilot from ISI effects. The output of the bandpass filter after sampling is

$$l_m = \sqrt{\frac{E_l}{T_s}}\, z_m + n_{l_m} \tag{4.7.8}$$

where $\sigma_{n_l}^2 = N_0 B_p$. These outputs are further processed by a Wiener filter. Without loss of generality we can consider the estimate of $\hat{z}_0$ by a Wiener filter as

$$\hat{z}_0 = \mathbf{h}^{\mathrm{H}}\mathbf{l} \tag{4.7.9}$$

where $()^{\mathrm{H}}$ is the Hermitian operator, combining transposition and conjugation. For an N_l–point estimate, the tap input vector $\mathbf{l} = \left[l_{-\frac{N_l-1}{2}}, ..., l_{-1}, l_0, l_1, ..., l_{\frac{N_l-1}{2}}\right]^T$. It is well known from Wiener filter theory [23] that the optimum (in an MMSE sense) choice for the tap weight vector $\mathbf{h}$ is $\mathbf{h} = \mathbf{R}^{-1}\mathbf{g}$ where $\mathbf{R} = \mathrm{E}\left[\mathbf{l}\mathbf{l}^{\mathrm{H}}\right]$ is the autocorrelation matrix of the tap input vector and $\mathbf{g} = \mathrm{E}[z_0^*\mathbf{l}]$ is the cross-correlation between the desired response and tap input vector. It is not difficult to show that the variance of the estimation error is

$$\mathrm{E}\left[|\hat{z}_0 - z_0|^2\right] = 1 - \mathbf{g}^{\mathrm{H}}\mathbf{R}^{-1}\mathbf{g}. \tag{4.7.10}$$

For the present problem we have

$$\begin{aligned}\mathbf{R} &= \mathrm{E}\left[\left(\sqrt{E_l}\mathbf{z} + \mathbf{n_l}\right)\left(\sqrt{E_l}\mathbf{z}^{\mathrm{H}} + \mathbf{n_l}^{\mathrm{H}}\right)\right] \\ &= E_l\,\mathrm{E}\left[\mathbf{z}\mathbf{z}^{\mathrm{H}}\right] + N_0\mathrm{E}\left[\mathbf{n_l}\mathbf{n_l}^{\mathrm{H}}\right]\end{aligned} \tag{4.7.11}$$

where

$$\mathbf{z} = \left[z_{-\frac{N_l-1}{2}}, ..., z_{-1}, z_0, z_1, ..., z_{-\frac{N_l-1}{2}}\right]^T \tag{4.7.12}$$

and

$$\mathbf{n_l} = \left[n_{l_{-\frac{N_l-1}{2}}}, ..., n_{l_{-1}}, n_{l_0}, n_{l_1}, ..., n_{l_{\frac{N_l-1}{2}}}\right]^T. \tag{4.7.13}$$

The $(i,j)^{th}$ element of $\mathbf{R}$ is given by

$$\mathbf{R}_{\mathrm{i,j}} = \frac{E_l}{T_s}J_0(2\pi f_D|i-j|\Delta t) + N_0 B_p \mathrm{sinc}(B_p(i-j)\Delta t) \tag{4.7.14}$$

and

$$\begin{aligned}\mathbf{g} &= \mathrm{E}\left[z_0^*\left(\sqrt{E_l}\mathbf{z} + \mathbf{n_l}\right)\right] \\ &= \sqrt{\frac{E_l}{T_s}}\,\mathrm{E}[z_0^*\mathbf{z}].\end{aligned} \tag{4.7.15}$$

The i^{th} element of g is given by

$$\mathbf{g_i} = \sqrt{\frac{E_l}{T_s}} J_0(2\pi f_D |i| \Delta t). \tag{4.7.16}$$

Let us assume $\Delta t = T_s$ and normalize the pilot bandpass filter bandwidth by the duration of a data symbol $\beta = B_p T_s$. We define the two $N_l \times N_l$ matrices $\mathbf{J_0}(\beta)$ with $(i,j)^{th}$ element $\mathbf{J_{0_{i,j}}}(\beta) = J_0(2\pi\beta|i-j|)$, $\mathbf{Sinc}(\beta)$ with $(i,j)^{th}$ element $\mathbf{Sinc_{i,j}}(\beta) = \text{sinc}(\beta(i-j))$, and the $N_l \times 1$ matrix $\mathbf{j_0}(\beta)$ with i^{th} element $\mathbf{j_{0_i}}(\beta) = J_0(2\pi\beta i)$. Then we can write

$$\sigma^2_{n_z} = \left(1 - \mathbf{j_0^H}(\beta)\left(\mathbf{J_0}(\beta) + \frac{N_0 B_p T_s}{E_l}\mathbf{Sinc}(\beta)\right)^{-1}\mathbf{j_0}(\beta)\right). \tag{4.7.17}$$

Let $f = E_l/E_s$ be the fraction of the total energy transmitted per data symbol which is allocated to the pilot. The total energy transmitted per data symbol is $E_s = E_a + E_l$ giving $E_a = E_s(1-f)$ and $E_l = E_s f$. Using these in (4.7.17)

$$\sigma^2_{n_z} = \left(1 - \mathbf{j_0^H}(\beta)\left(\mathbf{J_0}(\beta) + \frac{N_0}{E_s}\frac{\beta}{f}\mathbf{Sinc}(\beta)\right)^{-1}\mathbf{j_0}(\beta)\right) \tag{4.7.18}$$

and substituting in (4.7.6) yields for SNR′ of (4.7.3)

$$\text{SNR}' = \frac{\frac{E_s}{N_0}(1-f)}{1 + \frac{E_s}{N_0}(1-f)\left(1 - \mathbf{j_0^H}(\beta)\left(\mathbf{J_0}(\beta) + \frac{N_0}{E_s}\frac{\beta}{f}\mathbf{Sinc}(\beta)\right)^{-1}\mathbf{j_0}(\beta)\right)}. \tag{4.7.19}$$

The variation of $\sigma^2_{n_z}$ with N_l for several values of $\left(f, \beta, \frac{E_b}{N_0}\right)$ is shown in Figure 4.7. It can be seen that $\sigma^2_{n_z}$ is nearly independent of N_l, suggesting that $N_l = 1$ is an appropriate choice. This is because the noise components at the pilot filter output are strongly correlated. As N_l is increased to obtain less correlated noise components, the correlations of the pilot components with the desired component z_0 decrease, and these effects tend to cancel each other. With $N_l = 1$ (4.7.18) simplifies to

$$\begin{aligned} \sigma^2_{n_z} &= \frac{\beta}{\frac{E_s}{N_0}f + \beta} \\ &\approx \frac{N_0}{E_s}\frac{\beta}{f} \end{aligned} \tag{4.7.20}$$

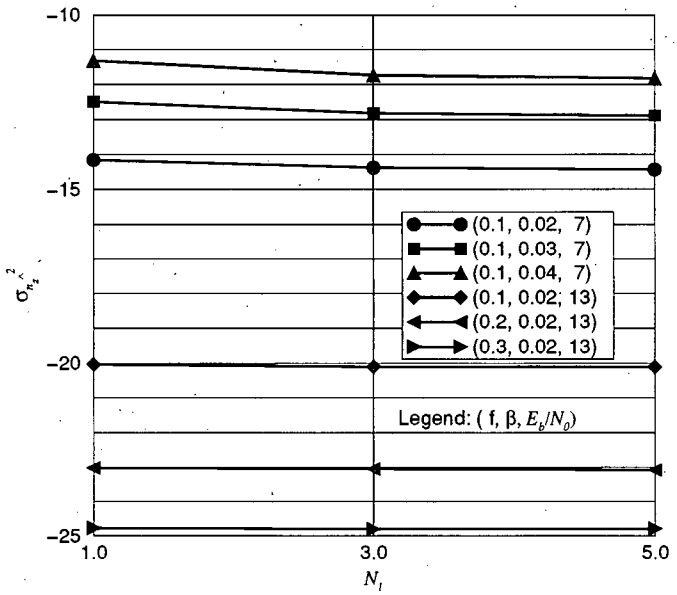

Figure 4.7 Variation of $\sigma^2_{n_z}$ with N_l for several values of $\left(f, \beta, \frac{E_b}{N_0}\right)$.

and (4.7.19) to

$$\mathrm{SNR}' = \frac{\left(\frac{E_s}{N_0} f + \beta\right)(1-f)}{f(1-\beta) + \beta\left(1 + \frac{N_0}{E_s}\right)}. \tag{4.7.21}$$

Figure 4.8 shows the variation of SNR′ with f for various $\left(\frac{E_s}{N_0}, \beta\right)$ pairs. It can be seen that the optimal allocation of power to the pilot signal is only 12.5% at $\beta = 0.02$ and increases only slightly as β is increased. There is very little variation with E_s/N_0. Compared to an ideal system having perfect knowledge of z_m at the receiver without having to expend power to measure it, the curves of Figure 4.8 at $\beta = 0.02$ predict a cost of approximately 1.3 dB for a system which must allocate power to channel measurement and subsequently use the noisy estimate which results.

4.7.1 Noisy Reference Simulation

Figure 4.9 compares the P_b measured by simulation for a noisy pilot reference verses an ideal reference, for $f_N = 0.64$ and $L = 3$. The MFB and ideal (noiseless) reference curves are the same as appeared in Figure 4.3.

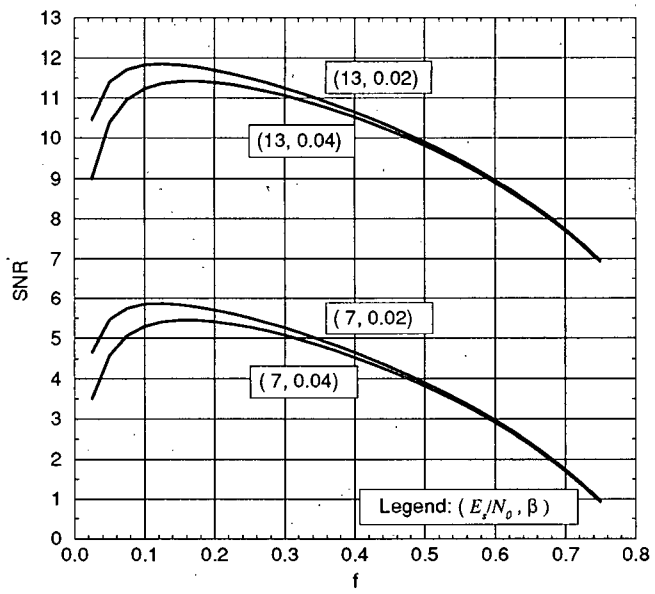

Figure 4.8 Variation of SNR′ with f for various $\left(\frac{E_s}{N_0}, \beta\right)$ pairs.

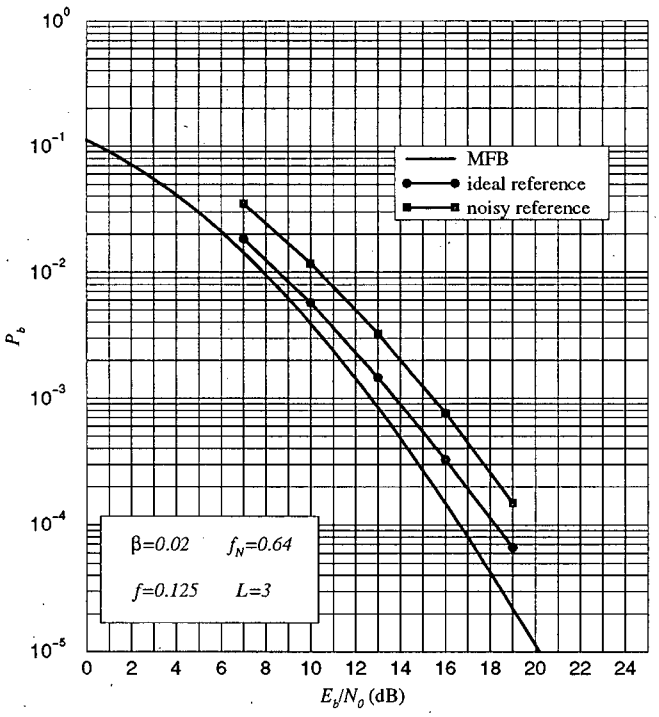

Figure 4.9 Effect on P_b of a noisy vs. ideal channel reference.

The curve for the noisy reference was obtained with the same simulation code as for the ideal reference case, except the ideal reference was replaced with a noisy reference as specified by (4.7.1), and having reference noise variance given by the first line of (4.7.20). The noisy reference was used by the MLSE receiver in calculating the matched filter outputs and the tone correlations, which are the only places a channel reference is required.

The E_b/N_0 numbers of the horizontal axis consider the total energy used to transmit a single bit; the actual E_b of a single bit was reduced by $f = 12.5\%$ to model the energy allocation to a pilot signal.

About 0.3 dB higher than predicted by the analysis, the energy required to measure the channel and the subsequent use of a noisy reference result in approximately a 1.6 dB penalty relative to an ideal, costless reference.

4.8 QOFDM

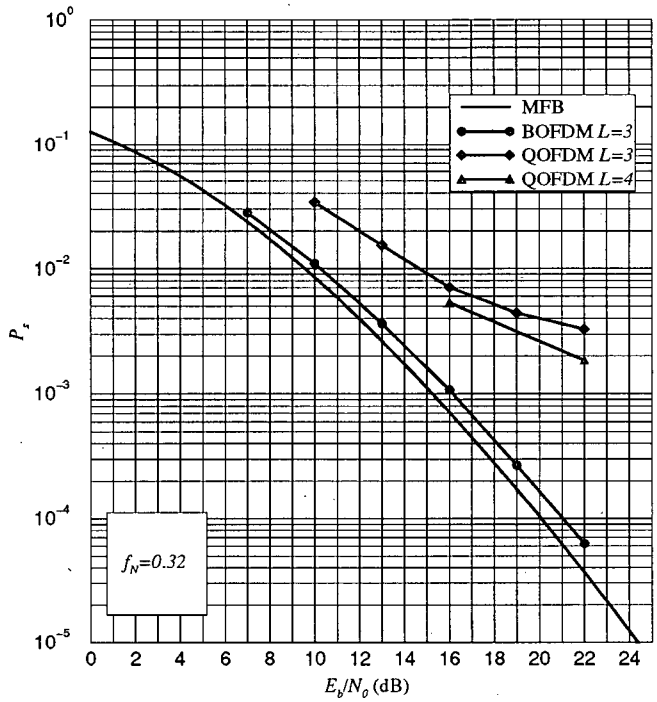

Figure 4.10 Limitation of truncated MLSE applied to QOFDM for $f_N = 0.32$

Thus far we have considered results only for BOFDM where we found the MFB at $P_b \geq 10^{-4}$ can be approached within 1 dB for practical values of L ranging from 3 to 5. Unfortunately, as shown in Figure 4.10, the required L for QOFDM is impractically large. There are two reasons for this. The first is the exponential dependence on L of the number of states which must be extended with each iteration of the truncated MLSE algorithm. For a given L, the number of states is *squared* for QOFDM compared to BOFDM. Secondly, there is more interference with QPSK symbols as opposed to BPSK symbols. This is because in addition to the ISI from nearby tones, there is also intrasymbol[13] distortion of the QPSK symbols.

[13] inphase-quadrature (IQ)

The truncated MLSE receiver in its present form is clearly inadequate for use with QOFDM. A more sophisticated approach, proposed in the context of serial modulation on an ISI channel, reduces the required MLSE constraint length with a linear prefilter [29]. Variations of this idea are developed in Chapter 5, which ultimately make the use of MLSE with QOFDM feasible.

4.9 Conclusion

In this chapter we have derived and simulated a truncated MLSE receiver for OFDM on flat Rayleigh fading channels. The metric used by the sequence estimator is evaluated by the Viterbi algorithm. Key quantities input to the algorithm can be interpreted as frequency-domain matched filter outputs and tone correlations. These quantities can be efficiently evaluated using FFTs. For BOFDM, with the assumption of perfect channel knowledge, it is possible to approach the MFBs of chapter 3 to within 1 dB for bit error rates as low as $P_b = 10^{-4}$ using constraint lengths of only $L = 3 - 5$ for normalized Doppler rates of $f_N = 0.32 - 1.28$. Compared to uncoded serial schemes which are unable to take advantage of channel averaging, there are gains of several dB for OFDM at P_b rates of 10^{-2} and below. These gains are of course contingent on the normalized Doppler rate being high enough to allow channel averaging to occur, but not so high as to require an excessive constraint length. The examples simulated covered the range from $f_N = 0.32 - 1.28$.

The use of pulse shaping of the OFDM block to reduce the spectral sidelobes of its tones was investigated but found to have little effect on P_s. The implication is that the sidelobes themselves are relatively unimportant at the simulated bit error rates, and that the visible error is due to a combination of mainlobe ISI resulting from the flat Rayleigh fading and AWGN.

While useful for comparison purposes, an ideal channel reference is unobtainable in practice. An analysis was presented to determine the dB loss of using a noisy as

opposed to an ideal reference, resulting in an estimated loss of about 1.6 dB for the example considered.

Application of the receiver to QOFDM proved impractical due to the required constraint length, which is longer than that required for BOFDM. Further work with QOFDM is deferred to Chapter 5.

Chapter 5

Linear and Decision Feedback Receivers for OFDM on Flat Rayleigh Fading Channels

In the previous chapter a truncated MLSE receiver was derived for channel-averaging OFDM which was able to approach the MFB quite closely for a range of normalized Doppler rates. A serious limitation of this approach is its complexity, which increases exponentially with the channel constraint length L. For serial modulations, the traditional alternatives have been linear and nonlinear decision feedback equalization techniques whose complexity is only linearly dependent on L. While there has been substantial activity in this area, particularly since the early seventies, to date (1997) there are few publications, [5], [7] and [17] in which equalization techniques have been applied to channel-averaging versions of OFDM.

In this chapter, we look quite closely at the theory of equalization as modified for OFDM in flat Rayleigh fading, ultimately resulting in the derivation of a new decision feedback equalization structure having substantial complexity and performance benefits over the current state of the art.

Section 5.1 derives the optimal linear MMSE equalizer for OFDM in flat Rayleigh fading. Section 5.2 derives a discrete symbol-spaced equalizer, also by the MMSE criterion. Section 5.3 reviews classic DFE as developed for serial modulation and Section 5.4 describes the application of this approach to OFDM in previous work.

The idea of reshaping the overall impulse response of the transmitter, channel, and front-end filter[14] to some desired impulse response (DIR) is reviewed in Section 5.5. Section 5.6 derives a DIR DFE based on the zero-forcing criterion (ZFDIRDFE) and in Section 5.7 an improved DIR DFE based on the MMSE criterion (MSEDIRDFE)

---

[14] The term "front-end filter" is defined in Section 5.3.

is derived. The combination of a Viterbi-type sequence estimator in combination with MSEDIR shaping is considered in Section 5.8.

In Section 5.9 MSE performance surfaces are defined for a simplified fading channel model and used to compare MSE (LMSE) equalization to ZFDIRDFE and MSEDIRDFE. Simulation results for the receivers are presented in Sections 5.10 and 5.8. Section 5.12 summarizes the conclusions of this chapter.

5.1 An Optimal Linear Equalizer

We consider an OFDM system in which the transmitted signal is represented as

$$s(t) = \frac{1}{\sqrt{T_0}} \sum_{n=0}^{N-1} a_n e^{j\frac{2\pi}{T_0}nt}, \quad 0 \le t \le T_0. \tag{5.1.1}$$

In (5.1.1) the pulse shaping $p(t)$ has been assumed rectangular primarily to simplify the notation to follow, but also because the investigation of other pulse shapes in Chapter 4 showed no advantage in terms of P_b.

The received signal is given by

$$\begin{aligned} r(t) &= z(t)\frac{1}{\sqrt{T_0}} \sum_{n=0}^{N-1} a_n e^{j\frac{2\pi}{T_0}nt} + n(t) \\ &= q(t) \sum_{n=0}^{N-1} a_n e^{j\frac{2\pi}{T_0}nt} + n(t) \end{aligned} \tag{5.1.2}$$

where $z(t)$ is the fading waveform, $q(t) = z(t)/\sqrt{T_0}$ and $n(t)$ is independent AWGN. We require for the equalizer a linear structure whose estimate of the n^{th} data symbol is given by

$$\hat{a}_n = \frac{1}{\sqrt{T_0}} \int_0^{T_0} r(t) c_n(t) e^{-j\frac{2\pi}{T_0}nt} dt \tag{5.1.3}$$

and where $c_n(t)$ is a weighting function to be determined by the MMSE criterion. The MSE is

$$\begin{aligned} \text{MSE} &= \mathrm{E}\left[|\hat{a}_n - a_n|^2\right] \\ &= \mathrm{E}\left[|\hat{a}_n|^2\right] - 2\mathrm{E}[\mathrm{Re}[\hat{a}_n a_n^*]] + E_a. \end{aligned} \tag{5.1.4}$$

Expanding $r(t)$ it can be shown that

$$\begin{aligned} \mathrm{E}\left[|\hat{a}_n|^2\right] = \frac{E_a}{T_0} &\int_0^{T_0} q(t)c_n(t) \sum_{m=0}^{N-1} e^{-j\frac{2\pi}{T_0}(n-m)t} dt \\ &\times \int_0^{T_0} q^*(u)c_n^*(u)e^{j\frac{2\pi}{T_0}(n-m)u} du + \frac{N_0}{T_0}\int_0^{T_0} |c_n(t)|^2 dt \end{aligned} \tag{5.1.5}$$

and

$$2\mathrm{E}[\mathrm{Re}[\hat{a}_n a_n^*]] = \frac{E_a}{\sqrt{T_0}}\int_0^{T_0} (q(t)c_n(t) + q^*(t)c_n^*(t))dt. \tag{5.1.6}$$

Combining (5.1.4), (5.1.5) and (5.1.6) we obtain the MSE as a function of $c_n(t)$

$$\begin{aligned} \text{MSE} = \frac{E_a}{T_0} &\int_0^{T_0} q(t)c_n(t) \sum_{m=0}^{N-1} e^{-j\frac{2\pi}{T_0}(n-m)t} dt \\ &\times \int_0^{T_0} q^*(u)c_n^*(u)e^{j\frac{2\pi}{T_0}(n-m)u} du + \frac{N_0}{T_0}\int_0^{T_0} |c_n(t)|^2 dt \\ &- \frac{E_a}{\sqrt{T_0}}\int_0^{T_0} (q(t)c_n(t) + q^*(t)c_n^*(t))dt + E_a. \end{aligned} \tag{5.1.7}$$

The derivative of (5.1.7) w.r.t. $c_n(x)$ is

$$\begin{aligned} \frac{\partial \text{MSE}}{2\partial c_n(x)} = \frac{E_a}{T_0} &\int_0^{T_0} q(t)c_n(t) \sum_{m=0}^{N-1} e^{-j\frac{2\pi}{T_0}(n-m)t} dt \\ &\times q^*(x)e^{j\frac{2\pi}{T_0}(n-m)x} + \frac{N_0}{T_0}c_n(x) \\ &- \frac{E_a}{\sqrt{T_0}}q^*(x). \end{aligned} \tag{5.1.8}$$

Setting $\frac{\partial \text{MSE}}{2\partial c_n(x)} = 0$, scaling by T_0/E_a and substituting $x = u$ we obtain the integral equation whose solution yields $c(t)$

$$\eta^2 c_n(u) = q^*(u) - \sqrt{T_0} q^*(u) \sum_{m=0}^{N-1} e^{j\frac{2\pi}{T_0}(n-m)u} \int_0^{T_0} q(t) c_n(t) e^{-j\frac{2\pi}{T_0}(n-m)t} dt \tag{5.1.9}$$

where $\eta^2 = N_0/E_a$ is the noise to signal ratio.

Defining

$$B_{n-m} = \int_0^{T_0} q(t) c_n(t) e^{-j\frac{2\pi}{T_0}(n-m)t} dt \tag{5.1.10}$$

(5.1.9) can be written as

$$\eta^2 c_n(u) = q^*(u) - \sqrt{T_0} q^*(u) \sum_{m=0}^{N-1} B_{n-m} e^{j\frac{2\pi}{T_0}(n-m)u}. \tag{5.1.11}$$

If we apply the linear operator

$$\mathrm{L}[\cdot] = \int_0^{T_0} q(u)[\cdot] e^{-j\frac{2\pi}{T_0}(n-l)u} du \tag{5.1.12}$$

to (5.1.11) and define

$$V_{n-l} = \int_0^{T_0} |q(u)|^2 e^{-j\frac{2\pi}{T_0}(n-l)u} du \tag{5.1.13}$$

we obtain

$$\eta^2 B_{n-l} = \sqrt{T_0} V_{n-l} - \sum_{m=0}^{N-1} B_{n-m} V_{m-l}, \quad 0 \le n, l \le N-1 \tag{5.1.14}$$

a system of linear equations which can be solved for B_n. Equations (5.1.11), (5.1.13) and (5.1.14) specify the continuous linear MSE equalizer for calculating $\hat{a}_n$.

The solutions to (5.1.14) can be concisely expressed in matrix form. Defining $\mathbf{b_n} = [B_n, B_{n-1}, \ldots, B_{n-N+1}]$, $\mathbf{v_n} = [V_n, V_{n-1}, \ldots, V_{n-N+1}]$ and $\mathbf{V}$ a square Hermitian

Toeplitz matrix with $(m,l)^{th}$ element $\mathbf{V}_{\mathrm{m,l}} = V_{m-l}$, $0 \leq l, m \leq N-1$, (5.1.14) can be written

$$\eta^2 \mathbf{b_n} = \sqrt{T_0}\mathbf{v_n} - \mathbf{b_n}\mathbf{V} \tag{5.1.15}$$

which has for its solutions

$$\mathbf{b_n} = \sqrt{T_0}\mathbf{v_n}\left(\mathbf{V} + \eta^2\mathbf{I}\right)^{-1}. \tag{5.1.16}$$

Equation (5.1.16) indicates that $\mathbf{b_n}$ and consequently the weighting function $c_n(t)$ depend on n, the index of the data symbol being estimated. This dependency arises because ISI experienced by a given data symbol depends on its location (tone) within the OFDM block. For example, centrally located data symbols have several adjacent channel interferers on either side but data symbols at the edges ($n = 0$ and $N-1$) have interferers on only one side.

As can be expected from physical considerations, symmetries can be used to reduce the calculation required. The V_n of (5.1.13) are recognized as the tone correlations defined in Chapter 4. We have $V_n = V_{-n}^*$ and combined with definition of $\mathbf{v_n}$ it follows that $\mathbf{v_n^*} = \mathbf{v_{N-1-n}^B}$, where the superscript B indicates the vector's elements are reversed in order. Accordingly, we also have $\mathbf{b_n^*} = \mathbf{b_{N-1-n}^B}$.

In general, solution of (5.1.16) requires an $N \times N$ matrix inversion followed by $N/2$ row vector by square matrix multiplications. Thus the exact solution for the linear MMSE equalizer is fairly tedious unless N is restricted to be quite small, possibly $N \leq 16$. For the larger values of N used in this work we consider approximations to the optimal solution to reduce the complexity of the equalizer.

5.1.1 Transform Approximation

A very useful simplification would be to eliminate the explicit matrix inversion required by (5.1.16). For this purpose we will apply the discrete frequency Fourier

transform (DFFT)[15] defined by

$$X_n = \int x(t) e^{j\frac{2\pi}{T_0}nt} dt \tag{5.1.17}$$

and its inverse (iDFFT) defined by

$$\tilde{x}(t) = \sum_k X_k e^{j\frac{2\pi}{T_0}kt}. \tag{5.1.18}$$

This is done in Appendix C along with some relevant properties. Taking an iDFFT with respect to the index n of (5.1.14) yields

$$\eta^2 \sum_n B_{n-l} e^{j\frac{2\pi}{T_0}nt} = \sqrt{T_0} \sum_n V_{n-l} e^{j\frac{2\pi}{T_0}nt} - \sum_{m=0}^{N-1} \sum_n B_{n-m} e^{j\frac{2\pi}{T_0}nt} V_{m-l} \tag{5.1.19}$$

or

$$\begin{aligned} \eta^2 e^{-j\frac{2\pi}{T_0}lt} \tilde{b}(t) &= e^{-j\frac{2\pi}{T_0}lt} \sqrt{T_0} \tilde{v}(t) - \tilde{b}(t) \sum_{m=0}^{N-1} V_{m-l} e^{-j\frac{2\pi}{T_0}mt} \\ &= e^{-j\frac{2\pi}{T_0}lt} \sqrt{T_0} \tilde{v}(t) - e^{-j\frac{2\pi}{T_0}lt} \tilde{b}(t) \sum_{k=-l}^{N-1-l} V_k e^{-j\frac{2\pi}{T_0}kt} \end{aligned} \tag{5.1.20}$$

where the tilde accent $\tilde{(\cdot)}$ indicates a periodic or time-aliased function as in $\tilde{x}(t) = T_0 \sum_n x(t - nT_0)$.

The last summation in (5.1.20) is not quite an iDFFT of V_k. However if we assume V_k has significant values only over the range $-L \leq k \leq L$ then $\tilde{v}(t) = \sum_{k=-L}^{L} V_k e^{j\frac{2\pi}{T_0}kt}$. Comparing with (5.1.20), it is apparent that provided $L \leq l \leq N - 1 - L$ we can write

$$\tilde{b}(t) = \frac{\sqrt{T_0}\tilde{v}(t)}{\tilde{v}(t) + \eta^2}. \tag{5.1.21}$$

Note that (5.1.21) reveals $\tilde{b}(t)$ to be a smoothed function relative to $\tilde{v}(t)$, thus the restriction on the significant values of V_k imply a similar restriction on the values of

[15] Not to be confused with the DFT or FFT.

B_k. Therefore we assume that the significant values of B_k are also restricted to the range $-L \leq k \leq L$ and applying this to (5.1.11) yields

$$\eta^2 c(t) = \sqrt{T_0} q^*(t) - q^*(t)\tilde{b}(t) \tag{5.1.22}$$

from which with (5.1.21) it is readily shown that

$$\begin{aligned} c(t) &= \frac{\sqrt{T_0} q^*(t)}{\tilde{v}(t) + \eta^2} \\ &= \frac{\sqrt{T_0} q^*(t)}{T_0 \sum_m |q(t - mT_0)|^2 + \eta^2}. \end{aligned} \tag{5.1.23}$$

For the $q^*(t)$ used in (5.1.2) this reduces to

$$\begin{aligned} c(t) &= \frac{z^*(t)}{|z(t)|^2 + \eta^2} \\ &= \frac{z^*(t)}{x(t)}, \quad 0 \leq t \leq T_0 \end{aligned} \tag{5.1.24}$$

where $x(t) = |z(t)|^2 + \eta^2$ has been introduced due to its frequent appearance in what follows. The function $x(t)$ is the inverse Fourier transform of the channel autocorrelation function in the frequency-domain, i.e. a time-domain version of the channel's power spectrum.

Equation (5.1.23) is an optimal weighting function only for use in estimating those data symbols a_k whose indices are restricted to $L \leq k \leq N - 1 - L$, i.e. the data symbols transmitted near the band edges of the OFDM waveform optimally require different weighting functions determined from the more complicated expressions given previously, even with the restrictions on the significant values of V_k. Practically though, $c(t)$ as given by (5.1.23) is expected to be a useful approximation for estimating all data symbols, since although the data symbols near the band edges are suboptimally detected, they also suffer from the least ISI. We see the difference between exact equalization with $c_n(t)$ and approximate equalization with $c(t)$ is mainly a matter of edge effects. Thus there should be little difference in P_b, averaged over all N tones, when $L \ll N$.

Note that except for a-domain change (5.1.23) has the familiar form of a continuous matched filter followed by a filter having a periodic response implementable as an infinitely long tapped delay line [30]. However, since in this case the OFDM block has finite duration T_0, it is convenient to determine $c(t)$ directly in the time-domain using (5.1.23) or (5.1.24).

5.1.2 Aliasing Approximation

The two previous works, [5] [7][16] concerning the equalization of channel averaging OFDM in fading both used a discrete model of the OFDM signal. In the notation of this work[17], the model for the transmitted signal is

$$s_m = \frac{1}{\sqrt{N}} \sum_{n=0}^{N-1} a_n e^{j\frac{2\pi}{N}nm}, \quad 0 \leq m \leq N-1 \tag{5.1.25}$$

and for the received signal

$$r_m = z_m s_m + n_m, \quad 0 \leq m \leq N-1. \tag{5.1.26}$$

These equations may be interpreted as the result of sampling the waveforms of the continuous model at rate N/T_0 and then setting the scaling factor $1/\sqrt{T_0} = 1/\sqrt{N}$. As discussed in Chapter 4 this is a sub-Nyquist sampling rate and results in an aliasing effect which causes all tones to have the same pattern of ISI. Viewed in the frequency-domain, the linear convolution of the channel impulse response with the data is modified by the sub-Nyquist sampling into a circular convolution of an aliased impulse response with the data. Thus the rate N/T_0 sampling increases the level of ISI irreversibly, but following the arguments of the Transform Approximation this effect should be quite small on the error rate averaged over all tones, provided $L \ll N$. The principal benefit of the aliasing approximation is that the optimal (given the sampling rate) MMSE equalizer

[16] A third, [17] was concerned with an FM version of OFDM, OFDM-FM.

[17] The transform scaling has been adjusted to normalize energies; $E_s = E_a$.

has a weighting function which is independent of the data symbol's index as shown in Section 5.2. This follows directly from the fact that a finite discrete sequence and its DFT can be viewed as periodic functions.

5.2 A Discrete T_s Spaced Linear Equalizer

Accepting a sampling interval of $T_0/N = T_s$ seconds at the input to a discrete equalizer, we derive a linear MMSE (LMSE) equalizer which is optimal from that point on. The desired estimate is formed as

$$\hat{a}_n = \frac{1}{\sqrt{N}} \sum_{m=0}^{N-1} r_m c_m e^{-j\frac{2\pi mn}{N}}. \tag{5.2.1}$$

Substituting (5.1.25), (5.2.1) and (5.1.26) into (5.1.4) it can be shown that the normalized MSE for the discrete equalizer is

$$\frac{\text{MSE}}{E_a} = \sum_{m=0}^{N-1} |c_m|^2 |q_m|^2 + \frac{\eta^2}{N} \sum_{m=0}^{N-1} |c_m|^2 - \frac{1}{\sqrt{N}} \sum_{m=0}^{N-1} (c_m q_m + c_m^* q_m^*) + 1. \tag{5.2.2}$$

Setting $\frac{\partial \text{MSE}}{2E_a \partial c_l} = 0$ yields an equation for c_l

$$c_l |q_l|^2 + \frac{\eta^2}{N} - q_l^* = 0 \tag{5.2.3}$$

which has the solution

$$\begin{aligned} c_l &= \frac{\sqrt{N} q_l^*}{N|q_l|^2 + \eta^2} \\ &= \frac{z_l^*}{|z_l|^2 + \eta^2} \\ &= \frac{z_l^*}{x_l}, \qquad 0 \le l \le N-1 \end{aligned} \tag{5.2.4}$$

for $q_l = z_l/\sqrt{N}$ and $x_l = |q_l|^2 + \eta^2$. Equations (5.1.24) and (5.2.4) are deceptively similar in form, yet the approximations each represents are quite distinct. Again, with a-domain change, the equalizer can be recognized as a matched filter followed by a tapped delay

line, but now and without further approximation the delay line is finite with N elements used to circularly convolve the outputs of the matched filter. While in this case it is more efficient to implement the equalizer directly in the time-domain as specified by (5.2.4) and (5.2.1), the frequency-domain interpretation becomes important when the equalizer is generalized to include decision feedback.

The most important point concerning (5.2.4) is that like (5.1.24) it does not require an inversion of an $N \times N$ matrix, as does the expression in (5.1.16).

An expression essentially similar[18] to (5.2.4) was presented in [5]. In that work, the error criterion was defined as the difference between an estimate of the transmitted waveform and the actual transmitted waveform

$$\epsilon_m = \hat{s}_m - s_m \tag{5.2.5}$$

instead of the estimated and actual data as defined by (5.1.4). Thus (5.2.4) is not a new result, but merely establishes the equivalence of the two criteria for this case.

5.2.1 Optimal Linear Mean Squared Error

Unfortunately it is not possible to get an exact expression for P_b, thus we resort to the more tractable MSE. The normalized MSE resulting from use of the optimal c_l as given by (5.2.4) reduces to a simple form. Rearranging (5.2.2) yields

$$\frac{\text{MSE}}{E_a} = \frac{1}{N}\sum_{m=0}^{N-1} c_m x_m c_m^* - \frac{1}{N} 2\text{Re}\left[\sum_{m=0}^{N-1} c_m z_m\right] + 1 \tag{5.2.6}$$

and applying (5.2.4) yields

$$\frac{\text{MMSE}}{E_a} = 1 - \frac{1}{N}\sum_{m=0}^{N-1} c_m^O z_m \tag{5.2.7}$$

or

$$\frac{\text{MMSE}}{E_a} = \frac{\eta^2}{N}\sum_{m=0}^{N-1} \frac{1}{\phi_{z_m} + \eta^2} \tag{5.2.8}$$

where the superscript $(\cdot)^O$ designates optimal.

[18] An adjacent channel interference term was used in place of the noise term here.

5.3 Classic Decision Feedback Equalization

As with linear equalization, nearly all work with decision feedback equalization (DFE) has occurred within the context of serial modulation on an ISI channel in the time-domain. Consequently, the following description is presented within that context.

The structure of the classic DFE [31] is shown in Figure 5.1.

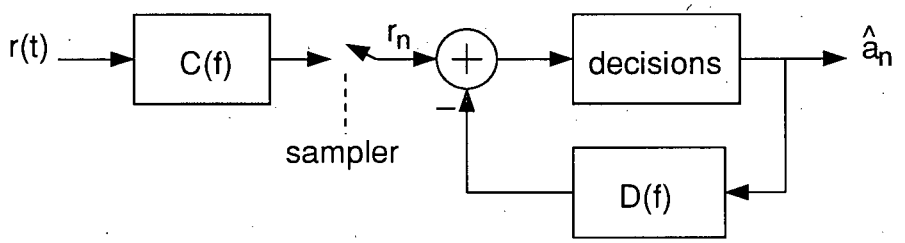

Figure 5.1 Classic DFE structure

It is designed to work with a received signal of the form

$$r(t) = \sum_{n=-\infty}^{\infty} a_n h(t - nT_s) + n(t) \tag{5.3.1}$$

where $h(t)$ is the combined response of the transmitter pulse shaping filter and the channel impulse response. The noise $n(t)$ is generally assumed to be AWGN.

There are two basic sections, the feedforward section containing the feedforward filter $C(f)$ operating on the received waveform, and the feedback section containing the feedback filter $D(f)$ operating on previous decisions. The impulse response of either filter may be finite or infinite in length. The feedforward section is a linear equalizer optimally consisting of a matched filter followed by a sampler and a tapped delay line with spacing equal to the symbol duration T_s, or optionally may consist of a fractionally spaced equalizer operating above the Nyquist rate [9] which incorporates matched filtering as part of its overall response. The feedback filter has the structure of a tapped delay line with spacing T_s and is used to form an estimate of the ISI due to the previously detected

data. ISI from future data is minimized by $C(f)$. The impulse responses of $C(f)$ and $D(f)$ are generally chosen by either the MMSE or zero-forcing (ZF)[19] criteria.

The idea of the DFE is to subtract this calculated ISI from the sample entering the decision element before making the current decision. Assuming previous decisions are correct, the DFE makes a decision based on a sample with less residual ISI than a comparable purely linear equalizer, and should therefore have a lower error rate. It has been shown [30] that with the perfect decision assumption, the MSE of the MMSE DFE is upper bounded by the MSE of the purely linear LMSE equalizer.

A potential problem that arises with DFE is error propagation due to incorrect decisions in the feedback section. While the derivation of a DFE requires the assumption of ideal decisions for tractability, to be useful a DFE must feed back data from previous decisions, some of which will be in error. Thus there is a tradeoff regarding the length of the feedback section. A long section removes more ISI when decisions are correct, but risks greater error propagation when an error is made.

5.4 Frequency Domain Zero-Forcing Decision Feedback Equalization

A technique called frequency-domain zero-forcing equalization (FDZFDFE) was developed for OFDM and presented in [7]. The basic idea is to immediately convert the received signal after sampling into the frequency-domain, and then to apply the classic [9] matrix-based DFE structure, originally posed in the time-domain for serial modulation, to the resulting signal.

In the notation of this work (5.1.26) is transformed into

$$R_k = \frac{1}{\sqrt{N}} \sum_{m=0}^{N-1} a_n Z_{k-n} + N_k \tag{5.4.1}$$

[19] ZF: elimination of ISI at the sampling instant over a certain range.

where $Z_k = \frac{1}{\sqrt{N}} \sum_{m=0}^{N-1} z_m e^{-j\frac{2\pi}{N}mk}$ and $N_k = \frac{1}{\sqrt{N}} \sum_{m=0}^{N-1} n_m e^{-j\frac{2\pi}{N}mk}$. The FDZFDFE has the form

$$\hat{a}_n = \sum_{k=-F}^{0} C_k R_{n-k} + \sum_{k=1}^{B} D_k \hat{a}_{n-k} \tag{5.4.2}$$

where the coefficients C_k were determined by the inversion of an $(F+1) \times (F+1)$ channel dependent matrix and the actual data, rather than the decisions, was used in the feedback section [32]. $F+1$ is the number of C_k tap coefficients and B the number of feedback coefficients. In [7] F was chosen as 10 and B as 15 for $N = 512$ and a normalized Doppler rate of $f_N = 2.05$. Simulation results showed FDZFDFE required 6.5 dB less E_b/N_0 than linear ZFE, and 2 dB less than an approximate method presented in [5], both at $P_s = 10^{-3}$. Thus these results represent the best P_s performance obtained for OFDM prior to the work being reported in this thesis.

5.5 Obtaining a Desired Impulse Response (DIR)

With the classic DFE structure the causal[20] component of the combined transmitter impulse response and channel impulse response may be so long as to preclude complete cancellation of ISI from previous decisions, either due to the required filter length or error propagation effects. Typically a workable length is found through simulation which is a compromise between error rate and complexity.

An alternative to the simple truncation described above is to reshape the combined impulse response to some desired impulse response (DIR) of fixed length. An important but not obvious point is the selection of the DIR. Simple examples include the preceding truncation, and the unit sample function which reduces to linear ZFE.

More sophisticated examples, in the context of serial modulation, have appeared in [29], [33], and [34]. The first two publications are principally concerned with obtaining a

[20] causal: that part defined for $t \geq 0$.

shortened impulse response to simplify a subsequent MLSE, but are of course applicable in the context of DFE as well. In [33], the DIR chosen was a truncated version of the original response and was shown to be an improvement over simple truncation without shaping.

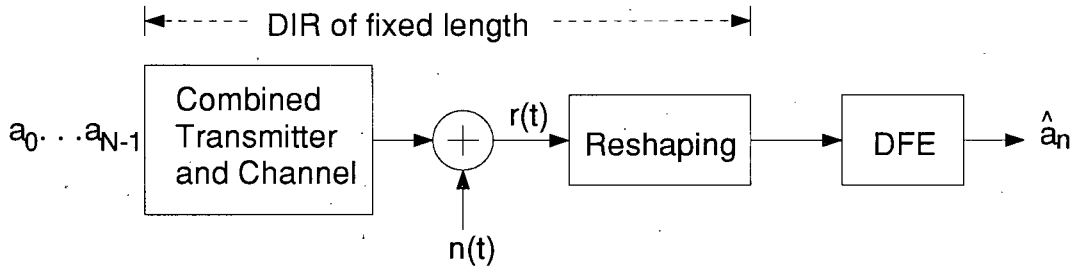

Figure 5.2 Forcing a DIR of fixed length before DFE

In [29] an MSE criterion in combination with a total energy constraint on the DIR is used to select the DIR, which is found by determining the eigenvector corresponding to the minimum eigenvalue of a certain channel dependent matrix. Included comparisons showed error rate improvements over the shaped truncation method of [33].

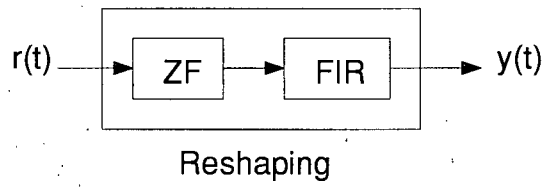

Figure 5.3 DIR obtained by concatenating ZF and FIR filters

Subsequently [34] suggested modifying a ZFE to obtain a finite impulse response for DFE. The idea is to obtain the DIR by concatenating a linear ZF filter with an FIR filter of fixed length. The FIR is determined by fixing the 0^{th} tap weight to a constant, and then selecting the remaining coefficients to minimize the noise variance at the equalizer output. Noise variance estimates indicated that most of the attainable improvement required a DIR length of only 4 or 5 for the channel investigated.

5.6 A Zero-Forcing Desired Impulse Response Decision Feedback Equalizer (ZFDIRDFE)

In the following we apply the approach of [34] in order to obtain a ZFDIRDFE for OFDM.

The estimate of the n^{th} data symbol is given by

$$\hat{a}_n = \frac{1}{\sqrt{N}} \sum_{k=0}^{N-1} C_k R_{n-k} - \frac{1}{\sqrt{N}} \sum_{k=1}^{B} D_k \hat{a}_{n-k} \tag{5.6.1}$$

where $R_k = \frac{1}{\sqrt{N}} \sum_{m=0}^{N-1} r_m e^{-j\frac{2\pi}{N}mk}$ is the DFT of r_m given by (5.1.26), and C_k and D_k are the coefficients of the equalizer filters.

Note that it is rather ambiguous to refer to C_k as a feedforward filter in this context for two reasons. The first is due to the circular nature of the ISI as viewed in the frequency-domain. The index k of Z_k increments and decrements modulo N, thus there is no clear distinction between past and future ISI. The second reason is that C_k will be designed to remove ISI due to a_{n-k} for $B < k \leq N-1$ when the estimate $\hat{a}_n$ is being formed. To avoid this ambiguity we will refer to C_k as the front-end filter, and continue to refer to D_k as the feedback filter.

Rather than perform the N circular convolutions indicated by the first term of (5.6.1) directly, it is more efficient to define a new sequence

$$y_m = r_m c_m \tag{5.6.2}$$

where

$$c_m = \frac{1}{\sqrt{N}} \sum_{k=0}^{N-1} C_k e^{j\frac{2\pi}{N}km} \tag{5.6.3}$$

and form the estimate

$$\hat{a}_n = Y_n - \frac{1}{\sqrt{N}} \sum_{k=1}^{B} D_k \hat{a}_{n-k} \tag{5.6.4}$$

where all N Y_n are obtained simultaneously from an FFT of y_m.

Of all the possible ZFE's, it is shown in [35] that the ZFE having a matched filter (MFZFE) is the ZFE which maximizes the SNR at the equalizer output. The output of a matched filter applied to the received signal (5.1.26) is

$$\begin{aligned} u_m &= r_m z_m^* \\ &= |z_m|^2 s_m + n_m z_m^* \\ &= \phi_{z_m} s_m + n_m z_m^* \end{aligned} \tag{5.6.5}$$

where

$$\phi_{z_m} = |z_m|^2. \tag{5.6.6}$$

Applying u_m to a filter with frequency response $1/\phi_{z_m}$ yields

$$u_m' = s_m + \frac{n_m z_m^*}{\phi_{z_m}}. \tag{5.6.7}$$

The sample u_m' can be interpreted as the MFZFE estimate of s_m. It is applied to a filter with response d_m to obtain a DIR of d_m, i.e.

$$c_m = \frac{z_m^* d_m}{\phi_{z_m}} \tag{5.6.8}$$

which yields for y_m

$$\begin{aligned} y_m &= s_m d_m + \frac{n_m z_m^* d_m}{\phi_{z_m}} \\ &= s_m d_m + n_{y_m} \end{aligned} \tag{5.6.9}$$

where $n_{y_m} = \frac{n_m z_m^* d_m}{\phi_{z_m}}$ is a colored Gaussian noise term. Its average variance is

$$\sigma_{n_y}^2 = \frac{N_0}{N} \sum_{m=0}^{N-1} \frac{|d_m|^2}{\phi_{z_m}}. \tag{5.6.10}$$

The noise variance of (5.6.10) is minimized by the selection of the frequency-domain coefficients D_k where

$$d_m = \frac{1}{\sqrt{N}} \sum_{k=0}^{B} D_k e^{j\frac{2\pi}{N}mk} \tag{5.6.11}$$

and $D_0 = \sqrt{N}$. Note this method has the peculiar feature that D_k must have some constraint or the minimum variance solution would $D_k = 0$, $0 \leq k \leq B$, i.e. no output at all.

Defining

$$h_m = 1/\phi_{z_m} \tag{5.6.12}$$

(5.6.10) can be written as

$$\sigma_{n_y}^2 = \frac{N_0}{N} \sum_{m=0}^{N-1} d_m^* h_m d_m \tag{5.6.13}$$

which has the equivalent frequency-domain expression

$$\sigma_{n_y}^2 = \frac{N_0}{N\sqrt{N}} \sum_{n=0}^{B} D_n \sum_{l=0}^{B} D_l^* H_{l-n} \tag{5.6.14}$$

where $H_k = \frac{1}{\sqrt{N}} \sum_{m=0}^{N-1} h_m e^{-j\frac{2\pi}{N}mk}$.

Defining $\mathbf{d}^{\mathrm{H}} = [D_1, D_2, \ldots, D_B]^*$, $\mathbf{h}^{\mathrm{H}} = [H_1, H_2, \ldots H_B]^*$ and $B \times B$ Hermitian Toeplitz matrix $\mathbf{H}$ with $(l,n)^{th}$ element $\mathbf{H}_{\mathrm{l,n}} = H_{l-n}$ (5.6.13) in matrix form is

$$\sigma_{n_y}^2 = \frac{N_0}{N\sqrt{N}} \Big(N H_0 + 2\sqrt{N} \mathrm{Re}\Big[\mathbf{d}^{\mathrm{H}}\mathbf{h}\Big] + \mathbf{d}^{\mathrm{H}}\mathbf{H}\mathbf{d} \Big). \tag{5.6.15}$$

The value of $\mathbf{d}$ for which (5.6.15) attains its minimum is determined by setting $\frac{\partial \sigma_{n_y}^2}{2\partial \mathbf{d}} = 0$. This yields

$$\frac{N_0}{N\sqrt{N}} \Big(\sqrt{N}\mathbf{h} + \mathbf{H}\mathbf{d} \Big) = 0 \tag{5.6.16}$$

which has the solution

$$\mathbf{d} = -\sqrt{N}\mathbf{H}^{-1}\mathbf{h}. \tag{5.6.17}$$

Using (5.6.17) in (5.6.15) we obtain a frequency-domain expression for the optimal noise variance

$$\sigma_{n_y}^{2^O} = \frac{N_0}{\sqrt{N}} \Big(H_0 - \mathbf{h}^{\mathrm{H}}\mathbf{H}^{-1}\mathbf{h} \Big). \tag{5.6.18}$$

5.6.1 Optimal Mean Squared Error

Taking a DFT of (5.6.9) to obtain Y_n yields

$$Y_n = \frac{1}{\sqrt{N}} \sum_{k=0}^{B} D_k a_{n-k} + N_{Y_n} \tag{5.6.19}$$

where $N_{Y_n} = \frac{1}{\sqrt{N}} \sum_{m=0}^{N-1} n_{y_m} e^{-j\frac{2\pi}{N}mn}$ is the DFT of n_{y_m}. Using (5.6.19) in (5.6.4) yields

$$\hat{a}_n = a_n + N_{Y_n} \tag{5.6.20}$$

which shows that the ZFDIRDFE has no residual ISI when previous decisions are correct. Therefore for this equalizer the MSE is equivalent to the noise variance (5.6.18), and the normalized MSE, for the optimal choice of D_k is

$$\text{mse}^{O} = \frac{\eta^2}{\sqrt{N}} \Big(H_0 - \mathbf{h}^{\mathrm{H}} \mathbf{H}^{-1} \mathbf{h} \Big). \tag{5.6.21}$$

5.6.2 Algorithm Summary

1. matrices h and **H** are formed using (5.6.6) and (5.6.12)
2. **H** is inverted to obtain **d** from (5.6.17)
3. (5.6.11) yields d_m, (5.6.8) c_m, and (5.6.2) with an FFT yields Y_n
4. $\hat{a}_n$ is obtained from (5.6.4)

The first three steps need only be performed once per OFDM block. The final step is repeated once per data symbol.

5.6.3 Structural Comparison to FDZFDFE

An interesting structural difference between ZFDIRDFE and FDDIRDFE concerns the pattern of ISI which is cancelled. The ZFDIRDFE exploits the circularity of the ISI to cancel all ISI except that from B previous (in a circular sense) data symbols. The FDZFDFE does not exploit the circularity; consequently less ISI is cancelled by the front-end filter and B must be larger for FDZFDFE than ZFDIRDFE.

Of course, the FDZFDFE could be modified to provide the same ISI cancellation pattern as does the ZFDIRDFE. However this could pose a problem for large F because the complexity of the required matrix inversion varies with $(F+1)^2$.

5.7 A Minimum Mean Squared Error Desired Impulse Response Decision Feedback Equalizer (MSEDIRDFE)

While the ZFDIRDFE is interesting for its structure and performance, it is reasonable to question whether the ZF criterion is a very good choice to use for the basis of a nonlinear DIRDFE. Certainly in the context of *linear* equalization for serial modulations it is well understood that ZF generally causes increased noise enhancement relative to a comparable LMSE. The LMSE results in a lower error rate than the ZFE when the combination of noise and residual ISI is less damaging than no ISI in combination with enhanced noise, and this is generally found to be the case[21].

Motivated by this observation we apply a minimum MSE criterion in the following to the selection of a DIR to derive an MSEDIRDFE for OFDM. Aside from changes to accommodate OFDM in fading, the formulation here differs from [29] in that there is no energy constraint placed on the DIR, and the DIR is not obtained in terms of an eigenvector.

In order obtain the same structure for the MSEDIRDFE as found for the ZFDIRDFE, the form of the estimate is unchanged. It is repeated here for convenience.

The estimate of the n^{th} data symbol is given by

$$\hat{a}_n = \frac{1}{\sqrt{N}} \sum_{k=0}^{N-1} C_k R_{n-k} - \frac{1}{\sqrt{N}} \sum_{k=1}^{B} D_k \hat{a}_{n-k} \tag{5.7.1}$$

where $R_k = \frac{1}{\sqrt{N}} \sum_{m=0}^{N-1} r_m e^{-j\frac{2\pi}{N}mk}$ is the DFT of r_m given by (5.1.26), and C_k and D_k are the equalizer coefficients. In the time-domain c_m is again given by (5.6.3), but the

[21] Constant amplitude, purely phase distorting channels are an exception since there is no noise enhancement problem.

expression for d_m in the context of MSEDIRDFE is modified to

$$d_m = \frac{1}{\sqrt{N}} \sum_{k=1}^{B} D_k e^{j\frac{2\pi}{N}km}. \tag{5.7.2}$$

Rather than perform the N circular convolutions indicated by the first term of (5.7.1) directly, it is more efficient to define a new sequence

$$y_m = r_m c_m \tag{5.7.3}$$

and form the estimate

$$\hat{a}_n = Y_n - \frac{1}{\sqrt{N}} \sum_{k=1}^{B} D_k \hat{a}_{n-k} \tag{5.7.4}$$

where all N Y_n are obtained simultaneously from an FFT of y_m.

We begin with a coupled equation approach [36] to obtain some insight into the nature of the front–end filter C_k and to derive some expressions for the MSE of relatively simple form.

Defining

$$\mathbf{c}^{\mathrm{H}} = \frac{1}{\sqrt{N}}[C_0, C_1, \ldots, C_{N-1}], \tag{5.7.5}$$

$$\mathbf{d}^{\mathrm{H}} = \frac{1}{\sqrt{N}}[D_1, D_2, \ldots, D_B], \tag{5.7.6}$$

$$\mathbf{r}_{\mathbf{n}}^{\mathrm{T}} = [R_{n-0}, R_{n-1}, \ldots, R_{n-N+1}], \tag{5.7.7}$$

and

$$\mathbf{a}_{\mathbf{n}}^{\mathrm{T}} = [a_{n-0}, a_{n-1}, \ldots, a_{n-B}] \tag{5.7.8}$$

(5.7.1) in matrix form is

$$\begin{aligned} \hat{a}_n &= \mathbf{c}^{\mathrm{H}}\mathbf{r}_{\mathbf{n}} - \mathbf{d}^{\mathrm{H}}\mathbf{a}_{\mathbf{n}} \\ &= \mathbf{f}^{\mathrm{H}}\mathbf{t} \end{aligned} \tag{5.7.9}$$

where $\mathbf{f}^{\mathrm{H}} = \left[\mathbf{c}^{\mathrm{H}}, -\mathbf{d}^{\mathrm{H}}\right]$ and $\mathbf{t}^{\mathrm{T}} = \left[\mathbf{r}_{\mathbf{n}}^{\mathrm{T}}, \mathbf{a}_{\mathbf{n}}\right]$. It is well known [23] that the MMSE solution for $\mathbf{f}$ satisfies

$$\mathbf{\Phi f} = \mathbf{p} \tag{5.7.10}$$

where

$$\mathbf{\Phi} = \begin{bmatrix} \mathrm{E}\left[\mathbf{r_n r_n^H}\right] & \mathrm{E}\left[\mathbf{r_n a_n^H}\right] \\ \mathrm{E}\left[\mathbf{a_n r_n^H}\right] & \mathrm{E}\left[\mathbf{a_n a_n^H}\right] \end{bmatrix} \tag{5.7.11}$$

and

$$\mathbf{p} = \begin{bmatrix} \mathrm{E}[\mathbf{r_n} a_n^*] \\ \mathrm{E}[\mathbf{a_n} a_n^*] \end{bmatrix}. \tag{5.7.12}$$

Evaluating the moments

$$\mathrm{E}\left[R_{n-l} R_{n-k}^*\right] = \frac{E_a}{\sqrt{N}} \Phi_{Z_{k-l}} + N_0 \delta_{k-l} \tag{5.7.13}$$

$$\mathrm{E}\left[R_{n-l} a_{n-k}^*\right] = \frac{E_a}{\sqrt{N}} Z_{k-l} \tag{5.7.14}$$

and

$$\mathrm{E}\left[a_{n-l} a_{n-k}^*\right] = E_a \delta_{k-l} \tag{5.7.15}$$

where

$$\Phi_{Z_k} = \frac{1}{\sqrt{N}} \sum_{m=0}^{N-1} Z_{m+k} Z_m^*. \tag{5.7.16}$$

Expanding (5.7.10) yields a pair of coupled which must be simultaneously satisfied;

$$\sum_{k=0}^{N-1} \left(\frac{1}{\sqrt{N}} \Phi_{Z_{k-l}} + \eta^2 \delta_{k-l} \right) C_k^* - \frac{1}{\sqrt{N}} \sum_{k=1}^{B} Z_{k-l} D_k^* = Z_{-l}, \quad 0 \le l \le N-1 \tag{5.7.17}$$

and

$$\frac{1}{\sqrt{N}} \sum_{k=0}^{N-1} Z_{l-k}^* C_k^* - D_l^* = \sqrt{N} \delta_l, \quad 1 \le l \le B. \tag{5.7.18}$$

The form of C_k can be deduced by expanding $\Phi_{Z_{k-l}}$ in (5.7.17) and defining Q_i, the linearly equalized fading samples (frequency-domain) as

$$Q_i = \frac{1}{\sqrt{N}} \sum_{k=0}^{N-1} Z_{i-k} C_k \tag{5.7.19}$$

which yields

$$\eta^2 C_l^* = Z_{-l} + \frac{1}{\sqrt{N}} \sum_{k=1-l}^{B-l} Z_k D_{k+l}^* - \frac{1}{\sqrt{N}} \sum_{k=0}^{N-1} Q_{k+l}^* Z_k, \quad 1 \le l \le B \tag{5.7.20}$$

from which it is apparent

$$C_l = \frac{1}{\sqrt{N}} \sum_{k=0}^{N-1} Z_k^* W_{k+l}. \tag{5.7.21}$$

Equation (5.7.21) shows that the front-end filter can be viewed as the cascade of a filter matched to the channel fading waveform followed by an additional feedback dependent filter specified by the coefficients W_k.

The W_k expressed in terms of the DIR and linearly equalized fading samples are

$$\begin{aligned} W_0 &= \frac{\sqrt{N} - Q_0}{\eta^2} \\ W_k &= \frac{D_k - Q_k}{\eta^2}, \quad 1 \le k \le B \\ W_k &= \frac{-Q_k}{\eta^2}, \quad B+1 \le k \le N-1. \end{aligned} \tag{5.7.22}$$

We shall return to (5.7.22) with further developments.

Using (5.7.21) and applying the linear operator

$$L[\cdot] = \frac{1}{\sqrt{N}} \sum_{l=0}^{N-1} [\cdot] Z_{-l-p}^* \tag{5.7.23}$$

to (5.7.17) yields

$$\frac{1}{N} \sum_{k=0}^{N-1} \Phi_{Z_k} \sum_{m=0}^{N-1} \Phi_{Z_{m+p}} W_{m+k}^* + \frac{\eta^2}{\sqrt{N}} \sum_{m=0}^{N-1} \Phi_{Z_{m+p}} - \frac{1}{\sqrt{N}} \sum_{m=1}^{B} \Phi_{Z_{m+p}} D_m^* = \Phi_{Z_p} \qquad 0 \le p \le N-1. \tag{5.7.24}$$

Transforming (5.7.24) and dividing by ϕ_{z_m} yields

$$\phi_{z_m} w_m^* + \eta^2 w_m^* - d_m^* - 1 = 0 \tag{5.7.25}$$

from which we obtain an explicit time-domain expression for the optimal w_m in terms of the feedback filter

$$w_m^O = \frac{(d_m + 1)}{\phi_{z_m} + \eta^2} \tag{5.7.26}$$

or equivalently

$$c_m^O = \frac{z_m^*(d_m + 1)}{\phi_{z_m} + \eta^2}. \tag{5.7.27}$$

Equation (5.7.27) shows that the time-domain response of the front–end filter for MSEDIRDFE is the product of the responses for the LMSE equalizer and a factor based on the DIR. This factor has the frequency-domain transform

$$(d_m + 1) \rightleftharpoons \left[\sqrt{N}, D_1, D_2, \ldots, D_B\right] \tag{5.7.28}$$

which is the DIR augmented with a coefficient $D_0 = \sqrt{N}$. Defining the frequency-domain sequence in (5.7.28) as the augmented DIR, we see that MSEDIRDFE determines an augmented DIR which is effectively constrained to have $D_0 = \sqrt{N}$.

Further insight is obtained by rewriting (5.7.18) as

$$\frac{1}{\sqrt{N}} \sum_{k=0}^{N-1} \Phi_{Z_{k-l}} W_k^* - D_k^* - \sqrt{N}\delta_k = \Gamma_k \tag{5.7.29}$$

where

$$\Gamma_k = \begin{cases} 0, & 1 \le k \le B \\ \text{undefined}, & \text{otherwise.} \end{cases} \tag{5.7.30}$$

Transforming and conjugating (5.7.29)

$$\phi_{z_m} w_m^* - d_m^* - 1 = \gamma_{-k} \tag{5.7.31}$$

and subtracting from (5.7.25) yields

$$w_m = \frac{-\gamma_{-k}^*}{\eta^2} \tag{5.7.32}$$

or with a further transform

$$W_k = \frac{-\Gamma_k^*}{\eta^2}. \tag{5.7.33}$$

From the definition of Γ_k in (5.7.30) and assuming $\eta^2 > 0$, (5.7.33) shows that $W_k = 0$, $1 \leq k \leq B$, precisely the range where the DIR is allowed nonzero values. This in turn implies, with (5.7.22), that $D_k = Q_k, \quad 1 \leq k \leq B$, i.e. the DIR coefficients are exactly equal to the linearly equalized fading samples.

There still remains the problem of determining the DIR. Recalling the MSE

$$\begin{aligned} \text{MSE} &= \mathrm{E}\left[|\hat{a}_n - a_n|^2\right] \\ &= \mathrm{E}\left[|\hat{a}_n|^2\right] - 2\mathrm{E}[\mathrm{Re}[\hat{a}_n a_n^*]] + E_a \end{aligned} \tag{5.7.34}$$

we seek the joint minimization of (5.7.34) with respect to C_k and D_k. For the first term in (5.7.34)

$$\begin{aligned} \mathrm{E}\left[|\hat{a}_n|^2\right] = \frac{1}{N}\sum_{l=0}^{N-1}\sum_{k=0}^{N-1} C_l C_k^* \mathrm{E}\left[R_{n-l}R_{n-k}^*\right] - 2\mathrm{Re}\left[\frac{1}{N}\sum_{l=0}^{N-1}\sum_{k=1}^{B} C_l D_k^* \mathrm{E}\left[R_{n-l}a_{n-k}^*\right]\right] \\ + \frac{1}{N}\sum_{l=1}^{B}\sum_{k=1}^{B} D_l D_k^* \mathrm{E}\left[a_{n-l}a_{n-k}^*\right]. \end{aligned} \tag{5.7.35}$$

Evaluating the moments in (5.7.35) and defining

$$X_{k-l} = \Phi_{Z_{k-l}} + \sqrt{N}\,\eta^2 \delta_{k-l} \tag{5.7.36}$$

yields

$$\begin{aligned} \frac{\mathrm{E}\left[|\hat{a}_n|^2\right]}{E_a} = \frac{1}{N\sqrt{N}}\sum_{l=0}^{N-1}\sum_{k=0}^{N-1} C_l C_k^* X_{k-l} - 2\mathrm{Re}\left[\frac{1}{N\sqrt{N}}\sum_{l=0}^{N-1}\sum_{k=1}^{B} C_l D_k^* Z_{k-l}\right] \\ + \frac{1}{N}\sum_{l=1}^{B} |D_l|^2. \end{aligned} \tag{5.7.37}$$

Similarly, the second and third terms of (5.7.34) are

$$\frac{2\mathrm{Re}[\hat{a}_n a_n^*]}{E_a} = 2\mathrm{Re}\left[\frac{1}{N}\sum_{l=0}^{N-1} C_l Z_{-l}\right] \tag{5.7.38}$$

and

$$\frac{\mathrm{E}\left[|a_n|^2\right]}{E_a} = 1. \tag{5.7.39}$$

Combining (5.7.34), (5.7.37) and (5.7.38) and transforming to the time-domain yields the normalized MSE

$$\begin{aligned}\frac{\mathrm{MSE}}{E_a} = \frac{1}{N}\sum_{m=0}^{N-1} c_m x_m c_m^* - \frac{1}{N}\sum_{m=0}^{N-1} 2\mathrm{Re}[c_m^* z_m^* d_m] \\ - \frac{1}{N}\sum_{m=0}^{N-1} 2\mathrm{Re}[c_m^* z_m^*] + \frac{1}{N}\sum_{m=0}^{N-1} d_m d_m^* + 1\end{aligned} \tag{5.7.40}$$

in terms of c_m and d_m. Expanding the first term of (5.7.40) with (5.7.27) and expanding d_m^* with its transform yields

$$\begin{aligned}\sum_{m=0}^{N-1} c_m x_m c_m^* &= \sum_{m=0}^{N-1} \frac{(z_m^* + z_m^* d_m)(z_m + z_m d_m^*)}{x_m} \\ &= \sum_{m=0}^{N-1} \frac{(z_m^* + z_m^* d_m)\left(z_m + z_m \frac{1}{\sqrt{N}} \sum_{l=1}^{B} D_l^* e^{-j\frac{2\pi}{N}lm}\right)}{x_m}.\end{aligned} \tag{5.7.41}$$

This expression can now be differentiated w.r.t. D_k to obtain

$$\begin{aligned}\frac{\partial}{2\partial D_k}\sum_{m=0}^{N-1} c_m x_m c_m^* &= \frac{1}{\sqrt{N}}\sum_{m=0}^{N-1}(g_m + g_m d_m)e^{-j\frac{2\pi}{N}km} \\ &= G_k + \frac{1}{\sqrt{N}}\sum_{l=1}^{B} D_l G_{k-l}\end{aligned} \tag{5.7.42}$$

where

$$g_m = \frac{\phi_{z_m}}{x_m}. \tag{5.7.43}$$

Similarly it can be shown for the remaining terms

$$\frac{\partial}{2\partial D_k}\sum_{m=0}^{N-1} 2\mathrm{Re}[c_m^* z_m^* d_m] = G_k + \frac{2}{\sqrt{N}}\sum_{l=1}^{B} D_l G_{k-l}, \tag{5.7.44}$$

$$\frac{\partial}{2\partial D_k}\sum_{m=0}^{N-1} 2\mathrm{Re}[c_m^* z_m^*] = G_k, \tag{5.7.45}$$

and

$$\frac{\partial}{2\partial D_k}\sum_{m=0}^{N-1} |d_m|^2 = D_k. \tag{5.7.46}$$

Combining (5.7.40)-(5.7.46) yields an implicit expression for the optimal D_k

$$\frac{1}{\sqrt{N}}\sum_{l=1}^{B} G_{k-l} D_l = D_k - G_k. \tag{5.7.47}$$

Defining the $B \times B$ Hermitian Toeplitz matrix $\mathbf{G}$ with $(k,l)^{th}$ element $\mathbf{G}_{k,l} = G_{k-l}$, $\mathbf{d}^{\mathrm{T}} = [D_1, D_2, \ldots, D_B]$ and $\mathbf{g}^{\mathrm{T}} = [G_1, G_2, \ldots, G_B]$, (5.7.47) in matrix form is

$$\frac{1}{\sqrt{N}}\mathbf{G}\mathbf{d} = \mathbf{d} - \mathbf{g} \tag{5.7.48}$$

which has for its solution

$$\mathbf{d} = \left(\mathbf{I} - \frac{1}{\sqrt{N}}\mathbf{G}\right)^{-1}\mathbf{g}. \tag{5.7.49}$$

The elements of $\mathbf{d}$ as determined from (5.7.49) are the desired D_k^O.

5.7.1 Minimum Mean Squared Error

A frequency-domain expression for the MMSE is readily obtained from [23]

$$\mathrm{MMSE} = E_a - \mathbf{f}^{\mathrm{H}}\mathbf{p}. \tag{5.7.50}$$

Evaluating $\mathbf{f}^{\mathrm{H}}\mathbf{p}$ and normalizing by E_a yields

$$\begin{aligned}\frac{\mathrm{MMSE}}{E_a} &= 1 - \frac{1}{N}\sum_{k=0}^{N-1} C_k^O Z_{-k} \\ &= 1 - \frac{1}{\sqrt{N}} W_0^O.\end{aligned} \tag{5.7.51}$$

Alternatively, applying Parseval's relation to (5.7.51) yields

$$\begin{aligned}\frac{\text{MMSE}}{E_a} &= 1 - \frac{1}{N}\sum_{m=0}^{N-1} c_m^O z_m \\ &= 1 - \frac{1}{N}\sum_{m=0}^{N-1} \frac{\phi_{z_m}\left(d_m^O + 1\right)}{\phi_{z_m} + \eta^2},\end{aligned} \tag{5.7.52}$$

a pair of time-domain expressions in terms of the front–end and feedback filters respectively.

Note that the first line of (5.7.52) is identical in form to (5.2.7) found for linear equalization, but differs due to the choice of c_m^O . It can also be seen that in the absence of feedback (5.7.52) reduces to (5.2.8) as found for linear equalization.

5.7.2 Algorithm Summary

1. matrices $\mathbf{g}$ and $\mathbf{G}$ are formed using (5.7.43)
2. $\left(\mathbf{I} - \frac{1}{\sqrt{N}}\mathbf{G}\right)$ is inverted to obtain $\mathbf{d}$ from (5.7.49)
3. (5.7.2) yields d_m, (5.7.27) c_m, and (5.7.3) with an FFT yields Y_n
4. $\hat{a}_n$ is obtained from (5.7.4)

The first three steps need only be performed once per OFDM block. The final step is repeated once per data symbol.

5.7.3 Structural Comparison

The MSEDIRDFE has the same structure as the ZFDIRDFE, the difference between the two lies in the selection of the DIR. In addition both require essentially the same amount of computation when each has the same number of feedback taps B. Thus the comparison of Section 5.6.3 between ZFDIRDFE and FDZFDFE applies as well between MSEDIRDFE and FDZFDFE.

A key advantage of MSEDIRDFE over ZFDIRDFE carries over from their linear counterparts. An MSEDIRDFE exists in cases where a ZFDIRDFE does not, specifically

when some values of z_m are 0 as can be seen from (5.6.12) and (5.6.17). Due to finite wordlength effects it is not necessary for z_m to be exactly equal to 0 to encounter numerical difficulties with the latter.

5.8 Combined Mean-Squared Error Desired Impulse Response Shaping and Sequence Estimation (MSEDIRSE)

The truncated MLSE of Chapter 4 was quite successful when applied to BOFDM, but its use with QOFDM was precluded by the required constraint length. We are now in a position to rectify that situation by setting the constraint length to a desired value using the methods derived for MSEDIRDFE, and then processing the resulting controlled ISI sequence with a truncated MLSE based on the DIR.

Assuming we have obtained the sequences D_n and Y_n as per Section 5.7, we express Y_n in terms of the DIR as

$$Y_n = \frac{1}{\sqrt{N}} \sum_{k=0}^{B} D_k \hat{a}_{n-k} + N_n \tag{5.8.1}$$

where $D_0 = \sqrt{N}$ and N_n is a Gaussian noise term with correlation function

$$\mathrm{E}[N_n N_m^*] = \frac{N_0}{N} \sum_{k=0}^{N-1} |c_k|^2 e^{-j\frac{2\pi}{N}k(n-m)}. \tag{5.8.2}$$

Equation (5.8.2) indicates that the noise terms of (5.8.1) are generally correlated in the presence of fading. However, we shall treat the N_n as if they were AWGN to obtain a suboptimal but simplified sequence estimator (simulation results presented in Figure 5.16 validate this approach). With this assumption it is easily shown that the ML metric to be maximized w.r.t. a_n, $0 \leq n \leq N-1$ is

$$\lambda = -\sum_{n=0}^{N-1} \left| Y_n - \frac{1}{\sqrt{N}} \sum_{k=0}^{B} D_k a_{n-k} \right|^2. \tag{5.8.3}$$

Equation (5.8.3) may be evaluated by defining

$$\lambda_m = -\sum_{n=0}^{m} \left| Y_n - \frac{1}{\sqrt{N}} \sum_{k=0}^{B} D_k a_{n-k} \right|^2 \tag{5.8.4}$$

for which

$$\lambda_m = \lambda_{m-1} - \left| Y_m - \frac{1}{\sqrt{N}} \sum_{k=0}^{B} D_k a_{m-k} \right|^2 \tag{5.8.5}$$

and determining the sequence a_n which maximizes λ_m, $0 \leq m \leq N-1$, recursively via the Viterbi algorithm.

5.9 MSE Performance Surfaces

The preceding MSE expressions provide a basis for a theoretical comparison of the equalizers. These expressions have been used to generate sets of performance surfaces which present the mse^O for the LMSE, ZFDIRDFE, and MSEDIRDFE as functions of the noise to signal ratio η^2, the number of feedback taps B, and the particular channel fading waveform.

The fading waveform is modeled with a deterministic vector $\mathbf{z}$ to make the MSE evaluations tractable. It is

$$\mathbf{z}^T = [z_0, z_1, \cdots, z_{63}], \quad \begin{cases} z_k = 1, & k \neq 4,5,6,42,43 \\ z_k = \epsilon, & k = 4,5,6,42,43 \end{cases} \tag{5.9.1}$$
$$0 \leq \epsilon \leq 1.$$

Selection of $\epsilon < 1$ models fading at the indexes designated in (5.9.1). Two sets of surfaces are presented in Figures 5.4 and 5.5, to illustrate the effects of fade depth. In Figure 5.4 $\epsilon = 0.1$ and in Figure 5.5 $\epsilon = 0.001$. The normalized optimal MSE (mse^O) for a specific equalizer is represented by the vertical height of its performance surface. The horizontal axes, pictured as a plane orthogonal to the vertical dimension, show the variation of mse^O with B and η^2. Note that for equalizers designed by the MMSE criterion, $\text{mse}^O = \text{MMSE}/E_a$.

Figure 5.4 shows that with the shallow fades, for most of the explored ranges of B and η^2, that mse^O for ZFDIRDFE is lower than for LMSE, and it is lowest of all for MSEDIRDFE. This statement has been verified by plotting a version of Figure 5.4 (not

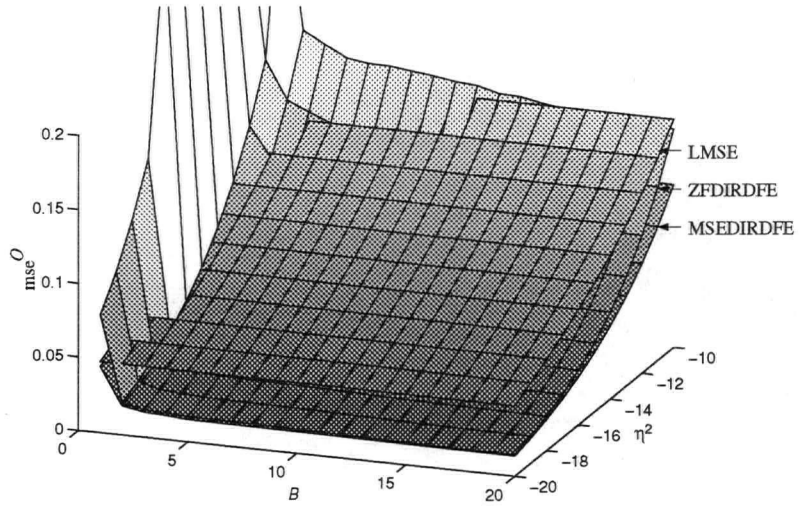

Figure 5.4 Normalized optimal mse surfaces for LMSE, ZFDIRDFE, and MSEDIRDFE at $N = 64$ and $\epsilon = 0.1$; shallow fades

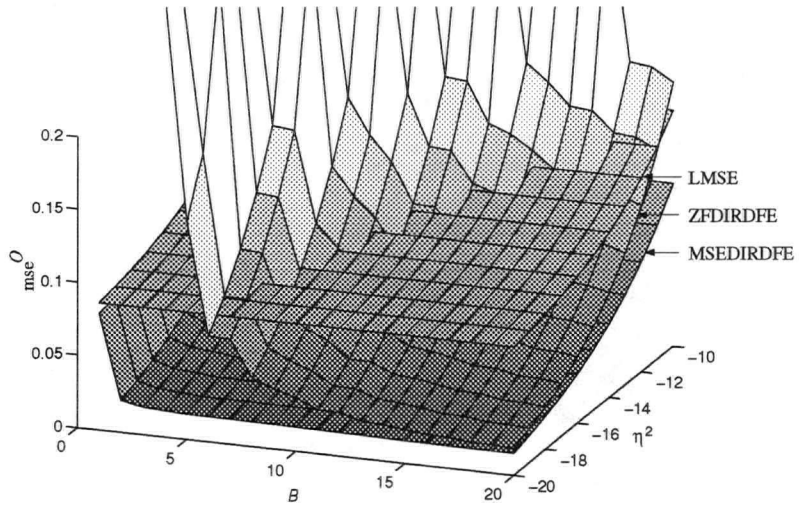

Figure 5.5 Normalized optimal mse surfaces for LMSE, ZFDIRDFE, and MSEDIRDFE at $N = 64$ and $\epsilon = 0.001$; deep fades

shown) without the LMSE surface so as to render the entire ZFDIRDFE surface visible. It is interesting that for small B and high η^2 there are regions where the performance of ZFDIRDFE is actually worse than for LMSE. In these areas the ZFDIRDFE is approaching a ZFE and the noise enhancement characteristic of ZFE is significant.

At $\eta^2 \approx -20$ dB there is very little difference between ZFDIRDFE and MSEDIRDFE, and in this region most of their improvement relative to LMSE is attained for only $B = 2$. As η^2 increases the performance of ZFDIRDFE deteriorates more rapidly than that of MSEDIRDFE, increasing the discrepancy between the two methods.

Figure 5.5 shows that for deeper fades, the performance differences between the methods increase. Again MSEDIRDFE has at every point the lowest mse^O and attains most of the improvement to be had relative to LMSE for $B = 2$ or 3. The situation is quite different for ZFDIRDFE. It can be seen that increasing B mitigates its noise enhancement problem, but we must have $B = 6$ at least, to do as well as LMSE, and this is adequate only for small η^2. Although increasing B improves its performance, at $B = 20$ it is still worse than MSEDIRDFE with only $B = 4$.

5.10 Simulation Results

The P_s performance of the equalizers derived in this chapter was evaluated by Monte Carlo simulation. The simulation framework, concerning OFDM in flat Rayleigh fading, is identical to that described in Chapter 4, except that the sampling rate was reduced to take advantage of the structural simplifications afforded by the aliasing approximation. As discussed in Chapter 4, perfect knowledge of the channel impulse response is assumed available at the receiver. The simulations were made long enough to obtain 95% confidence intervals of approximately $\pm 10\%$ of P_s.

We begin with a comparison of ZFDIRDFE and MSEDIRDFE, continue with an evaluation of MSEDIRDFE for a range of parameters, and then compare its performance to previous work.

5.10.1 Feedback Data

To include the effects of error propagation in the results which follow, all the simulations use the actual data symbol decisions in the feedback loop as opposed to the ideal (correct) decisions previously assumed to make the derivations tractable. An exception occurs with the initial decisions made for each OFDM block. Due to the circularity of the ISI resulting from the aliasing approximation, the detection of every data symbol requires knowledge of B previous, in a circular sense, data symbols. In order to preclude an error propagation problem damaging the first decision, the first decision is made with B correct data symbols in the feedback loop. This decision is then shifted into the feedback tapped delay line, and only $B-1$ ideal data symbols remain. Clearly, after the B initial decisions are made, all subsequent decisions involve only data symbols from actual previous decisions in the feedback loop. In the following, B turns out to be quite small, e.g. $B=3$ for $N=128$ and $f_D=0.01$, an overhead of less than 3%.

5.10.2 Comparison of ZFDIRDFE and MSEDIRDFE

Figure 5.6 shows the variation of P_s with B for both ZFDIRDFE and MSEDIRDFE. The curves are for QOFDM at $E_b/N_0=16$ dB and $f_N=1.28$. It can be seen that for both DFE's there is significant reduction in P_s as B increases, and essentially all the available improvement is achieved for only $B=3$ feedback coefficients. It is also clear that for a given value of B MSEDIRDFE has a lower P_s than ZFDIRDFE. Figure 5.7 shows explicitly the discrepancy in E_b/N_0, again for QOFDM and $f_N=1.28$, required for the two DFE's. The curves were produced with $B=3$ as suggested by Figure 5.6. It is clear that MSEDIRDFE has a consistent advantage of approximately 1 dB over ZFDIRDFE. Since there is no complexity penalty for MSEDIRDFE relative to ZFDIRDFE, there is little motivation to pursue the latter beyond this point. In fact, if the P_s achievable by ZFDIRDFE with $B \geq 3$ was considered adequate, essentially the same performance could be achieved by MSEDIRDFE with $B=1$. In the latter case, the matrix inversion

to obtain the feedback coefficients reduces to a simple scalar inversion. We also note that for $B \geq 2$ with MSEDIRDFE, there is no value of B which can be used with ZFDIRDFE to obtain as low a P_s. Consequently subsequent comparisons focus on MSEDIRDFE.

A P_s curve for the LMSE equalizer of Section 5.2 also appears in Figure 5.7. It is included in this and subsequent figures for comparison between linear and decision feedback equalization. It can be seen that the advantage of MSEDIRDFE over LMSE increases with increasing E_b/N_0, being near 3 dB at $P_s = 10^{-3}$.

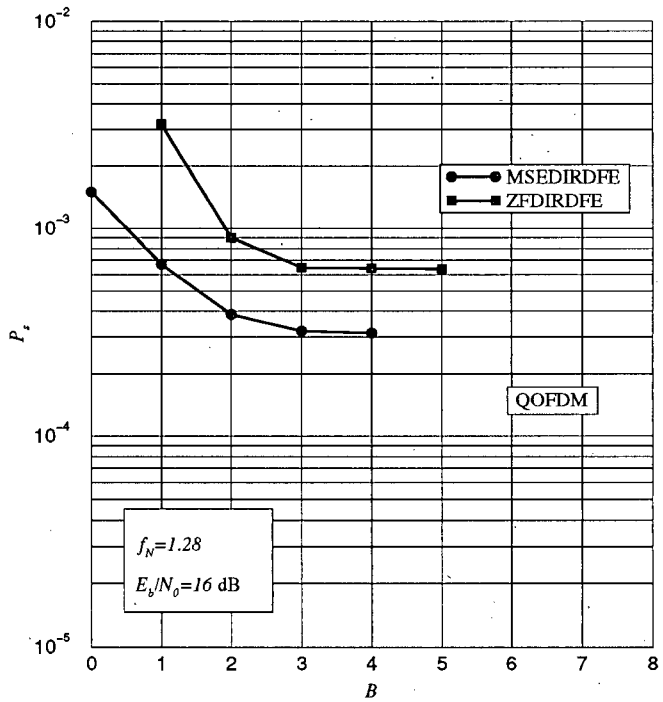

Figure 5.6 Variation of P_s with B for ZFDIRDFE and MSEDIRDFE, $f_N = 1.28$, $E_b/N_0 = 16$ dB, QOFDM

5.10.3 Evaluation of MSEDIRDFE

Figure 5.8 compares the variation of P_s with B for BOFDM and QOFDM, at $f_N = 0.32$ and $E_b/N_0 = 22$ dB. Nearly all the available improvement is attained with $B = 1$ for both cases.

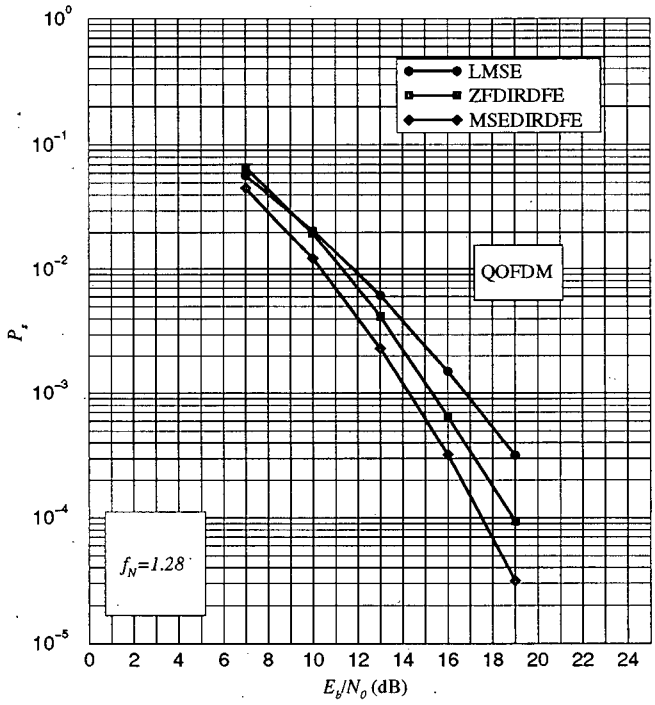

Figure 5.7 Comparison of MSE, ZFDIRDFE, and MSEDIRDFE, $f_N = 1.28$, QOFDM

The P_s for QOFDM would be very close to twice that for BOFDM if the channel were nonfading AWGN, since then there would be no ISI and QOFDM is equivalent to two BOFDM signals in quadrature. Figure 5.8 in contrast shows a ratio of approximately 3. This indicates, as found in Chapter 4, that QODFM suffers more from ISI than does BOFDM. A key difference however, is that here the significant contributors to ISI have been reduced to a number B which is small for QOFDM as well as BOFDM. This is important for the feasibility of MSEDIRSE with QOFDM.

Figure 5.9 makes the same comparison as Figure 5.8, but at $f_N = 1.28$ and $E_b/N_0 = 16$ dB. Most of the improvement is obtained for small B, possibly $B = 2$ or 3 for BOFDM and $B = 3$ for QOFDM.

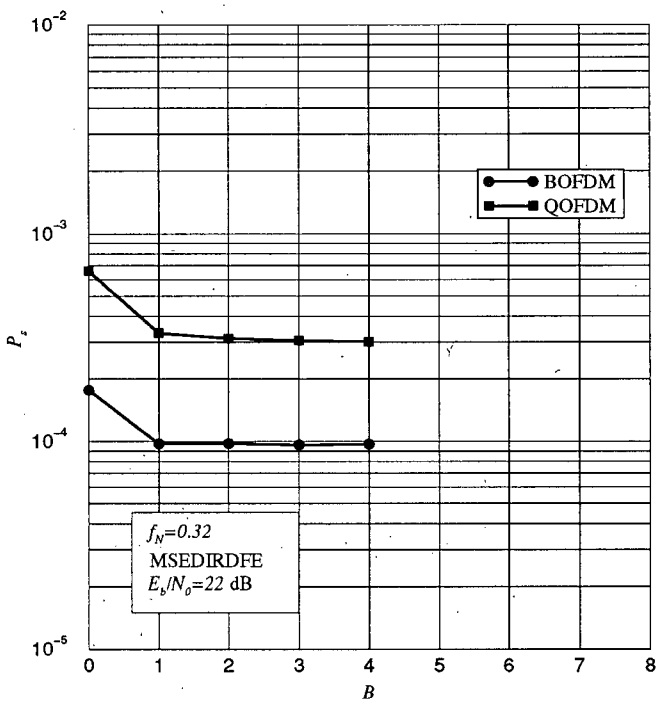

Figure 5.8 Variation of P_s with B for MSEDIRDFE, $f_N = 0.32$, $E_b/N_0 = 22$ dB.

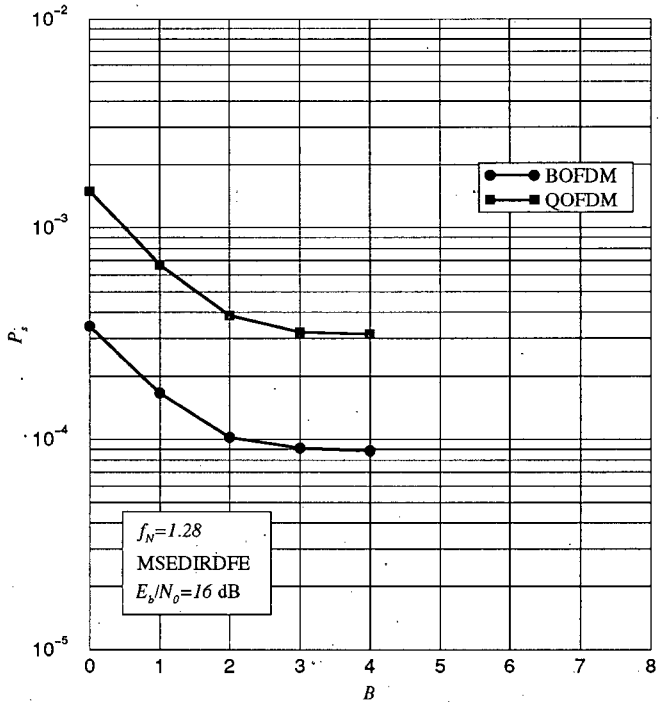

Figure 5.9 Variation of P_s with B for MSEDIRDFE, $f_N = 1.28$, $E_b/N_0 = 16$ dB.

P_s Comparison of LMSE and MSEDIRDFE Figures 5.10 and 5.11 compare MSEDIRDFE to LMSE for BOFDM and QOFDM, at $f_N = 0.32$ and $f_N = 1.28$. The B used to generate each curve is indicated on the graph legends. At $f_N = 0.32$ there is little to be gained with MSEDIRDFE compared to LMSE, less than 1 dB at $P_s = 10^{-3}$ for BOFDM. For QOFDM the improvement is slightly better, about 1.5 dB. We note though that obtaining this gain is simple since $B = 1$ for these curves. At higher f_N the advantage of MSEDIRDFE is more apparent. Figure 5.11 shows gains of about 1.5 dB for BOFDM and 2.7 dB for QOFDM at $P_s = 10^{-3}$. It can also be seen that the reduction in P_s with increasing E_b/N_0 is greater for MSEDIRDFE than LMSE, and that the relative improvement for QOFDM is again greater than for BOFDM.

P_s Comparison of MSEDIRDFE to MLSE and the MFB Figures 5.12 and 5.13 compare curves for MSEDIRDFE to the MFB and MLSE results of Chapter 4 for BOFDM. In both cases, $f_N = 0.32$ and $f_N = 1.28$, the MSEDIRDFE curve is slightly closer to the MLSE curve than the LMSE curve, indicating that over half the loss of LMSE relative to MLSE is recoverable with MSEDIRDFE, and the gain of MSEDIRDFE over LMSE increases with E_b/N_0 and f_N.

These curves also show the gain of MLSE over LMSE, about 1.7 dB at $f_N = 0.32$ and 2.9 dB at $f_N = 1.28$, both at $P_s = 10^{-3}$.

5.10.4 Comparison of MSEDIRDFE to Previous Work: FDZFDFE

Figure 5.14 shows a comparison between FDZFDFE from [7] and MSEDIRDFE developed here. The comparison was made by simulating on the basis of the OFDM parameters used in that work, $f_N = 2.05$ and $N = 512$, since the exact equations for calculating the front–end and feedback filter coefficients it used were not given.

The simulation of [7] used ideal decisions in the feedback loop with $B = 15$. The MSEDIRDFE simulation uses $B = 4$ and two curves are presented, one where ideal

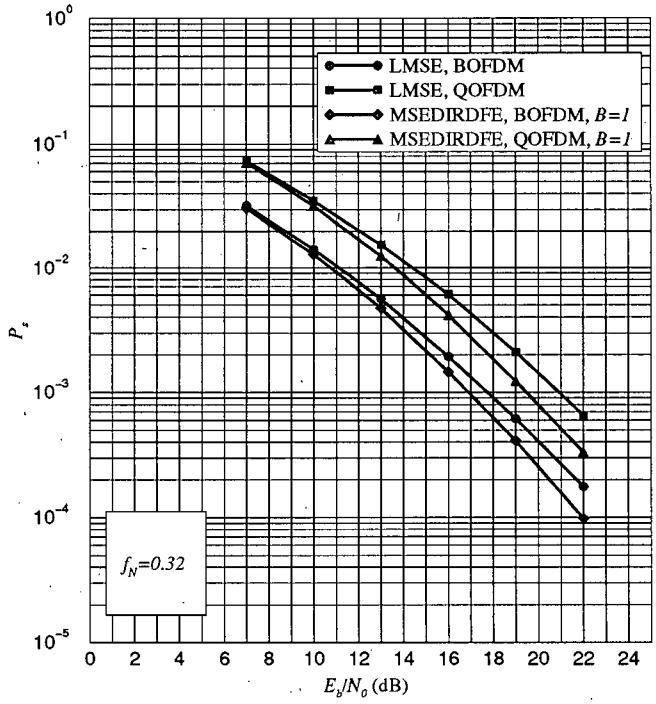

Figure 5.10 Comparison of LMSE and MSEDIRDFE, $B = 1$, $f_N = 0.32$.

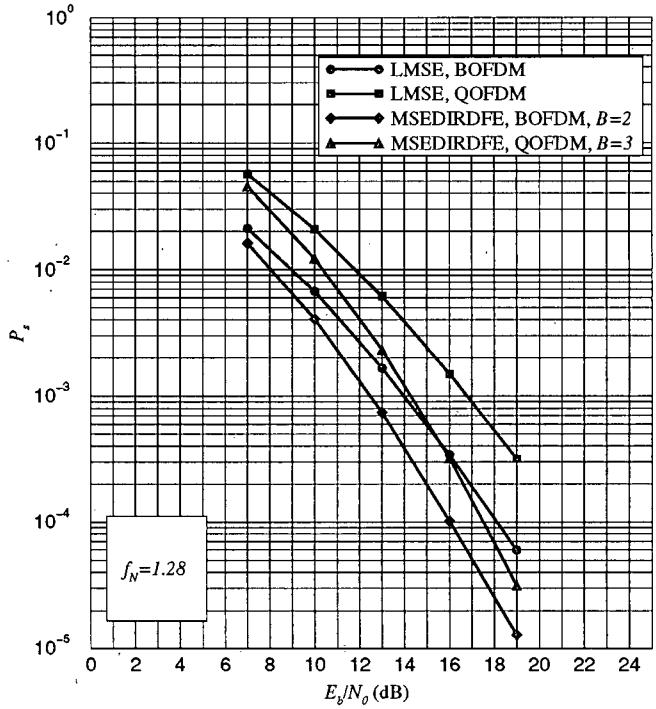

Figure 5.11 Comparison of LMSE and MSEDIRDFE for $f_N = 1.28$.

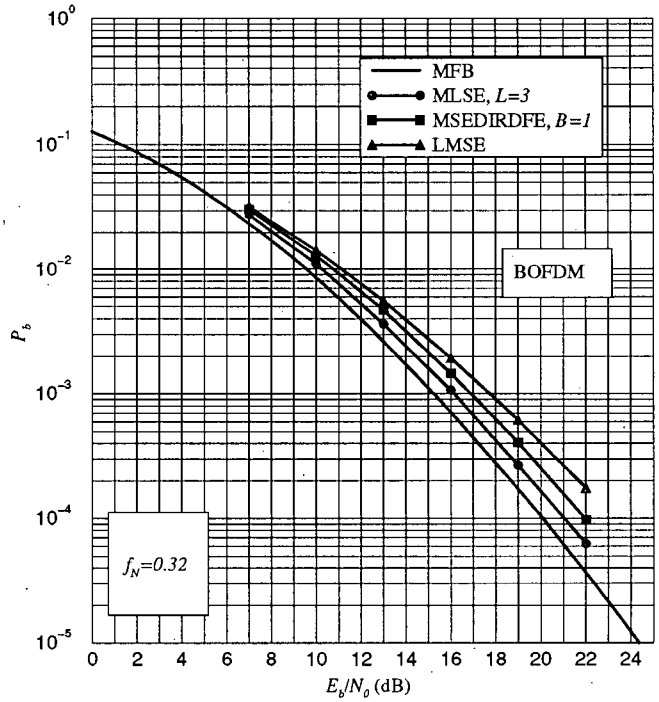

Figure 5.12 Comparison of LMSE and MSEDIRDFE to MLSE, $B = 1$, $f_N = 0.32$.

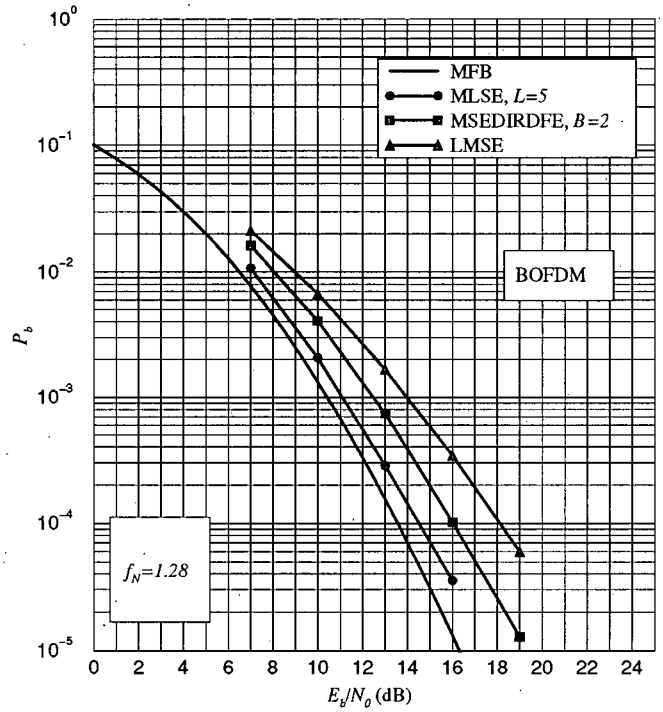

Figure 5.13 Comparison of LMSE and MSEDIRDFE to MLSE, $f_N = 1.28$.

decisions were used in the feedback loop and one where the actual decisions were used. Thus a fair comparison is between the left and rightmost curves. We see that

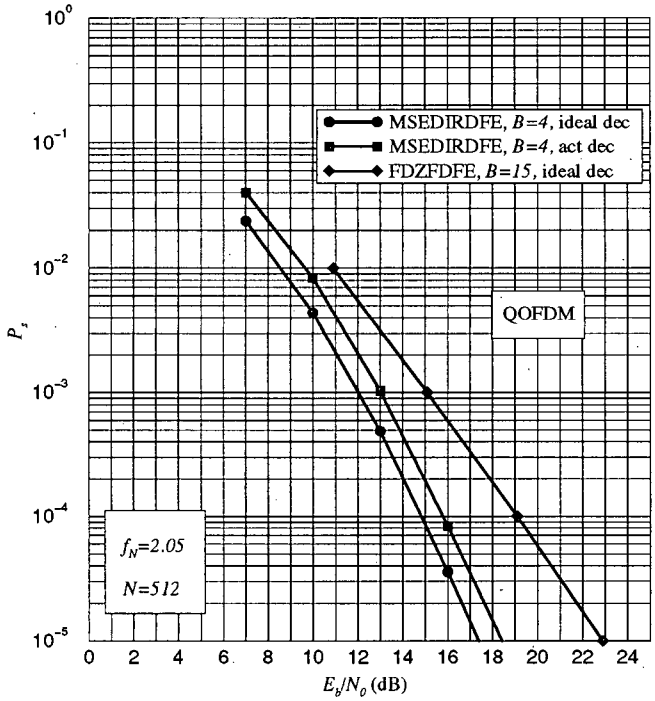

Figure 5.14 Comparison of MSEDIRDFE to FDZFDFE, for the parameters of [7], $f_N = 2.05$, $N = 512$, QOFDM.

MSEDIRDFE has about 3 dB gain over FDZFDFE at $P_s = 10^{-3}$ and this increases with increasing E_b/N_0. The middle curve, for MSEDIRDFE with actual decisions in the feedback loop loses only 1 dB compared to the ideal case, and still maintains a 2 dB advantage over ideal FDZFDFE at $P_s = 10^{-3}$.

5.11 MSEDIRSE Simulation Results

This section presents simulation results for the MSEDIRSE described in Section 5.8. Since both MSEDIRSE and MSEDIRDFE use the same front-end filter, a lower bound on P_s for MSEDIRSE given that filter is obtained from a simulation of MSEDIRDFE

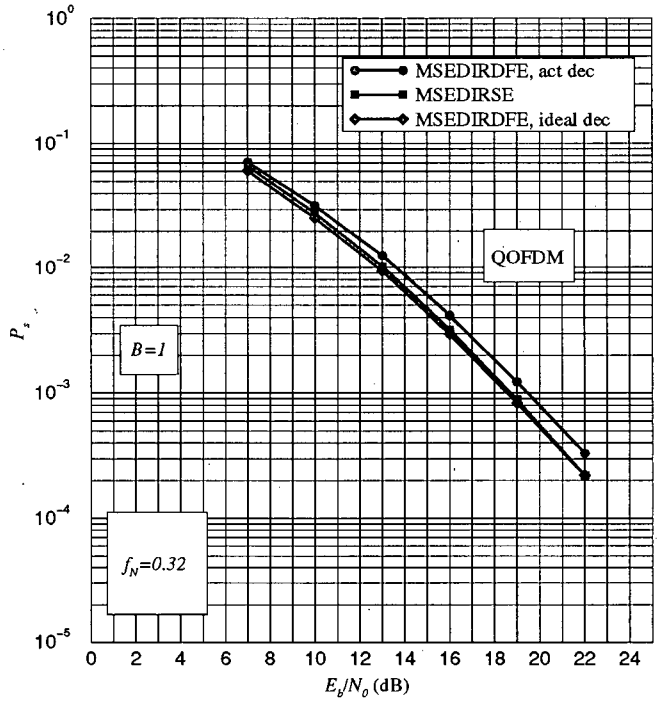

Figure 5.15 Performance of MSEDIRSE, $B = 1$, $f_N = 0.32$.

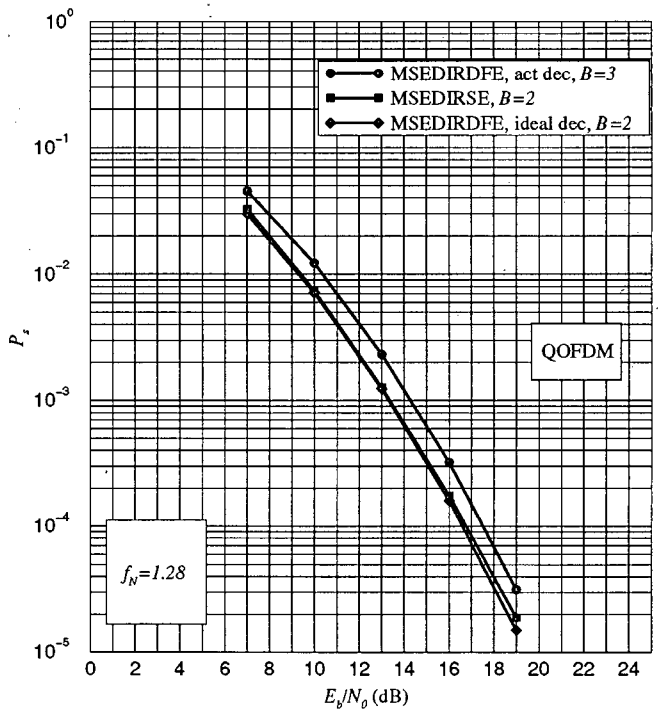

Figure 5.16 Performance of MSEDIRSE, $B = 2$, $f_N = 1.28$.

with ideal decisions in the feedback loop. This is because MSEDIRSE can do no better than to make no errors due to ISI from the DIR.

Figures 5.15 and 5.16 present P_s versus E_b/N_0 curves for MSEDIRDFE with both the actual and ideal decisions for comparison to MSEDIRSE. From the spread of the MSEDIRDFE curves with actual and ideal decisions it is apparent that the potential improvement at $P_s = 10^{-3}$ is limited to about 0.8 dB for $f_N = 0.32$ and about 1 dB for $f_N = 1.28$. As can be seen, nearly all of the potential gain over MSEDIRDFE with actual decisions is achieved by MSEDIRSE with only 4 and 16 state sequence estimators respectively.

Although the addition of a sequence estimator to obtain 1 dB or less available gain on a fading channel is not likely to be a desireable engineering tradeoff, these results validate the derivation of MSEDIRSE, and are in stark contrast to the poor performance of truncated MLSE with QOFDM shown in Chapter 4.

5.12 Conclusion

We have examined linear and decision feedback equalizer theory in the context of OFDM modulation on flat Rayleigh fading channels. The aliasing approximation was identified as a convenient means of obtaining simplified equalizer structures. This was combined with the idea of modifying the overall pulse response to obtain a desired impulse response, resulting in two new DFE structures for OFDM, ZFDIRDFE and MSEDIRDFE. The former is a translation of a previously existing idea for serial modulation to the OFDM problem here. The latter, MSEDIRDFE, is thought to be a new formulation with application broader than the OFDM context which inspired it.

A third structure, MSEDIRSE, combines the use of MSEDIR shaping with an approximate MLSE, and performs essentially as well as MSEDIRDFE with ideal decisions in the feedback loop.

Of the three, MSEDIRSE has the best performance, but MSEDIRDFE performs nearly as well and is slightly less complex, thus it may be preferable. Comparisons of MSEDIRDFE with previous best results show a significant improvement in terms of P_s without increased complexity.

Chapter 6

OFDM on Frequency-Selective Rayleigh Fading Channels

Although the flat fading model of previous chapters is frequently encountered in practice, it is not always applicable. As noted in Chapter 2, frequency selectivity is a function of both the transmitted signal and the delay spread of the channel. In urban environments the typical worst case excess delays[22] for arrivals which are within 10 dB of the maximum signal are less than 25 *u*sec [18]. For the delays near 25 *u*sec, this corresponds to the channel appearing frequency-selective for a signaling rates of about 4 kbaud and above. The delays can be even greater in suburban environments. For example the IS-54 [37] digital cellular channel model uses a two-ray model with a 40 *u*sec delay between the rays, which corresponds to one symbol period. Thus the applicability of any modulation proposed for land mobile radio to delay spread or frequency-selective channels is an important consideration.

In this chapter we extend some of our previous work for flat fading channels to frequency-selective channels. We derive receivers for OFDM on frequency-selective Rayleigh fading channels, based on the optimization of MLSE and MMSE performance criteria.

The chapter is organized as follows. Section 6.1 describes the channel modeling. Derivation of optimal and truncated MLSE receivers is presented in Section 6.2. Methods for evaluating matched filter outputs and tone correlations are given in Section 6.2.1, and the effect of pulse shaping on the tone correlations is considered in Section 6.2.2. Performance results obtained by simulation of the MLSE receivers are presented in Section 6.2.3.

---

[22] with a probability of 0.99

In Section 6.3 optimal linear MMSE receivers are derived. Direct and alternate implementations are described in Sections 6.3.1 and 6.3.2. Methods for evaluating matched filter outputs and tone correlations are given in Section 6.3.3. The relationship between integral equation and matrix formulations of the estimation problem is examined in Section 6.3.4, and an efficient matrix formulation for rate N/T_0 sampling is outlined in Section 6.3.5. The performance results obtained by simulation of the MMSE receivers are presented Section 6.3.6.

Section 6.4 summarizes the conclusions of this chapter.

6.1 A Frequency-Selective Rayleigh Fading Channel Model

The model introduced in Chapter 3 for a delay spread and time varying channel impulse response had a received signal $r(t)$ given by

$$r(t) = \int_0^{\tau_{max}} z(\sigma, t)s(t-\sigma)d\sigma + n(t) \tag{6.1.1}$$

where $z(\sigma, t)$ is the response of the channel at time t to an impulse applied at time $t-\sigma$, and τ_{max} is the maximum delay spread. The time variation models the fading process and the delay spread gives rise to the frequency selectivity. Although not much more difficult to work with than a flat fading model, the generality of (6.1.1) makes it difficult to obtain insight into some of the quantities[23] which arise in the following sections. For this purpose it is helpful to specialize the model slightly by considering a received signal consisting of N_b Rayleigh faded rays and AWGN. This model is still quite general because the rays may be correlated, and by assuming suitable weighting coefficients α_i for each ray, arbitrary delay spread profiles may be approximated. The model of the received signal is then

$$r(t) = \sum_{i=1}^{N_b} \alpha_i z_i(t-\tau_i)s(t-\tau_i) + n(t) \tag{6.1.2}$$

[23] i.e. the matched filter outputs and tone correlations

where N_b is the number of rays and τ_i is the delay associated with the i^{th} ray. The channel impulse response implied by (6.1.2) and (6.1.1) is

$$z(\sigma,t) = \sum_{i=1}^{N_b} \alpha_i \delta(\sigma - \tau_i) z_i(t - \tau_i). \tag{6.1.3}$$

Setting $N_b = 2$ in (6.1.3) gives the two-ray Rayleigh fading channel model as

$$z(\sigma,t) = \alpha_1 \delta(\sigma) z_1(t) + \alpha_2 \delta(\sigma - \tau) z_2(t - \tau). \tag{6.1.4}$$

Although the analyses are performed with the more general models, (6.1.4) is used to produce the simulation results of this chapter since it has the fewest parameters while still remaining able to model frequency-selective Rayleigh fading.

6.2 Derivation of the MLSE Receiver

The first problem encountered in generalizing the results of Chapter 4 to delay spread channels is in obtaining a discrete and sufficient statistic from the continuous received waveform. This statistic could then be processed by discrete structures similar to the MSEDIRDFE or MSEDIRSE derived previously. Although truncated MLSE can be expected to suffer the same limitations on frequency-selective channels as were found for flat fading channels, its derivation is useful because such a statistic is obtained as an intermediate result.

The derivation is similar to that of Chapter 4 but generalized to consider a received signal given by (6.1.1). Recalling the derivation of the MLSE receiver in Chapter 4, the signal dependent parameter $w(t, \mathbf{a})$ is generalized to

$$w(t, \mathbf{a}) = \int z(\sigma, t) s(t - \sigma) d\sigma. \tag{6.2.1}$$

Equation (4.2.3) gave the metric λ as a function of $w(t, \mathbf{a})$. It is repeated here for convenience

$$\lambda = \int \mathrm{Re}[r(t) w^*(t, \mathbf{a})] - \frac{1}{2} |w(t, \mathbf{a})|^2 dt. \tag{6.2.2}$$

Combining (6.2.1) and (6.2.2) and simplifying yields

$$\lambda = \mathrm{Re}\left[\sum_{n=0}^{N-1} a_n^* \int r(t) \int z^*(\sigma,t)p^*(t-\sigma)e^{-j\frac{2\pi}{T_0}n(t-\sigma)}d\sigma\ dt\right] - \frac{1}{2}\sum_{n=0}^{N-1}\sum_{m=0}^{N-1} a_n^* a_m \int\int z(\sigma_1,t)p(t-\sigma_1)e^{j\frac{2\pi}{T_0}m(t-\sigma_1)}d\sigma_1 \times \int z^*(\sigma_2,t)p^*(t-\sigma_2)e^{-j\frac{2\pi}{T_0}n(t-\sigma_2)}d\sigma_2\ \ dt \tag{6.2.3}$$

from which the quantities

$$U_n = \int r(t) \int z^*(\sigma,t)p^*(t-\sigma)e^{-j\frac{2\pi}{T_0}n(t-\sigma)}d\sigma\ dt \tag{6.2.4}$$

and

$$V_{m,n} = \int\int z(\sigma_1,t)p(t-\sigma_1)e^{j\frac{2\pi}{T_0}m(t-\sigma_1)}d\sigma_1 \times \int z^*(\sigma_2,t)p^*(t-\sigma_2)e^{-j\frac{2\pi}{T_0}n(t-\sigma_2)}d\sigma_2\ dt \tag{6.2.5}$$

can be defined. As per the observations of Section 4.2, U_n and $V_{m,n}$ will be referred to as the matched filter outputs and tone correlations respectively. The metric can now be written as

$$\lambda = \mathrm{Re}\left[\sum_{n=0}^{N-1} a_n^* U_n\right] - \frac{1}{2}\sum_{n=0}^{N-1}\sum_{m=0}^{N-1} a_n^* a_m V_{m,n} \tag{6.2.6}$$

which has the same general form as (4.2.11) except that $V_{m,n}$ can no longer be written as V_{n-m}. However the essential property for efficient recursive evaluation of (6.2.6) is that $V_{m,n} = V_{n,m}^*$, which can be seen to hold from (6.2.5). Using this property it may be shown (Appendix C) that λ may be found recursively by defining

$$\lambda_n = \mathrm{Re}[a_n^* U_n] - \mathrm{Re}\left[a_n^* \sum_{k=n-L}^{n-1} a_k V_{k,n}\right] - \frac{1}{2}|a_n|^2 V_{n,n} \tag{6.2.7}$$

and maximizing

$$\lambda = \sum_{n=0}^{N-1} \lambda_n. \tag{6.2.8}$$

Equation (6.2.7) results in an optimal sequence selection only for the selection of $L = n$, or equivalently if $V_n = 0$ for $n > L$.

The matched filter outputs U_n, $0 \leq n \leq N-1$ are the desired sufficient statistic.

6.2.1 Evaluation of U_n and V_n

We obtain expressions for U_n and V_n by specializing the channel impulse response to the N_b-ray model.

Matched Filter Outputs Using (6.1.3) in (6.2.4) we obtain

$$\begin{aligned} U_n &= \int r(t) \int \sum_{i=1}^{N_b} \alpha_i \delta(\sigma - \tau_i) z_i^*(t-\tau_i) p^*(t-\sigma) e^{-j\frac{2\pi}{T_0}n(t-\sigma)} d\sigma dt \\ &= \int r(t) \sum_{i=1}^{N_b} \alpha_i z_i^*(t-\tau_i) p^*(t-\tau_i) e^{-j\frac{2\pi}{T_0}n(t-\tau_i)} dt \\ &= \int r(t) \sum_{i=1}^{N_b} \alpha_i q_i^*(t-\tau_i) e^{-j\frac{2\pi}{T_0}n(t-\tau_i)} dt \\ &= \int \left[\sum_{i=1}^{N_b} \alpha_i r(t+\tau_i) q_i^*(t) \right] e^{-j\frac{2\pi}{T_0}nt} dt \end{aligned} \tag{6.2.9}$$

where $q_i(t) = z_i(t)p(t)$. Equation (6.2.9) has been manipulated into the form of a single Fourier transform of its argument in the square brackets. The interval of integration is over the range of non-zero values of its argument. In this case an appropriate range is $0 \leq t \leq T_0(1+\alpha)+\tau_m$ where α is the pulse rolloff and τ_m is the maximum delay spread.

There are N values of U_n required to calculate the data estimates by (6.2.6), but we note that approximation of integrals with the form of a Fourier transform via an FFT method was previously discussed in Section 4.3. Using this method all N values of U_n are calculated simultaneously with one FFT.

This calculation is essentially similar to that for the flat fading model of Chapter 4.

Specialized to the two-ray case (6.2.9) is

$$U_n = \int [\alpha_1 r(t) q_1^*(t) + \alpha_2 r(t+\tau) q_2^*(t)] e^{-j\frac{2\pi}{T_0}nt} dt. \tag{6.2.10}$$

Tone Correlations The tone correlations are defined in (6.2.5). Expanding this with (6.1.3) as above yields

$$\begin{aligned} V_{m,n} &= \int\int z(\sigma_1,t)p(t-\sigma_1)e^{j\frac{2\pi}{T_0}m(t-\sigma_1)}d\sigma_1 \\ &\quad \times \int z^*(\sigma_2,t)p^*(t-\sigma_2)e^{-j\frac{2\pi}{T_0}n(t-\sigma_2)}d\sigma_2\ dt \\ &= \int \sum_{i=1}^{N_b} \alpha_i \delta(\sigma_1-\tau_i)z(t-\tau_i)p(t-\sigma_1)e^{j\frac{2\pi}{T_0}m(t-\sigma_1)}d\sigma_1 \\ &\quad \times \sum_{k=1}^{N_b} \alpha_k \delta(\sigma_2-\tau_k)z^*(t-\tau_k)p^*(t-\sigma_2)e^{-j\frac{2\pi}{T_0}n(t-\sigma_2)}d\sigma_2 dt \\ &= \int \sum_{i=1}^{N_b}\sum_{k=1}^{N_b} \alpha_i\alpha_k q_i(t-\tau_i)q_k^*(t-\tau_k)e^{j\frac{2\pi}{T_0}m(t-\tau_i)}e^{-j\frac{2\pi}{T_0}n(t-\tau_k)}dt. \end{aligned} \tag{6.2.11}$$

Comparison of (6.2.11) with (4.2.13) shows the key difference between the flat fading and frequency-selective fading cases. In the former $V_{m,n} = V_{m-n}$, i.e. the tone correlations do not depend on m and n individually but only their difference. As can be seen above this is no longer the case for frequency-selective fading. The dependency of the $V_{m,n}$ on the individual values of m and n complicates their evaluation; they can no longer be found from a single Fourier transform as in the flat fading case. However it is still possible to express it as a sum of Fourier transforms. Upon collecting terms with a common index and moving exponential rotations outside the integral sign (6.2.11) becomes

$$\begin{aligned} V_{m,n} &= \int \left[\sum_{i=1}^{N_b} \alpha_i^2 |q_i(t)|^2\right] e^{-j\frac{2\pi}{T_0}(n-m)t}dt \\ &\quad + \sum_{i=1}^{N_b}\sum_{\substack{k=1\\k\neq i}}^{N_b} \alpha_i\alpha_k e^{-j\frac{2\pi}{T_0}m\tau_i}e^{j\frac{2\pi}{T_0}n\tau_k}\int q_i(t-\tau_i)q_k^*(t-\tau_k)e^{-j\frac{2\pi}{T_0}(n-m)t}dt. \end{aligned} \tag{6.2.12}$$

Defining the transforms

$$I_{1_n} = \int \left[\sum_{i=1}^{N_b} \alpha_i^2 |q_i(t)|^2\right] e^{-j\frac{2\pi}{T_0}nt}dt \tag{6.2.13}$$

and

$$I_{i,k_n} = \alpha_i \alpha_k \int q_i(t-\tau_i) q_k^*(t-\tau_k) e^{-j\frac{2\pi}{T_0}nt} dt \tag{6.2.14}$$

we can write (6.2.12) as

$$V_{m,n} = I_{1_{n-m}} + \sum_{i=1}^{N_b} \sum_{\substack{k=1 \\ k \neq i}}^{N_b} e^{-j\frac{2\pi}{T_0}m\tau_i} e^{j\frac{2\pi}{T_0}n\tau_k} I_{i,k_{n-m}} \tag{6.2.15}$$

which is a sum of $N_b(N_b-1)+1$ Fourier transforms. Noting I_{i,k_n} is conjugate symmetric, this can be reduced to $N_b(N_b-1)/2+1$ transforms. As with the matched filter outputs, these transforms can be evaluated with the FFT method of Chapter 4.

Equation (6.2.15) specialized to the two-ray case is

$$\begin{aligned} V_{m,n} &= I_{1_{n-m}} + e^{j\frac{2\pi}{T_0}n\tau} I_{1,2_{n-m}} + e^{-j\frac{2\pi}{T_0}m\tau} I_{2,1_{n-m}} \\ &= I_{1_{n-m}} + e^{j\frac{2\pi}{T_0}n\tau} I_{1,2_{n-m}} + e^{-j\frac{2\pi}{T_0}m\tau} I^*_{1,2_{m-n}} \end{aligned} \tag{6.2.16}$$

which requires only two transforms.

6.2.2 Pulse Shaping and the Tone Correlations

In Chapter 4 a criterion for pulse shaping was introduced as (4.5.1) which was shown to be satisfied by the root raised cosine family with rolloff parameter α. The specific criterion was to require that in the absence of fading the shaped basis functions should be orthogonal over the duration of $p(t)$, i.e.

$$\int |p(t)|^2 e^{-j\frac{2\pi}{T_0}(n-m)t} dt = \delta_{n-m} \tag{6.2.17}$$

and that this should hold for any choice of α. Equivalently, (6.2.17) states that the tone correlations in the absence of fading are

$$V_{n-m} = \delta_{n-m}. \tag{6.2.18}$$

The effect of flat Rayleigh fading is to modulate the pulse shape at frequencies at and below the maximum Doppler frequency. Since the tone correlations

$$V_n = \int |q(t)|^2 e^{-j\frac{2\pi}{T_0}nt} dt \tag{6.2.19}$$

are samples of the frequency spectrum of this modulated pulse shape it is apparent that the effect of the fading on V_n is to spread it out from a unit sample function by convolving the spectrum of $|p(t)|^2$ with the power spectrum of the fading process. However since the fading is lowpass and of much smaller bandwidth than that of the OFDM signal, the most significant values of the tone correlations are clustered on either side of any particular tone. It is this effect which allowed the use of truncated ($L < N-1$) MLSE for use in detecting BOFDM, with little degradation of P_b. Simulation results showed that pulse shaping with moderate ($\alpha \leq 0.25$) values of α had negligible effect on P_b, as might be expected from (6.2.17) and (6.2.18).

The situation for the case of a delay spread channel is markedly different. This can be seen by comparing (6.2.19) and (6.2.15) of the tone correlations for the flat and frequency-selective cases respectively. The principal difference is the presence of cross–terms between the rays in the latter. Considering any one of these cross–terms

$$I_{i,k_n} = \alpha_i \alpha_k \int q_i(t-\tau_i) q_k^*(t-\tau_k) e^{-j\frac{2\pi}{T_0}nt} dt \tag{6.2.20}$$

it can be seen that even in the absence of fading where (6.2.20) is

$$I_{i,k_n} = \alpha_i \alpha_k \int p_i(t-\tau_i) p_k^*(t-\tau_k) e^{-j\frac{2\pi}{T_0}nt} dt \tag{6.2.21}$$

we will find that in general

$$I_{i,k_n} \neq \delta_n \tag{6.2.22}$$

and consequently

$$V_{m,n} \neq \delta_{n-m}. \tag{6.2.23}$$

The important point of this is that pulse shaping is much more important on frequency-selective fading channels than flat fading channels. In particular the short constraint lengths used with rectangular pulse shaping and flat fading result in poor performance on frequency-selective channels. Fortunately (6.2.21) also indicates that pulse shaping can be used to control the spreading of $V_{m,n}$ and thereby make truncated MLSE feasible.

6.2.3 Simulation Results

The performance of the receivers developed in the preceding sections has been evaluated by simulation. Perfect channel knowledge is assumed available at the receiver and thus the results bound the best attainable performance for both receiver categories, nonlinear MLSE and linear MMSE respectively.

As in previous chapters, the figures presented are annotated with f_N since it is this parameter upon which the P_b of the MFB of Chapter 3 depends. A maximum Doppler rate of $f_D = 0.01$ times the data symbol rate is assumed and the sampling rate and number of samples per block is such that $f_N = f_D T_0 = f_D N$. Therefore we always have $N = 100 f_N$ data symbols per OFDM block.

The two-ray channel model was used to model frequency-selective Rayleigh fading. The delay spread τ is normalized by $T_s = T_0/N$, the data symbol interval. For example $\tau = 0.5$ indicates a difference in arrival times, or delay spread, of $0.5T_s$ between the two rays. The other channel model parameter is α_1^2, the proportion of total received power in the first ray. In the figures it is designated by γ to avoid confusion with α, the rolloff parameter of the root raised cosine pulse shape.

Figures 6.1 and 6.2 show the effect of delay spread on the symbol error rate, P_s, of an ideal MLSE receiver. By ideal MLSE we mean an optimal MLSE receiver as derived in Section 6.2 without truncation or other modification of the constraint length. This requires $L = N - 1$; thus simulation is practical only for small N due to complexity constraints.

Figure 6.1 shows the results for BOFDM with $N = 4$ and similarly Figure 6.2 for QOFDM. Both show results for three values of delay spread. The case of $\tau = 0.0$ is equivalent to flat fading. For $\tau = 0.5$ and $\tau = 1.0$, independent Rayleigh fading of two equal power rays was applied with amplitudes scaled so as to make the *total* received power of the two rays equal to that of the one ray flat fading case. Nevertheless, both figures show substantial gains in the presence of delay spread, of about 5 and 6 dB at

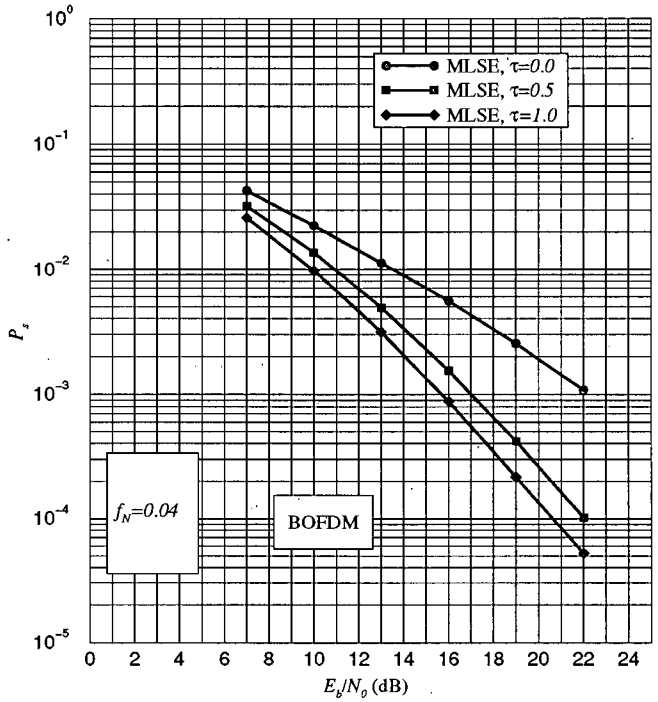

Figure 6.1 Effect of Delay Spread with Ideal MLSE for BOFDM, $N = 4$.

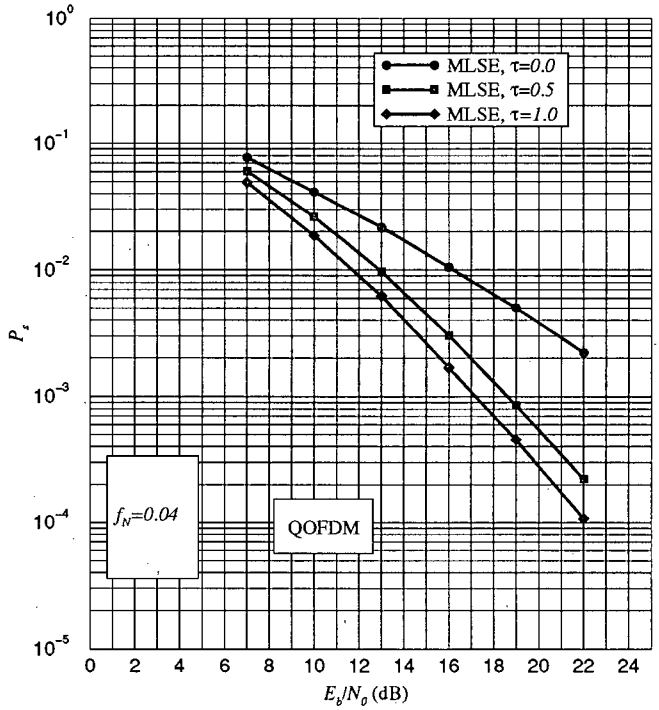

Figure 6.2 Effect of Delay Spread with Ideal MLSE for QOFDM, $N = 4$.

$P_s = 10^{-3}$ respectively. This is because such short blocks have negligible time diversity, so there is a large diversity gain due to the second ray. It is interesting that the MLSE receiver is able to attain such gain despite the ISI which must be substantial. At $\tau = 0.5$ the second arrival overlaps the first by $7/8$ of the OFDM block length and for $\tau = 1.0$ the overlap is $3/4$.

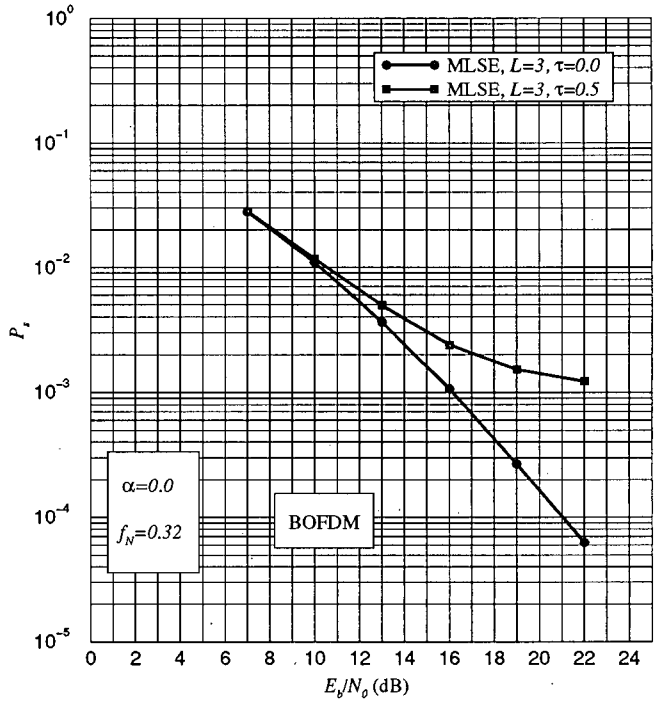

Figure 6.3 Effect of Delay Spread on Constraint Length for $f_N = 0.32$

Figure 6.3 shows the effect of delay spread on constraint length for $f_N = 0.32$. In this case ideal MLSE is not feasible[24] and so truncated MLSE with $L = 3$ is compared for flat fading and $\tau = 0.5$. Rectangular pulse shaping was used. The deterioration of the latter case is remarkable, about 5 dB at $P_s = 10^{-3}$. As discussed in Section 6.2.2, this effect is due to the emergence of cross-terms which are not present in the flat fading case.

One solution to the cross-term problem, the use of root raised cosine pulse shaping to modify the required constraint length is evaluated in Figure 6.4 for $f_N = 0.32$ and

[24] Ideal MLSE would require $L = N - 1$; it is precluded by the exponential complexity of the Viterbi algorithm

Figure 6.5 for $f_N = 1.28$. Values of $L = 3$ and 5 respectively were used to be consistent with the flat fading simulations of Chapter 4. Results are shown for various values of rolloff parameter α with $\tau = 0.5$. For $f_N = 0.32$ about 5 dB at $P_s = 10^{-3}$ is gained with $\alpha = 0.125$ compared to $\alpha = 0.0$, which is a substantial improvement. For $f_N = 1.28$ the improvement is not very significant above $P_s = 10^{-4}$, where it is only about 1 dB. In both cases, increasing α to 0.25 provides little benefit.

The relatively small improvement for the longer ($N = 128$) blocklength is because there is relatively little deterioration to improve upon. This is likely because $\tau = 0.5$ is a proportionately smaller delay spread for longer OFDM blocks.

Figures 6.6 and 6.7 show the effect of various power distributions between the rays, for $\alpha = 0.125$ and $\tau = 0.5$. In both cases, $f_N = 0.32$ and $f_N = 1.28$, the effect of the power distribution is seen to be nearly negligible. This is in contrast to the MFB results which show maximum benefit for equal power distribution. It appears that the additional factor of ISI, which also varies with the power distribution, is counterbalancing diversity gain from delay spread.

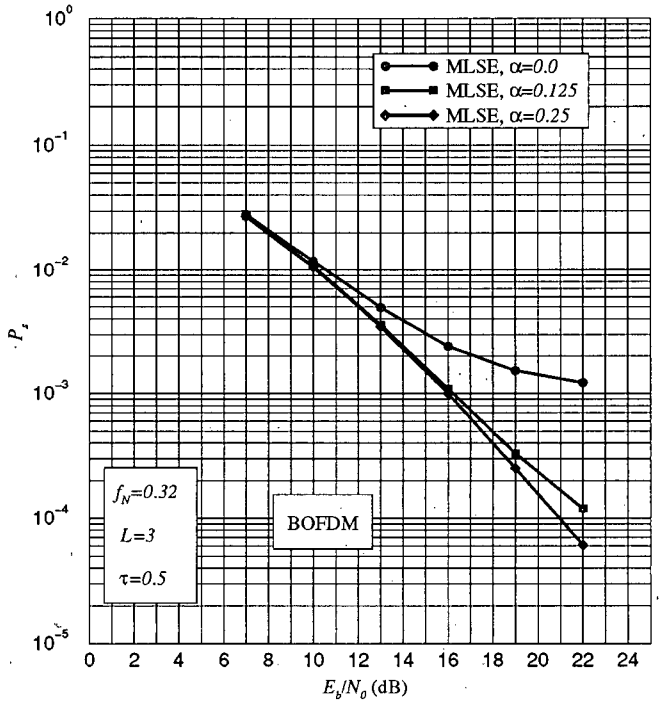

Figure 6.4 Effect of Pulse Shaping on Constraint Length for $f_N = 0.32$

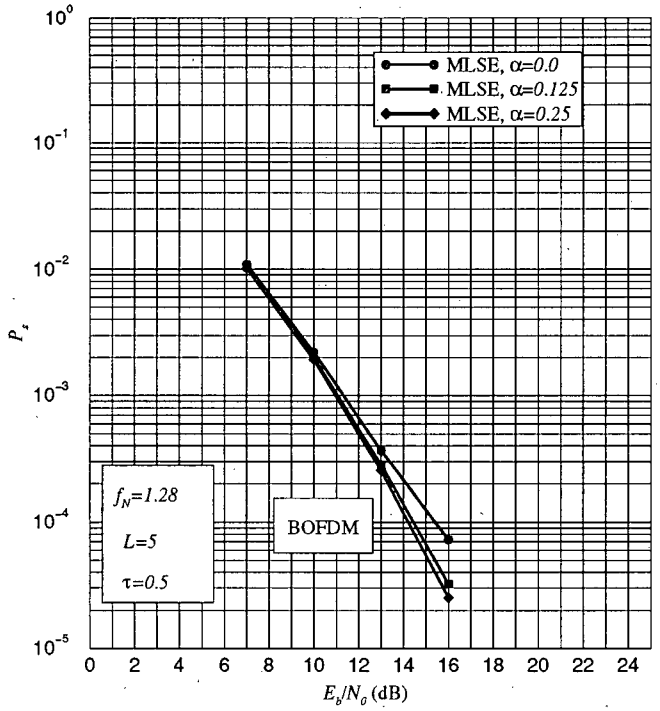

Figure 6.5 Effect of Pulse Shaping on Constraint Length for $f_N = 1.28$

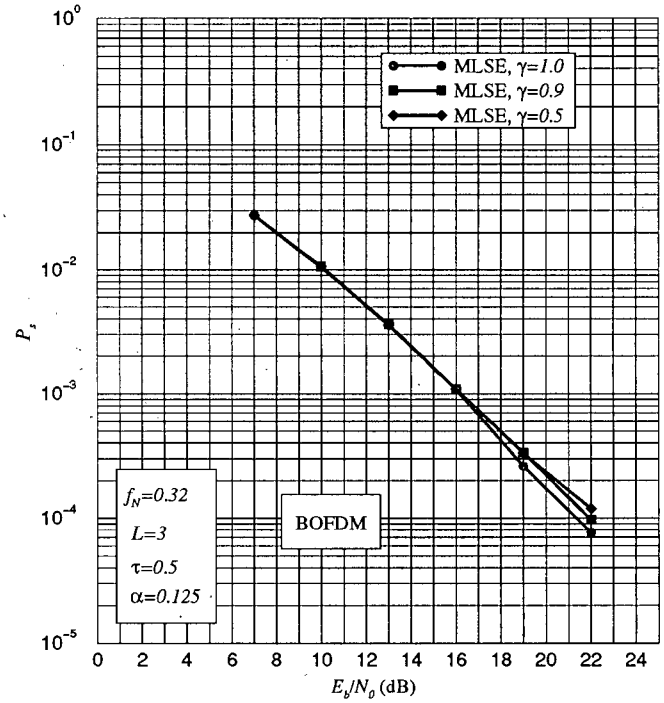

Figure 6.6 Effect of Power Distribution Between Rays for $f_N = 0.32$

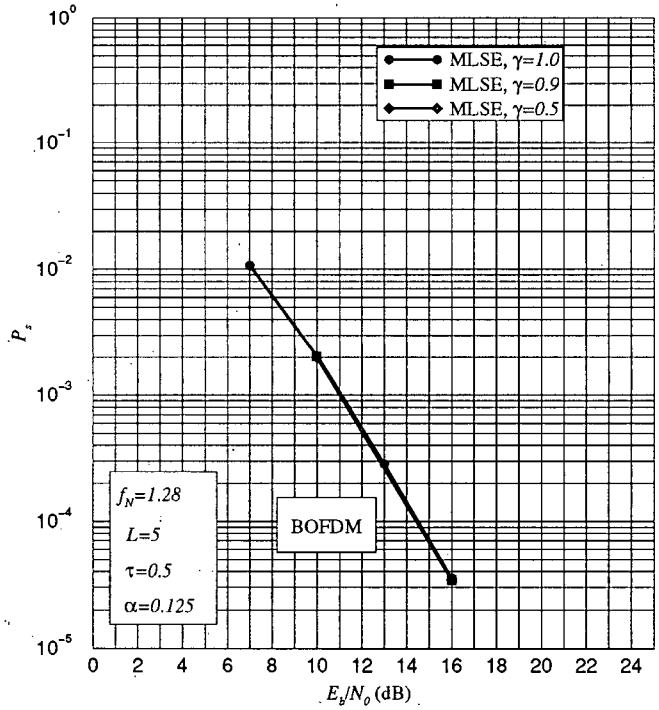

Figure 6.7 Effect of Power Distribution Between Rays for $f_N = 1.28$

6.3 Derivation of an MMSE Linear Receiver

In this section we derive the optimal linear receiver for frequency-selective (delay spread) channels based on the MMSE criterion. This allows us to compare the optimal linear receiver to the truncated MLSE receiver for BOFDM, and to obtain useful results for QOFDM of long blocklength. The latter was not possible for MLSE due to complexity constraints. In addition, simulation of the receiver from this derivation enables us to quantify the effect of the aliasing approximation used in Chapter 5, verifying the assumptions made there.

The approach taken is a generalized version of that used for the flat fading. Again we seek to minimize the MSE given by

$$\begin{aligned} \text{MSE} &= \mathrm{E}\left[|\hat{a}_n - a_n|^2\right] \\ &= \mathrm{E}\left[|\hat{a}_n|^2 - 2\mathrm{Re}[\hat{a}_n a_n^*] + E_a\right] \end{aligned} \tag{6.3.1}$$

and we assume a linear receiver structure of the form

$$\hat{a}_n = \int r(t) c_n(t) e^{-j\frac{2\pi}{T_0}nt} dt \tag{6.3.2}$$

where the interval of integration is over the time of the OFDM block being demodulated. The problem is to determine the weighting functions $c_n(t)$, $0 \leq n \leq N-1$, that are optimal in the MMSE sense. The difference compared to the flat fading case lies in $r(t)$ now having a more complicated form.

We can obtain an implicit expression for $c_n(t)$ using a variational argument [22], or more concisely by differentiation with respect to a function. Using (6.3.2) in (6.3.1) yields

$$\begin{aligned} \text{MSE} = \mathrm{E}[\hat{a}_n \int r^*(t) c_n^*(t) e^{j\frac{2\pi}{T_0}nt} dt - a_n \int r^*(t) c_n^*(t) e^{j\frac{2\pi}{T_0}nt} dt - \\ - a_n^* \int r(t) c_n(t) e^{-j\frac{2\pi}{T_0}nt} dt] + E_a \end{aligned} \tag{6.3.3}$$

and taking the derivative of (6.3.3) with respect to $c_n(u)$ yields

$$\frac{\partial \text{MSE}}{2\partial c_n(u)} = \text{E}\left[\hat{a}_n r^*(u) e^{j\frac{2\pi}{T_0}nu}\right] - \text{E}\left[a_n r^*(u) e^{j\frac{2\pi}{T_0}nu}\right]. \tag{6.3.4}$$

Setting (6.3.4) to 0 and again using (6.3.2) for $\hat{a}_n$ yields

$$\int \text{E}[r^*(u)r(t)]c_n(t)e^{-j\frac{2\pi}{T_0}nt}dt = \text{E}[a_n r^*(u)]. \tag{6.3.5}$$

Equation (6.3.5) is the desired implicit solution for $c_n(t)$ in terms of a general received signal $r(t)$.

Expanding $s(t)$ in (6.1.2) and using $q_i(t) = z_i(t)p(t)$ yields

$$r(t) = \sum_{i=1}^{N_p} \alpha_i q_i(t-\tau_i) \sum_{m=0}^{N-1} a_m e^{j\frac{2\pi}{T_0}m(t-\tau_i)} + n(t). \tag{6.3.6}$$

Using (6.3.6) it is straightforward to evaluate the expectations in (6.3.5), which are

$$\begin{aligned}\frac{\text{E}[r^*(u)r(t)]}{E_a} &= \sum_{m=0}^{N-1}\sum_{i=1}^{N_p} \alpha_i q_i(t-\tau_i)e^{j\frac{2\pi}{T_0}m(t-\tau_i)} \sum_{k=1}^{N_p} \alpha_k q_k^*(u-\tau_k)e^{-j\frac{2\pi}{T_0}m(u-\tau_k)} \\ &\quad + \eta^2\delta(t-u) \\ &= \sum_{m=0}^{N-1} f_m(t)f_m^*(u) + \eta^2\delta(t-u)\end{aligned} \tag{6.3.7}$$

and

$$\frac{\text{E}[a_n r^*(u)]}{E_a} = f_n^*(u) \tag{6.3.8}$$

where for ease of manipulation we have defined

$$f_m(t) = \sum_{i=1}^{N_p} \alpha_i q_i(t-\tau_i)e^{j\frac{2\pi}{T_0}m(t-\tau_i)}. \tag{6.3.9}$$

Upon substituting these expectations into (6.3.5) we obtain

$$\eta^2 c_n(u)e^{-j\frac{2\pi}{T_0}nu} = f_n^*(u) - \sum_{m=0}^{N-1} f_m^*(u) \int f_m(t)c_n(t)e^{-j\frac{2\pi}{T_0}nt}dt. \tag{6.3.10}$$

Equation (6.3.10) is in the form of a Fredholm integral equation [38] of the second kind with a degenerate kernel.

Defining the constants

$$B_{m,n} = \int f_m(t) c_n(t) e^{-j\frac{2\pi}{T_0}nt} dt \tag{6.3.11}$$

(6.3.10) can be written

$$\eta^2 c_n(u) e^{-j\frac{2\pi}{T_0}nu} = f_n^*(u) - \sum_{m=0}^{N-1} B_{m,n} f_m^*(u) \tag{6.3.12}$$

which indicates that $c_n(u)$ is expressible as

$$c_n(u) = \frac{1}{\eta^2} \sum_{m=0}^{N-1} C_{m,n} f_m^*(u) e^{j\frac{2\pi}{T_0}nu}, \tag{6.3.13}$$

a weighted sum of the fading functions defined in (6.3.9). $C_{m,n}$ and $B_{m,n}$ are related by

$$C_{m,n} = \delta_{m-n} - B_{m,n}. \tag{6.3.14}$$

We can obtain a matrix form by defining the linear operator

$$\mathrm{L}[\cdot] = \int f_l(u)(\cdot) du \tag{6.3.15}$$

and applying it to (6.3.12) to yield

$$\eta^2 B_{l,n} = \int f_l(u) f_n^*(u) du - \sum_{m=0}^{N-1} B_{m,n} \int f_l(u) f_m^*(u) du. \tag{6.3.16}$$

Defining the constants $V_{l,n}$ as

$$V_{l,n} = \int f_l(u) f_n^*(u) du \tag{6.3.17}$$

(6.3.16) becomes

$$\eta^2 B_{l,n} = V_{l,n} - \sum_{m=0}^{N-1} V_{l,m} B_{m,n}, \qquad 0 \le l, n \le N-1. \tag{6.3.18}$$

Making some additional definitions, $\mathbf{b_n^T} = [B_{0,n}, B_{1,n}, \ldots, B_{N-1,n}]$, $\mathbf{v_n^T} = [V_{0,n}, V_{1,n}, \ldots, V_{N-1,n}]$, and square matrix $\mathbf{V}$ having $(l,m)^{th}$ element $\mathbf{V_{l,m}} = V_{l,m}$, $0 \le l, m \le N-1$, (6.3.18) can be written in matrix form as

$$\eta^2 \mathbf{b_n} = \mathbf{v_n} - \mathbf{V}\mathbf{b_n} \tag{6.3.19}$$

which has the solution

$$\mathbf{b_n} = \left(\mathbf{V} + \eta^2 \mathbf{I}\right)^{-1} \mathbf{v_n}. \tag{6.3.20}$$

6.3.1 Direct Implementation

It can be seen from the preceding that the operation of the optimal linear receiver is fairly complicated for large N. The sequence of operations is as follows. Channel measurements are used with (6.3.9) and (6.3.17) to obtain the $V_{l,m}$, and these are then used in (6.3.20), requiring an $N \times N$ matrix inversion, to obtain the $B_{m,n}$, which with (6.3.14) and (6.3.13) yield $c_n(u)$. Finally $c_n(u)$ is used in (6.3.2) to obtain the data symbol estimate $\hat{a}_n$.

The matrix inversion is performed only once per OFDM block, but the matrix multiplication in (6.3.20) and subsequent operations must be performed for each data symbol, or N times.

6.3.2 Alternate Implementation

Its possible to circumvent explicit evaluation of $c_n(t)$ by combining (6.3.13) and (6.3.2) to obtain

$$\hat{a}_n = \frac{1}{\eta^2} \sum_{m=0}^{N-1} C_{m,n} \int r(t) f_m^*(t) dt. \tag{6.3.21}$$

Defining the matched filter outputs

$$U_m = \int r(t) f_m^*(t) dt \tag{6.3.22}$$

and applying to (6.3.21) yields

$$\hat{a}_n = \frac{1}{\eta^2} \sum_{m=0}^{N-1} C_{m,n} U_m. \tag{6.3.23}$$

Equation (6.3.23) expresses the data estimates as weighted sums of the matched filter outputs. To use this expression the $C_{m,n}$ are calculated as in the direct implementation and the U_m are determined from (6.3.22). There is little difference in complexity compared to the direct implementation; (6.3.23) was derived to obtain the relationship between $\hat{a}_n$ and U_m explicitly.

6.3.3 Evaluation of U_m and V_m

Matched Filter Outputs Using the definitions of U_m in (6.3.22) and the fading functions $f_m(t)$ defined in (6.3.9) yields

$$\begin{aligned} U_m &= \int r(t) f_m^*(t) dt \\ &= \int \left[\sum_{i=1}^{N_b} \alpha_i r(t+\tau_i) q_i^*(t) \right] e^{-j\frac{2\pi}{T_0} mt} dt \end{aligned} \tag{6.3.24}$$

which is identical to (6.2.9). We see that both the MLSE and MMSE analyses prescribe calculation of the same matched filter outputs.

Tone Correlations The tone correlations are defined in (6.3.17). Expanding this with (6.3.9) as above yields

$$\begin{aligned} V_{l,n} &= \int f_l(t) f_n^*(t) dt \\ &= \int \sum_{i=1}^{N_b} \sum_{k=1}^{N_b} \alpha_i \alpha_k q_i(t-\tau_i) q_k^*(t-\tau_k) e^{j\frac{2\pi}{T_0} l(t-\tau_i)} e^{-j\frac{2\pi}{T_0} n(t-\tau_k)} \\ &= \int \left[\sum_{i=1}^{N_b} \alpha_i^2 |q_i(t)|^2 e^{-j\frac{2\pi}{T_0}(n-l)t} \right] dt \\ &\quad + \sum_{i=1}^{N_b} \sum_{\substack{k=1 \\ k\neq i}}^{N_b} e^{-j\frac{2\pi}{T_0} l\tau_i} e^{j\frac{2\pi}{T_0} n\tau_k} \alpha_i \alpha_k \int q_i(t-\tau_i) q_k^*(t-\tau_k) e^{-j\frac{2\pi}{T_0}(n-l)t} dt \end{aligned} \tag{6.3.25}$$

and using the definition (6.2.14) this can be written

$$V_{l,n} = I_{1_{n-l}} + \sum_{i=1}^{N_b} \sum_{\substack{k=1 \\ k\neq i}}^{N_b} e^{-j\frac{2\pi}{T_0} l\tau_i} e^{j\frac{2\pi}{T_0} n\tau_k} I_{i,k_{n-l}} \tag{6.3.26}$$

which is identical to (6.2.15). As with the matched filter outputs, both the MLSE and MMSE analyses prescribe calculation of the same tone correlations.

6.3.4 Relation between Integral Equation and Matrix Formulations

The preceding analysis based on solving the integral equation (6.3.5) determined that the optimal linear MMSE estimates have the form

$$\hat{a}_n = \frac{1}{\eta^2} \sum_{m=0}^{N-1} C_{m,n} U_m. \tag{6.3.27}$$

An alternative solution method for the $C_{m,n}$ can be obtained by *assuming* (6.3.27) as an optimal form for the solution and applying matrix based MMSE estimation theory. It is instructive to compare the solutions obtained by the two methods.

We obtain (6.3.27) in matrix form by defining the vectors $\mathbf{c_n^T} = [C_{0,n}, C_{1,n}, \cdots, C_{N-1,n}]$ and $\mathbf{u}^{\mathrm{T}} = [U_0, U_1, \cdots, U_{N-1}]$, then

$$\hat{a}_n = \frac{1}{\eta^2} \mathbf{c_n^T u}. \tag{6.3.28}$$

It is well known that the MMSE solution for an equation having the form of (6.3.28) is given by [23]

$$\mathbf{c_n} = \eta^2 \mathbf{R}^{-1*} \mathbf{p_n^*} \tag{6.3.29}$$

where

$$\mathbf{R} = \mathrm{E}\left[\mathbf{u}\mathbf{u}^{\mathrm{H}}\right] \tag{6.3.30}$$

and

$$\mathbf{p_n} = \mathrm{E}[\mathbf{u} a_n^*]. \tag{6.3.31}$$

The $(l,k)^{th}$ element of $\mathbf{R}$ is $\mathbf{R_{l,k}} = R_{l,k}$. It is determined from (6.3.30) and (6.3.22) yielding

$$\begin{aligned} R_{l,k} &= \mathrm{E}[U_l, U_k^*] \\ &= \int\int \mathrm{E}[r(t) r^*(u)] f_l^*(t) f_k(u)\, dt\, du. \end{aligned} \tag{6.3.32}$$

Expanding $\mathrm{E}[r(t)r^*(u)]$ with (6.3.7) and using (6.3.17) it is readily shown

$$R_{l,k} = E_a \sum_{m=0}^{N-1} V_{k,m} V_{m,l} + N_0 V_{k-l} \tag{6.3.33}$$

or

$$\mathbf{R} = E_a \mathbf{V}^{\mathrm{T}} \mathbf{V}^{\mathrm{T}} + N_0 \mathbf{V}^{\mathrm{T}}. \tag{6.3.34}$$

Similarly it can be shown

$$\mathbf{p_n} = E_a \mathbf{v_n^*}. \tag{6.3.35}$$

Combining (6.3.34) (6.3.35) and (6.3.29) yields $\mathbf{c_n}$ as

$$\begin{aligned} \mathbf{c_n} &= \eta^2 \left(\mathbf{V}^{\mathrm{T}} \mathbf{V}^{\mathrm{T}} + \eta^2 \mathbf{V}^{\mathrm{T}} \right)^{-1*} \mathbf{v_n} \\ &= \eta^2 \left(\mathbf{V}\mathbf{V} + \eta^2 \mathbf{V} \right)^{-1} \mathbf{v_n} \end{aligned} \tag{6.3.36}$$

where we have also used $\mathbf{V} = \mathbf{V}^{\mathrm{H}} = \mathbf{V}^{\mathrm{T}*}$ to obtain the last line of (6.3.36).

The matrix based solution for $\mathbf{c_n}$ in (6.3.36) has a different form than that from the integral equation solution, and so it is not obvious that they are the same. Using the definition of $\mathbf{c_n}$ and combining with (6.3.20) we have from the latter method

$$\mathbf{c_n} = \mathbf{d_n} - \left(\mathbf{V} + \eta^2 \mathbf{I} \right)^{-1} \mathbf{v_n} \tag{6.3.37}$$

where $\mathbf{d_n}$ has a 1 in the n^{th} position and $0's$ elsewhere.

We demonstrate the equivalence of (6.3.36) and (6.3.37) by contradiction. Assuming inequality

$$\eta^2 \left(\mathbf{V}\mathbf{V} + \eta^2 \mathbf{V} \right)^{-1} \mathbf{v_n} \neq \mathbf{d_n} - \left(\mathbf{V} + \eta^2 \mathbf{I} \right)^{-1} \mathbf{v_n} \tag{6.3.38}$$

from which it follows

$$\begin{aligned} \eta^2 \left(\mathbf{V} + \eta^2 \mathbf{I} \right)^{-1} \mathbf{V}^{-1} \mathbf{v_n} &\neq \mathbf{d_n} - \left(\mathbf{V} + \eta^2 \mathbf{I} \right)^{-1} \mathbf{v_n} \\ \eta^2 \mathbf{V}^{-1} \mathbf{v_n} &\neq \mathbf{v_n} + \eta^2 \mathbf{d_n} - \mathbf{v_n} \\ \eta^2 \mathbf{v_n} &\neq \eta^2 \mathbf{V} \mathbf{d_n} \end{aligned} \tag{6.3.39}$$

and

$$\eta^2 \mathbf{v_n} \neq \eta^2 \mathbf{v_n}. \tag{6.3.40}$$

Equation (6.3.40) is a contradiction, establishing the equivalence of (6.3.36) and (6.3.37).

Stability Comparison In terms of numerical stability (6.3.37) from the integral equation approach is a more desirable form than (6.3.36). This can be seen by comparing the condition numbers of the matrices which must be inverted in each case.

The condition number $\mathrm{cn}(\mathbf{M})$ of a matrix $\mathbf{M}$ is defined as the ratio of the magnitude of its minimum to maximum eigenvalues [39]

$$\mathrm{cn}(\mathbf{M}) = \left| \frac{\lambda min}{\lambda max} \right| \tag{6.3.41}$$

where λmin and λmax are the minimum and maximum eigenvalues respectively. By definition $\mathrm{cn}(\mathbf{M})$ ranges between 0 and 1. A condition number close to zero implies the matrix is nearly singular [25] and problems of numerical stability can be expected with its attempted inversion.

Since $\mathbf{V} = \mathbf{V}^{\mathrm{H}}$ it is possible to perform an eigenvector decomposition and express it as

$$\mathbf{V} = \sum_{k=0}^{N-1} \lambda_k \mathbf{e_k} \mathbf{e_k^H} \tag{6.3.42}$$

where the $\mathbf{e_k}$ are the eigenvectors of $\mathbf{V}$. Using (6.3.42) we can write the relevant matrix of (6.3.37) as

$$\begin{aligned} \left(\mathbf{V} + \eta^2 \mathbf{I}\right) &= \sum_{k=0}^{N-1} \lambda_k \mathbf{e_k} \mathbf{e_k^H} + \eta^2 \mathbf{I} \\ &= \sum_{k=0}^{N-1} \left(\lambda_k + \eta^2\right) \mathbf{e_k} \mathbf{e_k^H} \end{aligned} \tag{6.3.43}$$

which reveals the condition number of $\left(\mathbf{V} + \eta^2 \mathbf{I}\right)$ to be

$$\mathrm{cn}\left(\mathbf{V} + \eta^2 \mathbf{I}\right) = \left| \frac{\lambda_{min} + \eta^2}{\lambda_{max} + \eta^2} \right|. \tag{6.3.44}$$

Similarly, the condition number of $(\mathbf{VV}+\eta^2\mathbf{V})$ is

$$\begin{aligned}\mathrm{cn}(\mathbf{VV}+\eta^2\mathbf{V}) &= \mathrm{cn}(\mathbf{V}(\mathbf{V}+\eta^2\mathbf{I})) \\ &= \mathrm{cn}\left(\sum_{k=0}^{N-1}\lambda_k\mathbf{e_k}\mathbf{e_k^H}\left(\sum_{i=0}^{N-1}(\lambda_i+\eta^2)\mathbf{e_i}\mathbf{e_i^H}\right)\right) \\ &= \mathrm{cn}\left(\sum_{k=0}^{N-1}\lambda_k(\lambda_k+\eta^2)\mathbf{e_k}\mathbf{e_k^H}\right) \\ &= \left|\frac{\lambda_{min}(\lambda_{min}+\eta^2)}{\lambda_{max}(\lambda_{max}+\eta^2)}\right|\end{aligned} \tag{6.3.45}$$

which shows

$$\mathrm{cn}(\mathbf{VV}+\eta^2\mathbf{V}) = \left|\frac{\lambda_{min}}{\lambda_{max}}\right|\mathrm{cn}(\mathbf{V}+\eta^2\mathbf{I}). \tag{6.3.46}$$

Two conclusions that can be drawn from (6.3.44)-(6.3.46) is that $(\mathbf{V}+\eta^2\mathbf{I})$ cannot be exactly singular for non-zero η^2, but it can be close for η^2 small. In contrast the matrix $(\mathbf{VV}+\eta^2\mathbf{V})$ can be singular for non-zero η^2 if $\lambda_{min}=0$, and will in any case be closer to singularity than $(\mathbf{V}+\eta^2\mathbf{I})$ by the factor $|\lambda_{min}/\lambda_{max}|$.

6.3.5 An Efficient Matrix Formulation for Rate N/T_0 Sampling

The transmitted OFDM signal $s(t)$ is given by

$$s(t) = p(t)\sum_{n=0}^{N-1} a_n e^{j\frac{2\pi}{T_0}nt}, \quad 0\le t\le T_0(1+\alpha). \tag{6.3.47}$$

Using the two-ray Rayleigh fading model, the received signal is given by

$$\begin{aligned}r(t) = \alpha_1 z_1(t)s(t) + \alpha_2 z_2(t-\tau)s(t-\tau) + n(t), \\ 0\le t\le T_0(1+\alpha)+\tau.\end{aligned} \tag{6.3.48}$$

In Chapter 5 we reasoned that the aliasing introduced by sub-Nyquist sampling at rate N/T_0 should not noticeably increase the error rate for large N. This suggests we could model equations (6.3.47) and (6.3.48) sufficiently accurately by sampling at rate

$1/\Delta t = N/T_0$ to obtain a discrete model which is then suitable for a matrix description. The discrete versions of the transmitted signal and received signal are then

$$s_m = p_m \sum_{n=0}^{N-1} a_n e^{j\frac{2\pi}{N}nm}, \quad 0 \le m \le N_\alpha - 1 \tag{6.3.49}$$

where

$$\begin{aligned} N_\alpha &= \left\lfloor \frac{T_0(1+\alpha)}{\Delta t} \right\rfloor \\ &= \lfloor N(1+\alpha) \rfloor \end{aligned} \tag{6.3.50}$$

and

$$\begin{aligned} r_m = \alpha_1 z_{1_m} s_m + \alpha_2 z_{2_{m-\tau}} s_{m-\tau} + n_m, \\ 0 \le m \le N_\tau - 1 \end{aligned} \tag{6.3.51}$$

where

$$N_\tau = \lfloor N(1+\alpha) + \tau/\Delta t \rfloor \tag{6.3.52}$$

respectively.

Defining the following matrices

$$\mathbf{s}^{\mathrm{T}} = [s_0, s_1, \ldots s_{N_a-1}], \tag{6.3.53}$$

$$\mathbf{P} = \mathrm{diag}(p_0, p_1, \ldots, p_{N_\alpha - 1}), \tag{6.3.54}$$

$$\begin{aligned} \mathbf{D} = [\{\mathbf{D}_{\mathrm{m,n}}\}], \quad \mathbf{D}_{\mathrm{m,n}} = e^{j\frac{2\pi}{N}mn}, \\ 0 \le n \le N - 1 \\ 0 \le m \le N_\alpha - 1 \end{aligned} \tag{6.3.55}$$

and

$$\mathbf{a}^{\mathrm{T}} = [a_0, a_1, \ldots, a_{N-1}] \tag{6.3.56}$$

(6.3.49) can be written

$$\mathbf{s} = \mathbf{PDa}. \tag{6.3.57}$$

Similarly defining

$$\mathbf{Z} = \left[\left\{\mathbf{Z}_{\mathrm{l,m}}\right\}\right], \quad \mathbf{Z}_{\mathrm{l,m}} = \begin{cases} \alpha_1 z_{1_m}, & l = m, \\ \alpha_2 z_{2_m}, & l = m + \tau/\Delta t \\ 0, & l \neq m \end{cases} \tag{6.3.58}$$

$$0 \leq m \leq N_\alpha - 1$$

$$0 \leq l \leq N_\tau - 1$$

$$\mathbf{r}^{\mathrm{T}} = [r_0, r_1, \ldots, r_{N_\tau}] \tag{6.3.59}$$

and

$$\mathbf{n}^{\mathrm{T}} = [n_0, n_1, \ldots, n_{N_\tau}] \tag{6.3.60}$$

(6.3.51) is

$$\begin{aligned} \mathbf{r} &= \mathbf{Z}\mathbf{s} + \mathbf{n} \\ &= \mathbf{Z}\mathbf{P}\mathbf{D}\mathbf{a} + \mathbf{n} \\ &= \mathbf{Q}\mathbf{D}\mathbf{a} + \mathbf{n} \end{aligned} \tag{6.3.61}$$

where

$$\mathbf{Q} = \mathbf{Z}\mathbf{P}. \tag{6.3.62}$$

If we form the estimates of $\mathbf{a}$ with

$$\hat{\mathbf{a}} = \mathbf{C}^{\mathrm{H}}\mathbf{r} \tag{6.3.63}$$

then it is readily shown that the linear MMSE choice for the weighting matrix $\mathbf{C}^{\mathrm{H}}$ is found from

$$\begin{aligned} \mathbf{C} &= \left(\mathrm{E}\left[\mathbf{r}\mathbf{r}^{\mathrm{H}}\right]\right)^{-1}\mathrm{E}\left[\mathbf{r}\mathbf{a}^{\mathrm{H}}\right] \\ &= \left(\mathbf{Q}\mathbf{Q}^{\mathbf{H}} + \eta^2\mathbf{I}\right)^{-1}\mathbf{Q}\mathbf{D} \end{aligned} \tag{6.3.64}$$

or

$$\mathbf{C}^{\mathrm{H}} = \mathbf{D}^{\mathrm{H}}\mathbf{Q}^{\mathrm{H}}\left(\mathbf{Q}\mathbf{Q}^{\mathrm{H}} + \eta^2\mathbf{I}\right)^{-1} \tag{6.3.65}$$

which yields for the estimate

$$\hat{\mathbf{a}} = \mathbf{D}^{\mathrm{H}}\mathbf{Q}^{\mathrm{H}}\left(\mathbf{Q}\mathbf{Q}^{\mathrm{H}} + \eta^2\mathbf{I}\right)^{-1}\mathbf{r}. \tag{6.3.66}$$

Equation (6.3.66) is a more efficient way to obtain $\hat{\mathbf{a}}$ than to explicitly determine $\mathbf{C}^{\mathrm{H}}$ and use it in (6.3.63). By first premultiplying $\mathbf{r}$ by $\left(\mathbf{Q}\mathbf{Q}^{\mathrm{H}} + \eta^2\mathbf{I}\right)^{-1}$, premultiplying the result by $\mathbf{Q}^{\mathrm{H}}$ and then by $\mathbf{D}^{\mathrm{H}}$, the rectangular by rectangular matrix multiplications are replaced with rectangular matrix by vector multiplications. This requires approximately N times less computation. Further, with the computation organized in this way $\mathbf{D}^{\mathrm{H}}$ is multiplying a vector

$$\hat{\mathbf{s}} = \mathbf{Q}^{\mathrm{H}}\left(\mathbf{Q}\mathbf{Q}^{\mathrm{H}} + \eta^2\mathbf{I}\right)^{-1}\mathbf{r} \tag{6.3.67}$$

which can be interpreted as an estimate of the undistorted signal $\mathbf{s}$. Combining (6.3.67) and (6.3.66)

$$\hat{\mathbf{a}} = \mathbf{D}^{\mathrm{H}}\hat{\mathbf{s}} \tag{6.3.68}$$

which is efficiently evaluated by an inverse FFT of $\hat{\mathbf{s}}$.

Comparison to Integral Equation Solution The advantage of this formulation over that derived with the integral equation approach can be seen from the definitions of $\mathbf{Z}$ and $\mathbf{Q}$ in (6.3.58) and (6.3.62) respectively. These fading matrices are two–diagonal and consequently $\left(\mathbf{Q}\mathbf{Q}^{\mathrm{H}} + \eta^2\mathbf{I}\right)$ is three–diagonal. By n–diagonal it is meant that all matrix entries are zero except possibly those on n diagonals, where the diagonals are not necessarily adjacent. Therefore $\left(\mathbf{Q}\mathbf{Q}^{\mathrm{H}} + \eta^2\mathbf{I}\right)$ can be inverted with only $O(N)$ operations [25] as opposed to $O\left(N^3\right)$ operations for a general matrix inversion. For the more general N_b-ray fading model the complexity of the matrix inversion varies as $N_b^2 N$ with N_b typically 6 or less and independent of N. The principal limitation of this formulation is that the complexity of the matrix inversion varies with the sampling rate

as can be seen from (6.3.50). In (6.3.58) it is assumed that τ is an integer multiple of Δt. More generally the sampling rate must be increased to obtain finer resolution of τ since this resolution is limited to Δt. With the integral equation formulation the size of the matrix which must be inverted is independent of Δt.

6.3.6 Simulation Results

In this section we evaluate by simulation the performances of the various optimal linear MMSE receivers developed in the previous sections, and compare them to the MLSE receivers. As in the flat fading case, the complexity reduction of MMSE relative to MLSE receivers allows simulation of QOFDM as well as BOFDM.

For this work we also produced the first simulation of the ideal linear MMSE receiver based on the integral equation formulation. Consequently we are able to verify empirically certain comments made previously about the significance of the Transform Approximation made in Chapter 5 and about the relationship between the integral equation and rate N/T_0 matrix formulations made in Section 6.3.5 of this chapter.

Figure 6.8 shows the effect of delay spread on the ideal linear MMSE receiver determined by the integral equation approach (IEMSE) and also includes the corresponding results from the ideal MLSE for comparison. Blocklength $N = 4$ is chosen because it is the only blocklength for which ideal MLSE is feasible with QOFDM; this is shown in Figure 6.9. The performances of the two receivers are remarkably close for both modulation formats, within a fraction of 1 dB at $P_s = 10^{-3}$ in each case. As might be expected[25], the greater difference is for BOFDM. The closeness of the results indicate that ISI poses little problem at such a short blocklength. This is because the channel changes little during the duration of the block, therefore there is little intrablock ISI, and the small number of symbols means there are few contributors to interray ISI. Further,

[25] In Chapter 4 we showed BOFDM suffers less than QOFDM from ISI on flat fading channels

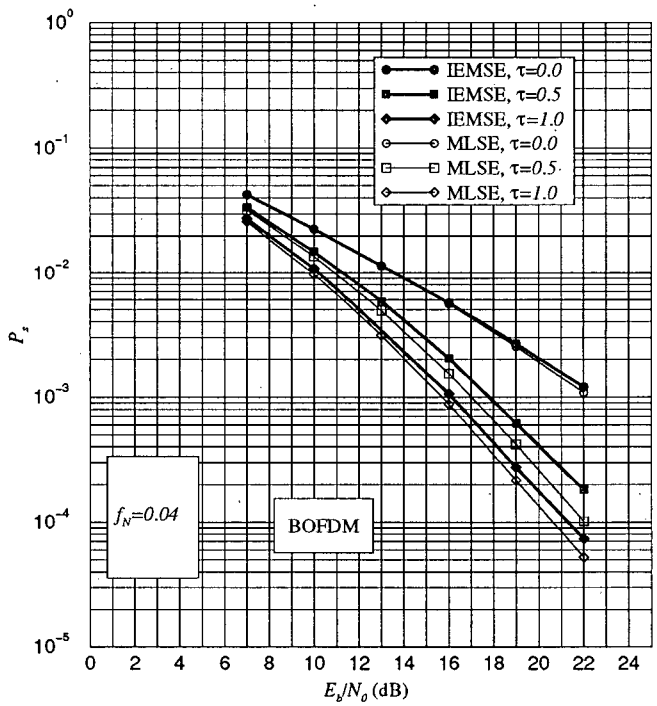

Figure 6.8 Effect of Delay Spread for Ideal MSE, for $f_N = 0.04$ and BOFDM

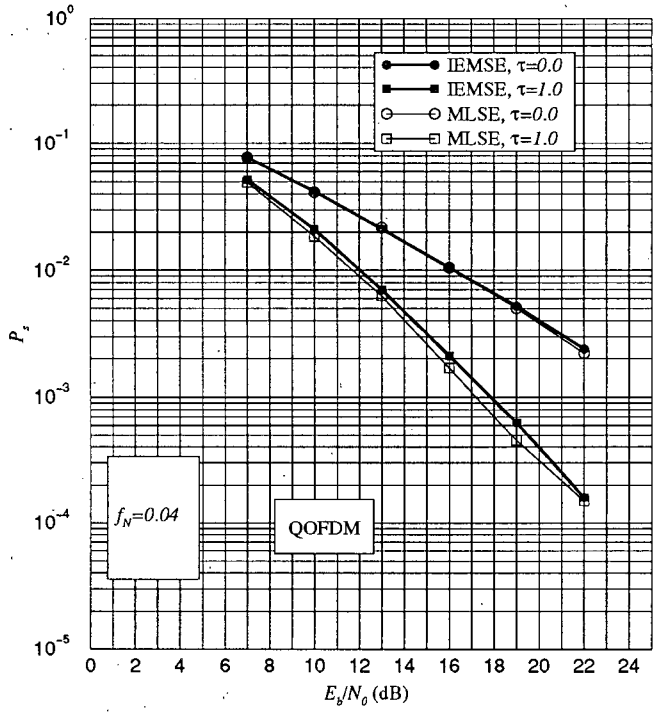

Figure 6.9 Effect of Delay Spread for Ideal MSE, for $f_N = 0.04$ and QOFDM

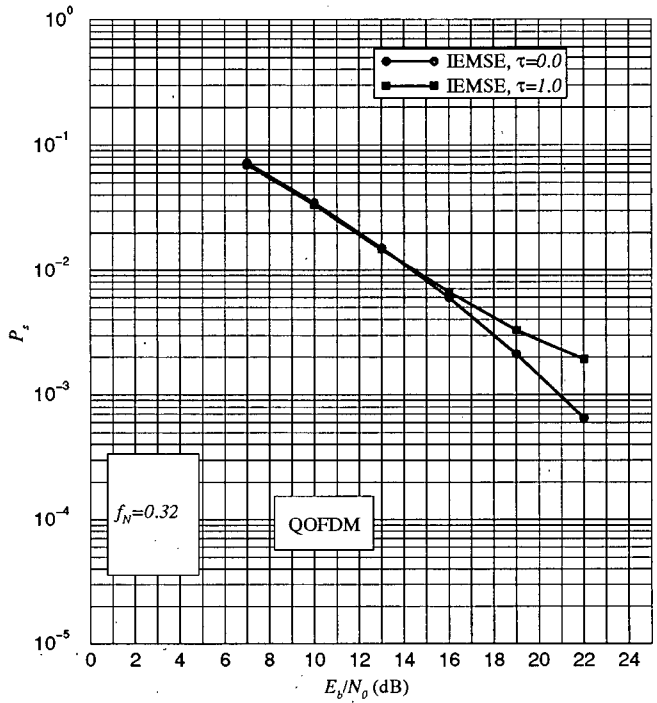

Figure 6.10 Effect of Delay Spread for Ideal MSE, for $f_N = 0.32$ and QOFDM

since the equalized block is essentially ISI free, the P_s for QOFDM is very nearly twice that for BOFDM, indicating a lack of intrasymbol ISI.

Figure 6.10 shows the effect of delay spread for IEMSE for QOFDM with $f_N = 0.32$. For this longer block, the accumulated effects of the various types of ISI make the delay spread case with $\tau = 1.0$ noticeably poorer than the flat fading case, causing the appearance of an error floor near $P_s = 10^{-3}$. Some deterioration can also be anticipated with longer blocks, such as $f_N = 1.28$.

Unfortunately, as discussed in the derivations, the complexity of the matrix inversion required for the IEMSE receiver varies with N^3, and is largely impractical for $N = 128$, as the simulations used to produce the results of this section process from $50,000$ to $100,000$ blocks. Using the insights developed concerning pulse shaping and constraint length in the context of the MLSE work, it is clearly possible to develop an approximation to the IEMSE of complexity proportional to L^2N which would then allow simulation of

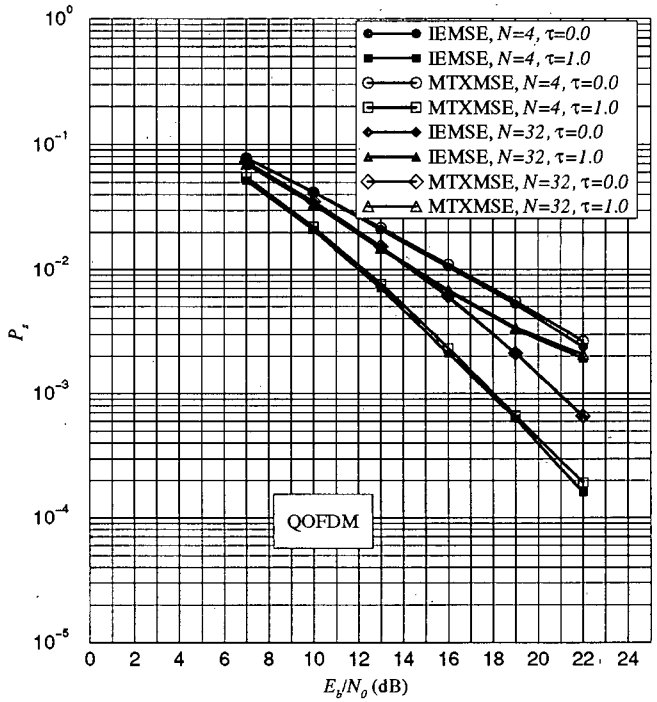

Figure 6.11 Proximity of the Matrix Formulation Results to the Ideal MSE Results

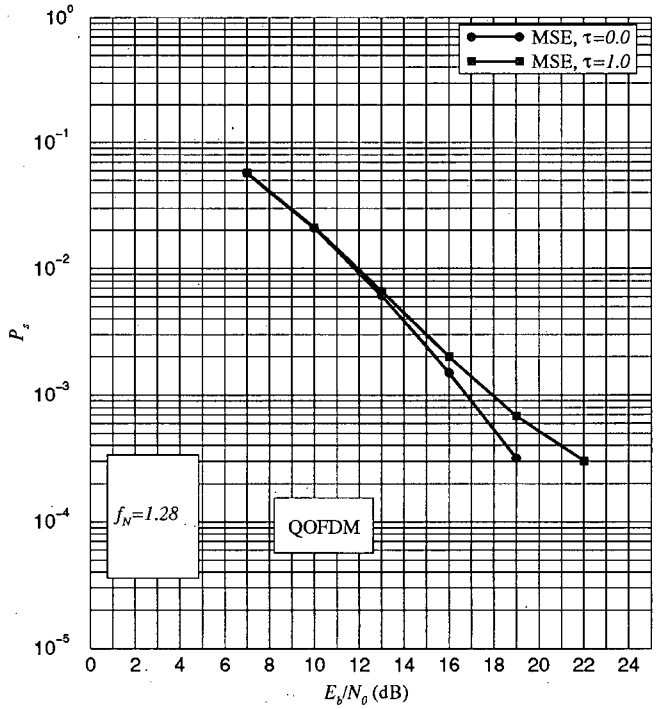

Figure 6.12 Effect of Delay Spread for $f_N = 1.28$

any blocklength of interest. An alternative approach, in which the frequency-selective channel was treated as a set of parallel flat fading channels was presented in [5].

However, we pursue instead means of determining the performance of the optimal linear MMSE receiver. The approach we take is to establish that the efficient matrix formulation of Section 6.3.5 produces results which are very close to those of the IEMSE receiver for $N \geq 32$, and may thus be used to determine the linear MMSE performance bound for $f_N = 1.28$.

In Chapter 5 we reasoned that the use of sub-Nyquist sampling at rate N/T_0 was an aliasing approximation which replaced a linear convolution with a circular convolution, and further that this effect would be insignificant for large values of N. We note that the only deviation of the matrix formulation of Section 6.3.5 (MTXMSE) from the ideal MMSE linear receiver is the use of this same aliasing approximation.

In Figure 6.11 results from the IEMSE are compared to the MTXMSE for QOFDM, for $N = 4$ and 32, and for both flat and delay spread fading channels. For the IEMSE results, the symbols identifying the curves are small and opaque. The corresponding curves for the MTXMSE use the same symbol shapes, but transparent and enlarged. In this way it can be seen that while there is a very small difference when $N = 4$, the curves for $N = 32$ are essentially coincident. The same coincidence would be expected for any N larger. Thus we obtain in Figure 6.12 the effect of delay spread for $f_N = 1.28$, and find about 1.2 dB of deterioration relative to the flat fading case at $P_s = 10^{-3}$.

Figure 6.13 shows comparisons of the ideal MLSE and IEMSE receivers to the MFB for $f_N = 0.04$. MFB's are given for three values of delay spread, with the amount of delay spread increasing from the top to the bottom of the graph. The results for the MLSE receiver are almost coincident with the MFB at all delay spreads, indicating negligible loss from ISI. The IEMSE receiver performs nearly as well for $\tau = 0.0$ and $\tau = 1.0$, but has about 1 dB deterioration at $P_s = 10^{-3}$ when $\tau = 0.5$.

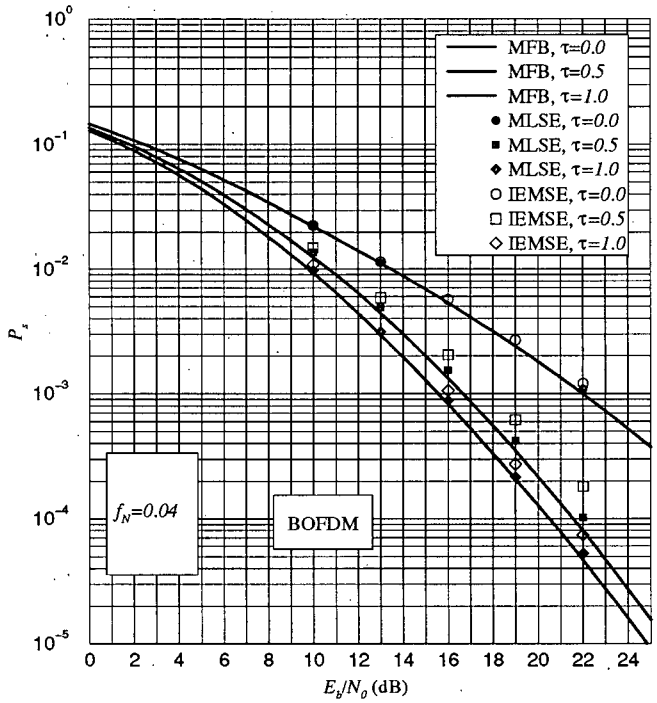

Figure 6.13 Comparison of the MFB to the IEMSE and MLSE Receivers for $f_N = 0.04$.

The discrepancies found between the MFB, MLSE, and MMSE receivers are greater for $f_N = 0.32$ and $f_N = 1.28$. This is expected because long blocklengths suffer substantial ISI which is neglected in the MFB formulation. Figure 6.14 shows a comparison of the MFB to the MLSE receiver for these two cases. The MLSE receiver, which at these blocklengths is the truncated MLSE receiver with $\alpha = 0.125$, still performs quite well, with about 0.7 dB discrepancy from the MFB for $f_N = 1.28$ and about 1.8 dB for $f_N = 0.32$, both compared at $P_s = 10^{-3}$. As shown in Figures 6.6 and 6.7, the MLSE receiver has essentially the same performance on delay spread as flat fading channels. The MFB in contrast has a larger diversity gain due to delay spread at $f_N = 0.32$ than at $f_N = 1.28$. This accounts for the relatively poorer performance of the MLSE receiver in the former case.

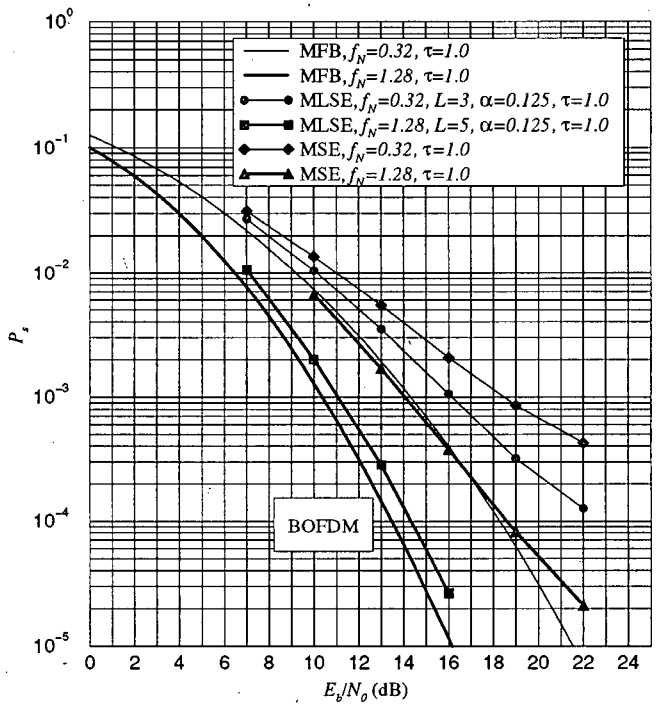

Figure 6.14 Comparison of the MFB to the MSE and MLSE Receivers for $f_N = 0.32$ and $f_N = 1.28$.

Figure 6.14 also shows results for a linear MMSE[26] receiver for $f_N = 1.28$. Its performance is about 3 dB worse at $P_s = 10^{-3}$ than the MLSE receiver. This is due to the inherent inferiority of linear compared to maximum likelihood estimation techniques in the presence of ISI.

6.4 Conclusion

We have derived optimal and suboptimal versions of an MLSE receiver for OFDM on frequency-selective fading channels, and evaluated their performance by simulation. In contrast to our previous results for the flat fading channel we found that pulse shaping has a large effect on the P_s of the truncated MLSE receiver when it is used on channels with delay spread. This is due to the presence of cross-correlations between the received OFDM blocks in the latter case.

[26] This is designated MSE on the figure, and was simulated by MTXMSE.

We also derived an optimal linear MMSE receiver for frequency-selective fading channels, based upon an integral equation formulation of the estimation problem. This approach allowed us, with P_s results generated by simulation, to quantify the effect of the aliasing approximation first discussed in Chapter 5 in the context of flat fading, as well as for the delay spread cases of this chapter. The effect was shown to be negligible for $N \geq 32$, and only a fraction of 1 dB for N as low as 4. This led to an MSE receiver form using the aliasing approximation whose complexity is only linear in N, with essentially optimal performance for long blocklengths.

We compared the solution form obtained from the integral equation approach to the solution form obtained from a conventional matrix analysis approach, and showed them to be theoretically equivalent when finite precision effects are neglected, but having the important difference that the integral equation form is more stable numerically. This difference was quantified in terms of the eigenvalues of a certain channel dependent tone correlation matrix.

For the short blocklength $N = 4$ it was shown that diversity gains are achieved by the MLSE and MMSE receivers which are very close to the MFB gains. For the longer blocklengths, it was found that the diversity gains were almost balanced by the increase in ISI with blocklength and diversity, yielding performance basically unchanged from the flat fading case. This result is based on the normalization choice which compares the flat fading and delay spread fading on the basis of same total received power. If we were to ask a slightly different, but equally valid, question by considering the performance on a flat fading channel, and then ask what would be the effect of the arrival of a second ray, we would then see a net gain due to the increase in total received power.

A key difference between the flat-fading and delay spread channels is revealed by comparing the results for QOFDM with $N = 4$, 32, and 128. These show that in contrast to the flat-fading case, on delay spread channels longer block lengths do not

necessarily have a lower P_s. This suggests that deliberately introduced delay spread via transmitter diversity in combination with short blocks might be more effective than channel averaging with long blocks.

Chapter 7

Conclusion and Suggestions for Future Work

7.1 Conclusion

The performance and receiver structures for channel-averaging OFDM on land mobile radio channels characterized by flat and frequency-selective Rayleigh fading have been studied. A new matched filter bound (MFB) applicable to fast fading was derived to establish lower limits on the P_b of any receiver structure applied to uncoded OFDM on these channels, and to provide a benchmark for receiver performance. The theory of equalization was developed in the context of OFDM using integral equation and matrix formulations. New nonlinear sequence estimating and decision feedback receiver structures were derived using MLSE and MMSE optimality criteria. The performance of these receivers was evaluated by simulation and found to equal or in most cases exceed previous results for the same modulation and channels.

Several insights were obtained into the nature of the ISI in OFDM caused by fading. BOFDM was found to be much less sensitive to ISI than QOFDM. With BOFDM, a simple truncated MLSE receiver can approach the MFB to within 1 dB, but it is effectively useless for long blocklength QOFDM due to the required constraint length. The channel impulse response is amenable to reshaping by the MSEDIR technique which was devised to reduce the constraint length of the ISI, making sequence estimation feasible and improving the performance of DFE substantially. ISI on frequency-selective fading channels is much worse than for flat fading channels. The problem was shown to be the appearance of certain cross-terms arising in the tone correlations due to the interaction of multiple received versions of the transmitted OFDM block, but controllable with by proper pulse shaping.

We conclude that the channel averaging ability of OFDM gives it a substantial P_b performance advantage over any other uncoded modulation on fast flat Rayleigh fading

channels, and that most of the gain indicated by the MFB is attainable by the nonlinear receiver structures devised in this thesis. On frequency-selective Rayleigh fading channels a comparison with conventional serial modulation schemes is less positive. This is mainly because of diminishing returns with increasing diversity, also predicted by the MFB. The presence of a second uncorrelated ray in the delay spread case causes a large diversity improvement for short blocklength OFDM and serial modulation schemes which is not available for long blocklength OFDM[27]. By comparing the results for $N = 4$ and $N = 32$ was found that given an equally sophisticated receiver, the performance of a serial modulation scheme would be comparable to OFDM if the powers in the two rays were similar. Of course, this is a very special case. Long blocklength OFDM maintains an important advantage when the relative strengths of the received rays are unknown a priori because it is fairly insensitive to the power distribution among the rays.

7.2 Suggestions for Future Work

1. *Interleaved OFDM* Interleaved OFDM (IOFDM) is a variation of OFDM originated during this investigation. The idea is shown in Figure 7.1. A serial data stream a_k is partitioned into short blocks of $N = 4$. These are transformed by a 4-point inverse FFT to obtain a new set of symbols b_k. The b_k stream is applied to an interleaver, and the output of the interleaver feeds a conventional serial modulator. At the receiver the process is reversed. The inverse FFT time-diversifies the a_k information over the b_k, and the interleaver decorrelates the samples of a particular OFDM block. This method provides the diversity gain of a much longer block with a block length short enough to allow ideal MLSE. Some preliminary results for BPSK IOFDM (BIOFDM) on a flat Rayleigh fading channel, plotted in Figure 7.2, show a comparison to BOFDM with $f_D = 0.01$ and $N = 128$. Ideal interleaving

[27] unless τ_{max} approaches $N/2$, an impractically large value.

(ideal interleaving results in uncorrelated received samples for $f_N > 0.0$) and perfect channel estimation were assumed in the simulation.

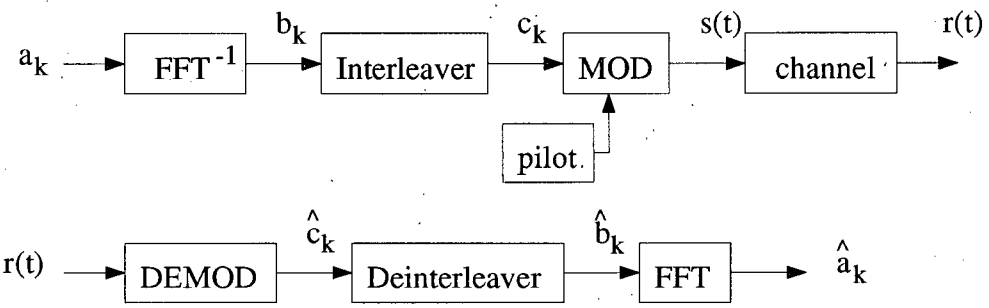

Figure 7.1 IOFDM

2. *DFE for frequency-selective channels* The MSEDIRDFE equalizer developed for flat fading could be extended to the frequency-selective fading case. A possible approach

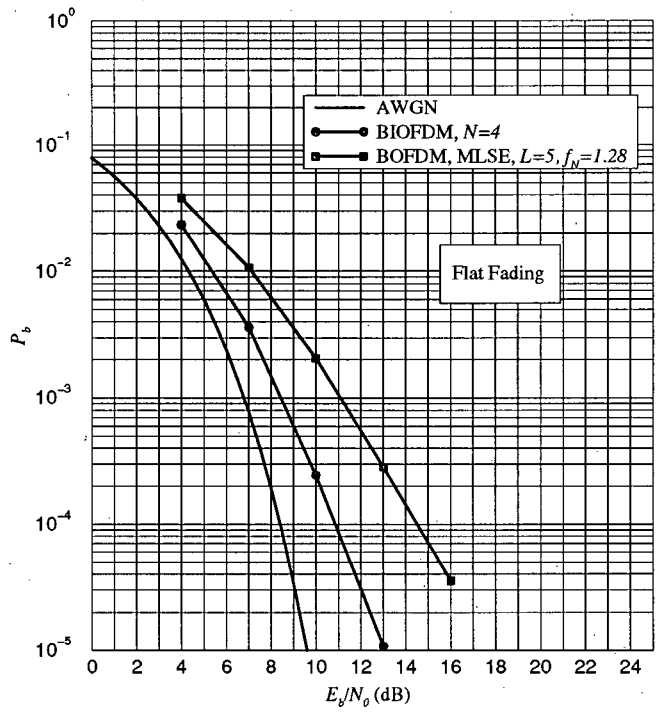

Figure 7.2 Comparison of BIOFDM with ideal interleaving to BOFDM with $f_N = 1.28$ on a flat fading Rayleigh channel.

might be to subdivide the OFDM block into smaller units that experience relatively flat fading, and then apply the flat fading techniques to each subunit.

3. *Trellis-coded blocks* The effectiveness of channel averaging obtained by trellis-coding of conventional serially-modulated data blocks should be compared to that of OFDM. Since trellis-coding requires a larger signal constellation to maintain the same data rate, it is unlikely that the two methods would have the same sensitivity to channel estimation noise, and this would be an important point of comparison.
4. *Channel estimation* Channel estimation for flat fading channels is well understood, but much remains to be done in the area of frequency-selective fading channels. Pilot tones, data sequences, and frequency chirps have all been applied ([5],[10], [11], [12],) but a comparative analysis of the costs and merits of each would be quite useful not only for OFDM, but other coherent techniques as well. It is also important to quantify the robustness of channel estimation methods in an interference limited environment.

Appendix A MFB Details

A.1 Evaluation of an Integral

In Chapter 3 the following integral occurs:

$$P_b = \frac{1}{2} - \frac{1}{2}\sum_{i=1}^{R}\sum_{k=1}^{n_i}\frac{A_{ik}}{(k-1)!\lambda_i^k}\int_0^\infty \operatorname{erf}\left(\sqrt{\frac{E_b y}{N_0}}\right) y^{k-1}e^{-y/\lambda_i}dy. \tag{A.1.1}$$

A closed form can be found by expanding the $\operatorname{erf}(\cdot)$ function within the integral as

$$I = \frac{2}{\sqrt{\pi}}\int_0^\infty \int_0^{\sqrt{\frac{E_b y}{T_0}}} e^{-t^2}dt\, y^{k-1}e^{-y/\lambda_i}dy. \tag{A.1.2}$$

Setting

$$u = \frac{2}{\sqrt{\pi}}\int_0^{\sqrt{\frac{E_b y}{N_0}}} e^{-t^2}dt \tag{A.1.3}$$

and

$$dv = y^{k-1}e^{-y/\lambda_i}dy \tag{A.1.4}$$

it is easily shown

$$du = \frac{\sqrt{E_b/N_0}}{\sqrt{\pi}}y^{-1/2}e^{-E_b y/N_0}dy \tag{A.1.5}$$

and

$$v = -\sum_{l=0}^{k-1}\frac{(k-1)!\lambda_i^{l+1}}{(k-1-l)!}y^{k-1-l}e^{-y/\lambda_i}. \tag{A.1.6}$$

Integrating by parts

$$\begin{aligned} I = &\left[-\sum_{l=0}^{k-1}\frac{(k-1)!\lambda_i^{l+1}}{(k-1-l)!}\operatorname{erf}\left(\sqrt{\frac{E_b y}{N_0}}\right)y^{k-1-l}e^{-y/\lambda_i}\right]_{y=0}^{y=\infty} \\ &+\left[\frac{\sqrt{E_b/N_0}}{\sqrt{\pi}}\sum_{l=0}^{k-1}\frac{(k-1)!\lambda_i^{l+1}}{(k-1-l)!}\int_0^\infty y^{k-\frac{3}{2}-l}e^{-(E_b/N_0+1/\lambda_i)y}dy\right] \end{aligned} \tag{A.1.7}$$

and noting the remaining integral above is in the form of the gamma function

$$I = \frac{1}{\sqrt{\pi}} \sum_{l=0}^{k-1} \frac{(k-1)!\lambda_i^{l+1}\Gamma\left(k-l-\frac{1}{2}\right)}{(k-1-l)!} \sqrt{\frac{E_b/N_0}{\left(E_b/N_0 + 1/\lambda_i\right)^{2(k-l)-1}}}. \tag{A.1.8}$$

where $\Gamma(\cdot)$ is the gamma function defined by [40]

$$\Gamma(x) = \int_0^\infty t^{x-1} e^{-t} dt. \tag{A.1.9}$$

Equation (A.1.8) may be simplified by modifying the summation index to $m = k - l$ to obtain

$$I = \frac{\lambda_i^k (k-1)!}{\sqrt{\pi}} \sum_{m=0}^{k-1} \frac{\Gamma\left(m+\frac{1}{2}\right)}{m!} \sqrt{\frac{\lambda_i E_b/N_0}{\left(\lambda_i E_b/N_0 + 1\right)^{2m+1}}} \tag{A.1.10}$$

and using the identity [40] $\Gamma\left(m+\frac{1}{2}\right) = \frac{\sqrt{\pi}(2m-1)!!}{(2m)!}$ yields

$$I = \lambda_i^k (k-1)! \sum_{m=0}^{k-1} \frac{(2m-1)!!}{(2m)!} \sqrt{\frac{\lambda_i E_b/N_0}{\left(\lambda_i E_b/N_0 + 1\right)^{2m+1}}} \tag{A.1.11}$$

where $(\cdot)!!$ is the double factorial function [40] defined by

$$(n)!! = \begin{cases} (n)(n-2)(n-4)\cdots(1), & n \text{ odd} \\ (n)(n-2)(n-4)\cdots(2), & n \text{ even} \end{cases}. \tag{A.1.12}$$

Combining (A.1.11) with (A.1.1) yields the desired expression for P_b:

$$P_b = \frac{1}{2} - \frac{1}{2} \sum_{i=1}^{R} \sum_{k=1}^{n_i} A_{ik} \sum_{l=0}^{k-1} \frac{(2l-1)!!}{(2l)!} \sqrt{\frac{\lambda_i E_b/N_0}{\left(\lambda_i E_b/N_0 + 1\right)^{2l+1}}}. \tag{A.1.13}$$

A.2 Mean and Variance of y in Flat Rayleigh Fading

For the flat Rayleigh fading model the matched filter output y is given by

$$y = \int |p(t)|^2 |z_1(t)|^2 dt. \tag{A.2.1}$$

The mean of y is

$$\begin{aligned} m_y &= \int |p(t)|^2 E\left[|z_1(t)|^2\right] dt \\ &= 2\sigma_{zr}^2 \end{aligned} \tag{A.2.2}$$

where we have used $E\left[|z_1(t)|^2\right] = 2\sigma_{zr}^2$ for a Rayleigh *pdf* and where σ_{zr}^2 is the variance of the real part of $z_1(t)$.

Finding the variance of y is more involved. We have

$$\sigma_y^2 = E\left[y^2\right] - 4\sigma_{zr}^2. \tag{A.2.3}$$

To simplify the notation let $v_1 = |z(t_1)|$ and $v_2 = |z(t_2)|$. Solving for the second moment

$$E\left[y^2\right] = \int\int |p(t_1)|^2 |p(t_2)|^2 E\left[v_1^2 v_2^2\right] dt_1 dt_2. \tag{A.2.4}$$

We seek

$$E\left[v_1^2 v_2^2\right] = \int_0^\infty \int_0^\infty \frac{v_1^3 v_2^3}{\sigma_{zr}^4(1-\rho^2)} e^{-\frac{v_1^2+v_2^2}{2\sigma_{zr}^2(1-\rho^2)}} I_0\left(\frac{\rho v_1 v_2}{\sigma_{zr}^2(1-\rho^2)}\right) dv_1\, dv_2. \tag{A.2.5}$$

In (A.2.18) we have used the joint *pdf* for two Rayleigh distributed random variables [22]

$$p_{v_1 v_2}(v_1, v_2) = \frac{v_1 v_2}{\sigma_{zr}^4(1-\rho^2)}\, e^{-\frac{v_1^2+v_2^2}{2\sigma_{zr}^2(1-\rho^2)}}\, I_0\left(\frac{\rho v_1 v_2}{\sigma_{zr}^2(1-\rho^2)}\right) \tag{A.2.6}$$

where ρ is the normalized cross correlation between two samples of the real part of the process $z_1(t)$ or equivalently two samples of the imaginary part. The real and imaginary parts are assumed to be independent. $I_0()$ is the zeroth order modified Bessel function of the first kind. Expanding $I_0()$ as [40]

$$I_0(x) = \sum_{k=0}^{\infty} \frac{\left(\frac{1}{4}x^2\right)^k}{(k!)^2} \tag{A.2.7}$$

and integrating term by term, it can be shown that

$$E\left[v_1^2 v_2^2\right] = 4\sigma_{zr}^4\left(1+\rho^2\right). \tag{A.2.8}$$

A result for the univariate case [9] is

$$\begin{aligned} E\left[v^k\right] &= \left(2\sigma_{zr}^2\right)^{\frac{k}{2}}\Gamma\left(1+\frac{k}{2}\right) \\ \Rightarrow E\left[v^2\right] &= 2\sigma_{zr}^2 \text{ and } E\left[v^4\right] = 8\sigma_{zr}^4. \end{aligned} \tag{A.2.9}$$

This provides two consistency checks of (A.2.21) by setting ρ to 0 or 1.

We assume [3]

$$\rho(\tau) = J_0(\omega_D \tau) \tag{A.2.10}$$

where $J_0()$ is the zeroth order Bessel function of the first kind, ω_D is the maximum Doppler frequency in radians, and $\tau = t_1 - t_2$ is the time interval between samples. Combining (A.2.16),(A.2.17),(A.2.21) and (A.2.23) we have

$$\sigma_y^2 = \int\int |p(t_1)|^2 |p(t_2)|^2 J_0^2(\omega_D(t_1 - t_2))dt_1\, dt_2. \tag{A.2.11}$$

Note that the evaluation of (A.2.24) can be reduced to at most the evaluation of two one dimensional integrals by rewriting it in terms of $\tau = t_1 - t_2$ as

$$\sigma_y^2 = \int\int |p(t_1)|^2 |p(t_1 - \tau)|^2 dt_1\, J_0^2(\omega_D \tau)d\tau. \tag{A.2.12}$$

The inner integral is the autocorrelation of the squared pulse magnitude

$$C_p(\tau) = \int |p(t)|^2 |p(t-\tau)|^2 dt. \tag{A.2.13}$$

$C_p(\tau)$ could be considered the autocorrelation of the pulse power. In many cases, $C_p(\tau)$ can be determined analytically. For example, if $p(t)$ is a rect pulse we have

$$\begin{aligned} C_{pr}(\tau) &= \frac{1}{T_0}\int_0^{T_0} \text{rect}^2(t)\text{rect}^2(t-\tau)dt \\ &= \frac{1}{T_0}\left(1 - \frac{\tau}{T_0}\right). \end{aligned} \tag{A.2.14}$$

Using (A.2.26) in (A.2.25) we obtain

$$\sigma_y^2 = \int_{-T_0}^{T_0} C_p(\tau) J_0^2(\omega_D \tau) d\tau. \tag{A.2.15}$$

A Limiting case Noting the normalized Doppler frequency in radians is $\omega_N = 2\pi f_N = w_D T_0$, we can obtain the limiting variance of y as $f_N \to \infty$ by holding w_D constant in (A.2.28) and taking the limit as $T_0 \to \infty$.

The pulse $p(t)$ has been defined as having unit energy and duration T_0. These features constrain the behavior of $C_p(t)$ and hence σ_y^2 as T_0 increases. Writing $p(t)$ in terms of $p_u(t)$, a pulse having unit energy and also unit duration

$$p(t) = \frac{1}{\sqrt{T_0}} p_u(t/T_0) \tag{A.2.16}$$

and combining this with (A.2.26) at $\tau = 0$ we have

$$\begin{aligned} C_p(0) &= \frac{1}{T_0^2} \int_0^{T_0} |p_u(t/T_0)|^4 dt \\ &= \frac{1}{T_0} \int_0^1 |p_u(x)|^4 dx \\ &= \frac{c}{T_0} \end{aligned} \tag{A.2.17}$$

where c is some finite constant defined as

$$c = \int_0^1 |p_u(x)|^4 dx. \tag{A.2.18}$$

Noting an autocorrelation function has its peak at lag 0,

$$C_p(\tau) \leq \frac{c}{T_0}. \tag{A.2.19}$$

Using (A.2.32) in (A.2.28) yields

$$\sigma_y^2 \leq \frac{2c \int_0^{T_0} J_0^2(\omega_D \tau) d\tau}{T_0} \tag{A.2.20}$$

and applying L'Hopital's rule

$$\lim_{T_0 \to \infty} \sigma_y^2 = \lim_{T_0 \to \infty} 2cJ_0^2(\omega_D T_0) d\tau = 0. \tag{A.2.21}$$

The variance σ_y^2 approaches 0 as the pulse duration T_0 or equivalently as the normalized Doppler frequency f_N increases without limit for any unit energy pulse.

A.3 Selection of M

Assuming fast fading, we first require that Δt in

$$y = \Delta t \sum_{i=1}^{M} |q_i|^2 \tag{A.3.1}$$

be much less than the *coherence time* $t_c = 1/f_D$ of the channel so that

$$\Delta t \sum_{i=1}^{M} |q_i|^2 \approx \int |q(t)| dt \tag{A.3.2}$$

is a close approximation, i.e.

$$\Delta t \ll t_c = \frac{1}{f_D}. \tag{A.3.3}$$

In (A.3.37) Δt was chosen so that $f_D \Delta t = 0.01$ was used to calculate the fast fading results of Section 3.5, and $f_D = 0.0$ was used for the slow fading results.

We have

$$f_N = f_D T_0 = f_D M \Delta t \tag{A.3.4}$$

and for fast fading the normalized Doppler rate was set by selecting

$$M = \frac{f_N}{f_D \Delta t}. \tag{A.3.5}$$

For the slow fading examples M was selected just large enough to allow an accurate representation of the desired delay spread, e.g. for normalized delay spread $\tau = 0.25$, $M = 4$ was selected.

Appendix B The DFFT and the iDFFT

The discrete frequency Fourier transform (DFFT) is defined by

$$X_k = \int x(t) e^{-j\frac{2\pi}{T_0}kt} dt \tag{B.1}$$

and its inverse (iDFFT) by

$$\tilde{x}(t) = \sum_k X_k e^{j\frac{2\pi}{T_0}kt} \tag{B.2}$$

where $\tilde{x}(t)$ is a periodic function in time related to $x(t)$ by

$$\tilde{x}(t) = T_0 \sum_n x(t - nT_0). \tag{B.3}$$

Equations (B.2) and (B.3) are readily established from the definition (B.1) using the conventional continuous Fourier transform $X(f) = \int x(t)e^{-j2\pi ft}dt$ and the Fourier transform pair $\sum_n \delta(t - nT_0) \rightleftharpoons \frac{1}{T_0}\sum_k \delta\left(f - \frac{k}{T_0}\right)$. We have $X_k = X(f) \times \sum_k \delta\left(f - \frac{k}{T_0}\right)$ which must then have for its inverse

$$\begin{aligned} X_k \rightleftharpoons & x(t) \otimes T_0 \sum_n \delta(t - nT_0) \\ &= T_0 \sum_n x(t - nT_0) \\ &= \tilde{x}(t) \end{aligned} \tag{B.4}$$

where $\otimes$ is the convolution operator. Another useful relation is found by applying the orthogonality property of complex exponentials to (B.2) yielding

$$\begin{aligned} \int_{T_0} \tilde{x}(t) e^{-j\frac{2\pi}{T_0}mt} dt &= \sum_k X_k \int_{T_0} e^{j\frac{2\pi}{T_0}kt} e^{-j\frac{2\pi}{T_0}mt} dt \\ &= T_0 X_m \end{aligned} \tag{B.5}$$

or

$$X_k = \frac{1}{T_0} \int_{T_0} \tilde{x}(t) e^{-j\frac{2\pi}{T_0}kt}. \tag{B.6}$$

Appendix C Derivation of a Metric Recursion

The MLSE receivers of Chapters 3 and 5 are implemented with a Viterbi algorithm which requires a recursive metric. Details of the derivation are given below. The original application of the Viterbi algorithm to ISI problems required a noise-whitening filter before the sequence estimator [26]. We use the approach of [41] which is able to avoid this requirement.

Consider the metric λ_l below for which we seek a recursive expression

$$\lambda_l = \mathrm{Re}\left[\sum_{n=0}^{l} a_n^* U_n\right] - \frac{1}{2}\sum_{n=0}^{l}\sum_{m=0}^{l} a_n^* a_m V_{m,n} \tag{C.7}$$

and expand the double summation as follows

$$\sum_{n=0}^{l}\sum_{m=0}^{l} a_n^* a_m V_{m,n} = \sum_{m=0}^{l}\left(a_l^* a_m V_{m,l} + \sum_{n=0}^{l-1} a_n^* a_m V_{m,n}\right). \tag{C.8}$$

Isolating the terms for which $m = l$ the R.H.S. above can be written

$$|a_l|^2 V_{l,l} + \sum_{n=0}^{l-1} a_n^* a_l V_{l.n} + \sum_{m=0}^{l-1}\left(a_l^* a_m V_{m,l} + \sum_{n=0}^{l-1} a_n^* a_m V_{m,n}\right) \tag{C.9}$$

and using $V_{m,n} = V_{n,m}^*$ the preceding is equivalent to

$$|a_l|^2 + 2\mathrm{Re}\left[a_l \sum_{n=0}^{l-1} a_n^* V_{l,n}\right] + \sum_{n=0}^{l-1}\sum_{m=0}^{l-1} a_n^* a_m V_{m,n}. \tag{C.10}$$

Using (C.4) in (C.1) yields

$$\begin{aligned}\lambda_l =& \mathrm{Re}[a_l^* U_l] - \frac{|a_l|^2 V_{l,l}}{2} - \mathrm{Re}\left[a_l \sum_{n=0}^{l-1} a_n^* V_{l,n}\right] \\ &+ \mathrm{Re}\left[\sum_{l=0}^{l-1} a_n^* U_n\right] - \sum_{n=0}^{l-1}\sum_{m=0}^{l-1} a_n^* a_m\end{aligned} \tag{C.11}$$

from which it is apparent

$$\lambda_l = \lambda_{l-1} + \mathrm{Re}[a_l^* U_l] - \mathrm{Re}\left[a_l \sum_{n=0}^{l-1} a_n^* V_{l,n}\right] - \frac{|a_l|^2 V_{l,l}}{2}. \tag{C.12}$$

Appendix D Matrix Notation Conventions

Matrix notation, when clearly defined, provides an elegant representation for systems of linear equations. We rely on it from Chapter 3 onwards. Unfortunately there is no one consensus on how to identify matrices and define their elements, therefore the conventions adopted for this work are explained below.

All matrices are represented by boldface characters. An uppercase boldface character represents a two-dimensional matrix, and a lower case boldface character represents one-dimensional matrix, which is a column vector. For example $\mathbf{Q}$ is a two-dimensional matrix and $\mathbf{q}$ is a column vector.

The $(i,k)^{th}$ element of $\mathbf{Q}$ is $\mathbf{Q}_{\mathrm{i,k}}$ and the i^{th} element of $\mathbf{q}$ is $\mathbf{q}_{\mathrm{i}}$. Note the subscripts are not bold.

Examples:

$$\mathbf{Q} = \begin{bmatrix} x_{1,1} & x_{1,2} & \cdots & x_{1,N} \\ x_{2,1} & x_{2,2} & \cdots & x_{2,N} \\ \vdots & \vdots & \cdots & \vdots \\ x_{M,1} & x_{M,2} & \cdots & x_{M,N} \end{bmatrix}, \qquad \mathbf{q} = \begin{bmatrix} x_1 \\ x_2 \\ \vdots \\ x_M \end{bmatrix} \tag{D.13}$$

where $\mathbf{Q}_{\mathrm{i,k}} = x_{i,k}$ and $\mathbf{q}_{\mathrm{i}} = x_i$. There is no relation between the case of a matrix and the case of its elements. We do this because it is helpful when checking the syntax of matrix equations to be able to distinguish two-dimensional matrices from column vectors at a glance; this determines the case of the matrix. Yet, depending on the situation, we need to assemble matrices of scalars defined in either the time-domain or frequency-domain. Following the well-established convention for Fourier Transforms, we consistently represent frequency-domain scalars with uppercase characters and time-domain scalars with lowercase characters. Thus $\mathbf{d} = [x_1, x_2, \cdots x_M]^{\mathrm{T}}$ and $\mathbf{d} = [X_1, X_2 \cdots, X_M]^{\mathrm{T}}$ are both valid constructs. The superscript $(\cdot)^{\mathrm{T}}$ denotes transposition.

Occasionally we need to define several related vectors. We do this with a *bold* subscript, e.g. $\mathbf{d_1}, \mathbf{d_2}, \cdots, \mathbf{d_N}$ represents N different column vectors. The i^{th} element of the k^{th} vector is $\mathbf{d_{k_i}}$. Note k is bold, i is not.

It follows an alternative way of describing $\mathbf{Q}$ above would be to first define $\mathbf{q_k} = \left[x_{1,k}, x_{2,k}, \cdots, x_{M,k}\right]^{\mathrm{T}}$ and then define $\mathbf{Q} = [\mathbf{q_1}, \mathbf{q_2}, \cdots, \mathbf{q_N}]$.

Another convenient way to define the same matrix $\mathbf{Q}$ is: $\mathbf{Q} = \left[\left\{\mathbf{Q_{i,k}}\right\}\right]$, $\mathbf{Q_{i,k}} = x_{i,k}$, where $1 \leq i \leq M$, $1 \leq k \leq N$. The $\left[\left\{\mathbf{Q_{i,k}}\right\}\right]$ denotes the set of elements $\mathbf{Q_{i,k}}$ are arranged in a matrix.

Note the order of the subscripts in $\mathbf{Q_{i,k}} = x_{i,k}$ can be reversed to obtain $\mathbf{Q^T}$, e.g. $\mathbf{Q^T} = \left[\left\{\mathbf{Q_{i,k}}\right\}\right]$, $\mathbf{Q_{i,k}} = x_{k,i}$.

Analogous to the vector case, a two-dimensional matrix can also be defined as an array of two-dimensional sub-matrices, e.g. $\mathbf{Y} = \left[\left\{\mathbf{X_{j,l}}\right\}\right]$, where the $(i,k)^{th}$ element of $\mathbf{X_{j,l}}$ is given by $\mathbf{X_{j,l}} = \mathbf{X_{j,l_{i,k}}}$.

We also use the *Hermitian*, $(\cdot)^{\mathrm{H}}$, to denote conjugate transpose, e.g. $\mathbf{Q}^{\mathrm{H}} = \mathbf{Q}^{\mathrm{T}*}$.

Bibliography

[1] J. E. Padgett, C. G. Gunther, and T. Hattori, "Overview of wireless personal communications," *IEEE Communications Mag.*, vol. 33, pp. 28–41, Jan. 1995.

[2] D. C. Cox, "Wireless network access for personal communications," *IEEE Communications Mag.*, vol. 30, pp. 96–115, Dec. 1992.

[3] W. C. Jakes, *Microwave Mobile Communications*. N.Y.: Wiley, 1974.

[4] A. J. Viterbi and R. Padovani, "Implications of mobile cellular CDMA," *IEEE Communications Mag.*, vol. 30, pp. 42–49, Dec. 1992.

[5] L. J. Cimini Jr., "Analysis and simulation of a digital mobile channel using orthogonal frequency division multiplexing," *IEEE Trans. Comm.*, vol. COM-33, pp. 665–675, July 1985.

[6] A. V. Oppenheim and R. W. Schaffer, *Digital Signal Processing*. Englewood Cliffs, N.J.: Prentice-Hall, 1973.

[7] J. Ahn and H. S. Lee, "Frequency domain equalisation of OFDM signals over frequency nonselective Rayleigh fading channels," *Electronics Letters*, vol. 29, pp. 1476–1477, Aug. 1993.

[8] J. M. Wozencraft and I. M.Jacobs, *Principles of Communications Engineering*. N.Y.: Wiley, 1965.

[9] J. G. Proakis, *Digital Communications*. N.Y.: McGraw-Hill, 1989.

[10] J. K. Cavers, "An analysis of pilot symbol assisted modulation for Rayleigh fading channels," *IEEE Trans. Veh. Tech.*, vol. 40, pp. 686–693, Nov. 1991.

[11] J. K. Cavers, "Performance of tone calibration with frequency offset and imperfect pilot filter," *IEEE Trans. Veh. Tech.*, vol. 40, pp. 426–434, May 1991.

[12] M. Mouly and M.-B. Pautet, *The GSM System for Mobile Communications*. 49 rue Louise Bruneau, F-91120 Palaiseau, France: Mouly & Pautet, 1992.

[13] J. Holsinger, *Digital Communication over fixed time continuous channels with memory.* PhD thesis, M.I.T., 1964.

[14] S. B. Weinstein and P. M. Ebert, "Data transmission by frequency division multiplexing using the discrete Fourier transform," *IEEE Trans. Comm. Tech.*, vol. COM-19, pp. 628–634, Oct. 1971.

[15] P. Bello, "Selective fading limitations of the kathryn modem and some system design considerations," *IEEE Trans. Comm.*, vol. 13, pp. 320–333, Sept. 1965.

[16] J. Rault, D. Castelain, and B. LeFloch, "The coded orthogonal frequency division multiplexing (COFDM) technique, and its application to digital radio broadcasting towards mobile receivers," in *IEEE Global Communication Conference (Globecom)*, pp. 428–432, 1989.

[17] E. F. Casas and C. Leung, "OFDM for data communication over mobile radio FM channels-part 1: Analysis and experimental results," *IEEE Trans. Comm.*, vol. COM-39, pp. 783–793, May 1991.

[18] J. Andersen, T. Rappaport, and S. Yoshida, "Propagation measurements and models for wireless communications channels," *IEEE Communications Mag.*, vol. 33, pp. 42–49, Jan. 1995.

[19] A. Papoulis, *Probability, Random Variables, and Stochastic Processes.* N.Y.: McGraw-Hill, 1984.

[20] J. Mazo, "Exact matched filter bound for two-beam Rayleigh fading," *IEEE Trans. Comm.*, vol. COM–39, pp. 1027–1030, July 1991.

[21] M. Clark, L. Greenstein, W. Kennedy, and M. Shafi, "Matched filter performance bounds for diversity combining receivers in digital mobile radio," *IEEE Trans. Veh. Tech.*, vol. 41, pp. 356–362, Nov. 1992.

[22] W. Davenport and W. Root, *An Introduction to the Theory of Random Signals and Noise.* N.Y.: McGraw-Hill, 1958.

[23] S. S. Haykin, *Introduction to Adaptive Filters.* N.Y.: MacMillan, 1984.

[24] A. V. Oppenheim, A. S. Willsky, and I. T. Young, *Signals and Systems.* Englewood Cliffs, N.J.: Prentice-Hall, 1983.

[25] W. Press, B. Flannery, S. Teukolsky, and W. Vetterling, *Numerical Recipes in C.* Cambridge: Cambridge University Press, 1988.

[26] G. D. Forney, Jr., "Maximum-likelihood sequence estimation of digital sequences in the presence of intersymbol interference," *IEEE Trans. Inf. Theory*, vol. IT-18, pp. 363–378, May 1972.

[27] G. Ungerboeck, "Nonlinear equalization of binary signals in Gaussian noise," *IEEE Trans. Comm. Tech.*, vol. COM-19, pp. 1128–1137, Dec. 1971.

[28] R. E. Blahut, *Digital Transmission of Information.* N.Y.: McGraw-Hill, 1982.

[29] D. D. Falconer and F. R. Magee, Jr., "Adaptive channel memory truncation for maximum likelihood sequence estimation," *Bell System Technical Journal*, vol. 52, pp. 1541–1562, Nov. 1973.

[30] J. Salz, "Optimum mean-square decison feedback equalization," *Bell System Technical Journal*, vol. 52, pp. 1341–1373, Oct. 1973.

[31] C. A. Belfiore and J. H. Park, Jr., "Decision feedback equalization," *Proc. of the IEEE*, vol. 67, pp. 1143–1156, Aug. 1979.

[32] J. M. Ahn, "private communication." re: ideal decisions in DFE feedback loop, July 1996.

[33] S. U. H. Qureshi and E. E. Newhall, "An adaptive receiver for data transmission over time-dispersive channels," *IEEE Trans. Inform. Theory.*, vol. IT-19, pp. 448–457, July 1969.

[34] D. G. Messerschmitt, "Design of a finite impulse response for the Viterbi algorithm and decision feedback equalizer," in *Rec. Int. Conf. Communications, ICC-74*, (Minneapolis, MN), June 1974.

[35] D. G. Messerschmitt, "A geometric theory of intersymbol interference," *Bell System Technical Journal*, vol. 52, pp. 1483–1519, Nov. 1973.

[36] P. Monsen, "Feedback equalization for fading dispersive channels," *IEEE Trans. Inform. Theory.*, vol. IT-17, pp. 56–64, Jan. 1971.

[37] D. D. Falconer, F. Adachi, and B. Gudmundson, "Time division multiple access methods for wireless personal communications," *IEEE Communications Mag.*, vol. 33, pp. 42–49, Jan. 1995.

[38] A. Jerri, *Introduction to Integral Equations with Applications*. N.Y.: Dekker, 1985.

[39] G. Strang, *Linear Algebra and its Applications*. San Diego: Harcourt, 1988.

[40] M. Abramowitz and I. E. Stegun, *Handbook of Mathematical Functions*. Washington, D. C.: National Bureau of Standards, 1972.

[41] G. Ungerboeck, "Adaptive maximum-likelihood receiver for carrier-modulated data-transmission systems," *IEEE Trans. Comm.*, vol. COM-22, pp. 624–636, May 1974.